

A Novel Micromechanics Based Approach  
in  
Modeling Pavement Response

By

Arun Bhattacharya

B.S.M.E. ( Jadavpur University) 1985  
M.S.M.E ( Wayne State University) 1987

DISSERTATION

Submitted in partial satisfaction of the requirements for the degree of

DOCTOR OF PHILOSOPHY

in

Engineering

in the

OFFICE OF GRADUATE STUDIES

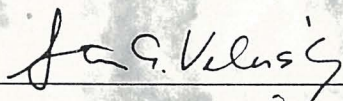
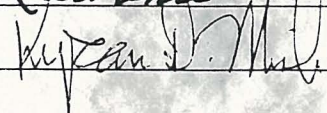
of the

UNIVERSITY OF CALIFORNIA

DAVIS

UCD - ARR -  
97 - 06 - 30 - 01

Approved:

  
\_\_\_\_\_  
  
\_\_\_\_\_  
  
\_\_\_\_\_

Committee in Charge

1997

i

**Committee in Charge:**

**Dr. Steven A. Velinsky, Chair  
Professor of Mechanical Engineering**

**Dr. Lawrence W. Rehfield  
Professor of Aeronautical Engineering**

**Dr. Kyran D. Mish  
Professor of Civil Engineering**

**A Novel Micromechanics Based Approach  
to  
Pavement Modeling and Response**

**Copyright 1997**

**by**

**Arun Bhattacharya**

Arun Bhattacharya  
June 1997  
Mechanical Engineering

**A Novel Micromechanics Based Approach  
to  
Pavement Modeling and Response**

**Abstract**

For maintaining a smooth flow of traffic in the nation's highway system, sections of pavements that are damaged need to be serviced frequently. Among the various types of damage, those caused by heavy trucks are a major concern. Based on a detailed and broad literature survey, it is apparent that no analytical model exists which could closely predict dynamic pavement response and progressive damage, even qualitatively, due to truck loading. It is such a model that is developed in this work. In order to predict pavement response and damage analytically, a model will have to be based on a theory that captures the essential features of the pavement material. The state-of-the-art Microplane Theory, which has never been applied before to pavement, is chosen to model the material behavior in this research. The theory is implemented in a finite element code to predict tri-axial pavement response. The pavement material damage due to traffic loading is also presented qualitatively. Furthermore, using Taguchi Methods, the critical parameters in a pavement design are determined. Finally, the response of pavement to various joint designs parameters is evaluated.

## Acknowledgments

I want to express my profound gratitude to Professor Steven A. Velinsky for his invaluable guidance throughout this research. While giving research direction, Professor Velinsky has provided inspiration through the highs and lows of this research during the last four years. My sincerest thanks also go to Professor Lawrence W. Rehfield for his advice during difficult periods in the research and for opening doors to new insights. Additional thanks go to Professor Bahram Ravani, Chairman of the Department of Mechanical and Aeronautical Engineering, for serving as the chairman on my Qualifying Committee and for providing valuable advice during the qualifying exam. I would like to thank Professor Kyran Mish for his constructive suggestions on my dissertation and to Professor Yanus Dafalias of the Department of Civil Engineering who has provided different perspectives on the concrete modeling work in my thesis. I am greatly indebted to Dr. Ty Lasky at the AHMCT Center for always helping me with various unexpected computing and networking problems, especially at odd hours. Thanks also to Jim Stiles and Kin Yen for providing assistance with other networking issues and apprising me of the computer resources available here at AHMCT.

On a personal note, I am greatly indebted to Susie Fann for her assistance with all of the necessary paperwork. Lastly, my heart goes out to my wife Sujata, and my son Arvind, for making things go smoothly during my graduate career at the Aeronautical/Mechanical Engineering Department of UC Davis and for bearing with me during the late hours when I continuously missed them. My overseas gratitude goes to my Dad and Mom in India for supporting me telepathically.

To  
my dad,  
wife and mom,  
who made it all possible

# CONTENTS

## ABSTRACT

|                                                       |    |
|-------------------------------------------------------|----|
| <b>CHAPTER 1 - INTRODUCTION</b>                       | 1  |
| 1.1 - Summary of the Problem                          | 1  |
| 1.2 - Focus                                           | 2  |
| 1.3 - Summary                                         | 3  |
| <b>CHAPTER 2 - SUMMARY OF LITERATURE SEARCH</b>       | 4  |
| 2.1 - Objective the Literature Search                 | 4  |
| 2.2 - Survey                                          | 4  |
| 2.3 - Status of Other Analytical Methods              | 14 |
| 2.4 - Justification for this research                 | 17 |
| 2.5 - Summary                                         | 18 |
| <b>CHAPTER 3 - MICROPLANE MODEL</b>                   | 20 |
| 3.1 - Introduction                                    | 20 |
| 3.2 - Bazant's Microplane Theory                      | 20 |
| 3.3 - Damage Rule                                     | 23 |
| 3.4 - Summary                                         | 24 |
| <b>CHAPTER 4 - IMPLEMENTATION OF MICROPLANE MODEL</b> | 25 |
| 4.1 - Introduction                                    | 25 |
| 4.2 - Constitutive Implementation                     | 25 |
| 4.3 - Program Checks                                  | 34 |
| 4.4 - Unloading and Reloading                         | 36 |

|                                                    |           |
|----------------------------------------------------|-----------|
| 4.5 - Explicit vs. Implicit Integration Methods    | 37        |
| 4.6 - Time Step Calculation                        | 40        |
| 4.7 - Mass Scaling                                 | 41        |
| 4.8 - Summary                                      | 42        |
| <b>CHAPTER 5 - VERIFICATION OF NUMERICAL MODEL</b> | <b>43</b> |
| 5.1 - Introduction                                 | 43        |
| 5.2 - Sensitivity Study                            | 43        |
| 5.3 - Taguchi Method and Its Application           | 45        |
| 5.4 - Verification of The Model                    | 52        |
| 5.5 - Taguchi Method Applied in Numerical Modeling | 59        |
| 5.6 - Avoiding Mesh Dependencies                   | 64        |
| 5.7 - Summary                                      | 66        |
| <b>CHAPTER 6 - PAVEMENT RESPONSE MODELING</b>      | <b>67</b> |
| 6.1 - Introduction                                 | 67        |
| 6.2 - Foundation Modeling                          | 67        |
| 6.3 - Pavement Modeling                            | 70        |
| 6.4 - Verification                                 | 71        |
| 6.5 - Damage Distribution                          | 84        |
| 6.6 - Summary                                      | 96        |
| <b>CHAPTER 7 - JOINT DESIGN</b>                    | <b>98</b> |
| 7.1 - Introduction                                 | 98        |
| 7.2 - A Typical Joint                              | 98        |
| 7.3 - Pavement Response under Dynamic Loads        | 99        |
| 7.4 - Dowel Design                                 | 101       |
| 7.5 - Jointed Pavement Response                    | 103       |
| 7.6 - Taguchi Sensitivity Study                    | 107       |

|                                                                            |     |
|----------------------------------------------------------------------------|-----|
| 7.7 - Discussion of The Results                                            | 109 |
| 7.8 - Joint Stiffness Study                                                | 110 |
| 7.9 - Summary                                                              | 113 |
| <b>CHAPTER 8 - CONCLUSIONS AND RECOMMENDATIONS<br/>FOR FUTURE RESEARCH</b> | 114 |
| 8.1- Contributions of this thesis                                          | 114 |
| 8.2 - Future Research                                                      | 116 |
| <b>BIBLIOGRAPHY</b>                                                        | 119 |
| <b>APPENDICES</b>                                                          | 137 |
| A - Derivation of the Incremental Tangent Stiffness Matrix                 | 137 |
| B - Taguchi Method                                                         | 139 |
| C - Steps to Calculate ANOVA                                               | 141 |
| D - Table of Dowel Diameter and Length                                     | 143 |
| E - The Developed Program                                                  | 144 |
| F - Stress-Strain Equations                                                | 160 |
| G - Nomenclature                                                           | 162 |

## LIST OF FIGURES

|      |                                            |    |
|------|--------------------------------------------|----|
| 1.1  | Typical cross section of a rigid pavement  | 2  |
| 2.1  | Load displacement curve before peak load   | 10 |
| 2.2  | Finite element meshes used                 | 10 |
| 2.3  | Truck model from Gillespie (1993)          | 12 |
| 2.4  | Simulated results Gillespie (1993)         | 12 |
| 2.5  | Simulated results Gillespie (1993)         | 12 |
| 4.1  | Microplane directions (Full Model)         | 32 |
| 4.2  | Microplane directions (Quarter Model)      | 32 |
| 4.3  | Numerical convergence                      | 34 |
| 5.1  | Finite element mesh                        | 45 |
| 5.2  | Main effects                               | 48 |
| 5.3  | Microplane component curves                | 51 |
| 5.4  | Uniaxial tension                           | 53 |
| 5.5  | Analysis results for uniaxial tension load | 53 |
| 5.6  | Cyclic loop                                | 54 |
| 5.7  | Post -peak and hysteresis loop compared    | 55 |
| 5.8  | Cyclic compression                         | 56 |
| 5.9  | Triaxial test                              | 57 |
| 5.10 | Triaxial test results                      | 57 |
| 5.11 | Three point bend test                      | 58 |
| 5.12 | Three point bending test                   | 59 |
| 5.13 | Monotonic and cyclic load                  | 60 |
| 5.14 | Numerical sensitivity                      | 62 |

|      |                                                         |     |
|------|---------------------------------------------------------|-----|
| 5.15 | Comparison between monotonic and cyclic loading         | 63  |
| 6.1  | Pavement element discretization                         | 69  |
| 6.2  | Finite element mesh of the quarter model                | 73  |
| 6.3  | Undeformed and deformed shape of the quarter model      | 74  |
| 6.4  | Deflected basin under a loaded wheel                    | 77  |
| 6.5  | Simulated deflected basin under a loaded wheel          | 77  |
| 6.6  | Rigid pavement influence function                       | 78  |
| 6.7  | Canadian test truck description                         | 80  |
| 6.8  | Axle load distribution in the test                      | 81  |
| 6.9  | Axle load distribution in the analysis                  | 81  |
| 6.10 | Finite element mesh                                     | 82  |
| 6.11 | Narrow strip of the pavement under load                 | 82  |
| 6.12 | Dynamic truck test simulation                           | 83  |
| 6.13 | One loading cycle                                       | 86  |
| 6.14 | Finite element mesh                                     | 86  |
| 6.15 | Instantaneous damage distribution after 5 cycles        | 87  |
| 6.16 | Instantaneous damage distribution after 10 cycles       | 88  |
| 6.17 | Extrapolated damage distribution along the vehicle path | 89  |
| 6.18 | Main effects in cyclic loading                          | 94  |
| 7.1  | A typical Joint                                         | 99  |
| 7.2  | Finite element mesh of the jointed pavement             | 100 |
| 7.3  | Pavement slab under tension                             | 102 |
| 7.4  | Deformed plot ( Loading on the joint)                   | 104 |
| 7.5  | Deformed plot (Loading next to the joint)               | 104 |

# Chapter 1. Introduction

## 1.1. Summary of the Problem

A well designed pavement, assisted by a good preventive maintenance scheme, ensures a smooth flow of traffic and a long service life. A pavement whose strength and stiffness deteriorates with time gradually fails to support the flow of traffic and eventually gives rise to various types of pavement distress. These distresses, when small, may initially cause a minor ride discomfort, but after cycles of traffic loading, grow adequately large to disrupt the flow of traffic. This costs considerable time and money. It is estimated that the United States government's annual expenditure on road maintenance caused by heavy vehicles is 9 billion dollars (Cebon, 1993), and this does not reflect the time lost in traffic hold-ups. Any means to curtail this expenditure is therefore highly desirable.

Among the wide spectrum of damage, including those having natural and catastrophic origins, the category of damage initiated by traffic is a chief contributor to pavement distress. The most severe in that category is the fatigue cracking caused by a dynamic transfer of forces from the vehicle tires onto the pavement. In order to plan better for the maintenance schemes and design longer lasting pavements for the future, the response of a pavement to a given dynamic loading needs to be fully understood. Additionally, variation in response with each cycle of traffic loading needs to be predicted. This prediction would then caution the highway engineers of an impending distress so that necessary maintenance could be appropriately planned. Predicting pavement response and damage experimentally is expensive, cumbersome, and can be disruptive to the flow of traffic. An analytical model can simulate the dynamic response in a more efficient manner and with this idea a literature survey was conducted to ascertain the status of such research. However, the literature search will show in the subsequent pages that no such analytical

technique exists today, capable of predicting a realistic pavement response due to the dynamic loading of a vehicle. Moreover, none exists that can identify even the sensitive design parameters responsible for pavement's dynamic performance and damage potential. This thesis establishes a major step to such a novel analytical technique capable of predicting the dynamic response of a pavement and identifying damage qualitatively.

## 1.2. Focus

Among the types of pavement in service (flexible, rigid and composite), rigid pavement is the subject of this research. A typical cross section of a rigid pavement (Huang, 1993) is shown in Figure 1.1. The depth of the layers marked by  $h_1$  and  $h_2$  in Figure 1.1 are usually within the range of 0.15 - 0.3 m (0.5 - 1.0 ft) and 0.1 - 0.3 m (0.3 - 1.0 ft) respectively. Rigid pavements are constructed of Portland Cement Concrete (PCC), and in contrast to flexible pavements, they are placed either directly on the prepared subgrade or on a single layer of granular or stabilized material. The rigid pavements are paved in section and employ various types of joints for connections and load transfer across them.

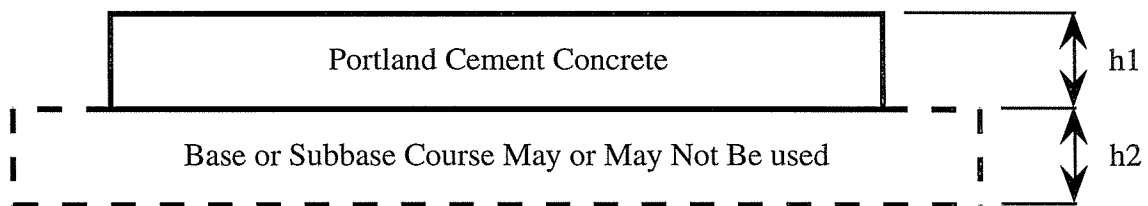


Figure 1.1: Typical cross section of a rigid pavement

Fatigue cracking has long been considered the major failure criterion for rigid pavement design. The focus of this work is to develop an analytical tool to predict the pavement response and the onset of these damages in Plain Concrete Pavements (PCP).

This can lead towards the planning of preventive maintenance. Also, the intent is to be capable of analyzing future design and construction of Transversely Jointed Plain Concrete Pavements (TJPCP) for a wide range of traffic loading and pavement construction environments.

### **1.3. Summary**

In this chapter, the specific problem of modeling pavement response and predicting damage under traffic loading is identified. The research will focus on the response of Plain Concrete Pavements. Additionally, the response of Transversely Jointed Plain Concrete Pavements under dynamic loading will be investigated in this dissertation.

## **Chapter 2. Summary of Literature Search**

### **2.1. Objective of the Literature Search**

As mentioned earlier, pavement-vehicle interaction is the leading cause of pavement distress. For predicting the response analytically, a vehicle model to compute the vehicle loads and a pavement model that uses those loads, can be used to generate the material response. Accordingly, an in-depth literature search has been conducted to establish the state-of-the-art in several areas that are relevant to the pavement-vehicle interaction problem.

### **2.2. Survey**

The areas surveyed encompass nine groups, as follows: Physical Observation, Fracture Mechanics, Statistical Mechanics, Micromechanics, Plasticity and Continuum Mechanics, Finite Element Methods, Damage Assessment on the pavement side and Vehicle Modeling and Tire Modeling, on the vehicle side. This section briefly describes the status of research in these various areas.

#### **2.2.1. Papers on Physical Observation**

Concrete, which is a primary building block of the pavement, shows certain types of physical behaviors, most of which are evident from a physical inspection of the material. Those characteristics are: (i) Brittleness, (ii) Cracking, (iii) Fracture, (iv) Strain-Softening, (v) Highly nonlinear stress-strain relationship, (vi) Inclusion toughening (vii) Notch Sensitivity, and (viii) Size-Effects, illustrating the complex nature of concrete. Shah et al. (1991) recommended that at least the first five should be represented by any reasonable model of concrete for purposes of analyzing pavement.

To acquire knowledge of concrete through a series of tests in a laboratory, the same type of concrete specimens having the same size and constituents must be used in each of those tests. Otherwise, the 'size effect' (Bazant et al., 1984) could become dominant particularly at high strain rates in the tension-softening regime of the stress-strain curve. Notch Sensitivity in concrete is also very significant when compared to metals like grey cast iron. For example, in the case of fracture tests, like the Izod Impact Test (Askeland, 1993) which requires a V-shaped notch on the specimen, the specimens should all be the same size and have identical specifications for the notches to produce experimental data from which a generalized inference about concrete behavior can be drawn. Much research conducted (Barsom, 1977; Aifantis, 1984; RILEM, 1985; Shah et al., 1991) brings out this difficulty in experimentally quantifying the generalized properties of concrete.

To simulate the response of a concrete part using finite element methods, one has to overcome the mesh dependencies caused at the onset of cracking. It is also difficult to relate an experimental fracture to a state of failure in the numerical modeling of concrete. Fracture in a concrete specimen tested in a laboratory is abrupt (Askeland, 1993), whereas in an analytical model, the damage may be slow and mesh dependent. Moreover, if the element size is not related to the aggregate size of the concrete used, the simulated damage tends to get confined to the width of the element being used. Researchers (Kotsovos et al., 1978; Shah et al, 1991; Souma et al., 1994) emphasized this problem in numerically simulating the concrete fracture phenomena. Based on the extensive literature reviewed, it appears that no technique exists today that could predict all the above features for concrete.

### **2.2.2. Papers on Fracture Mechanics**

From a fracture mechanics point of view, concrete, is known as a brittle heterogeneous material in which fracture is preceded by a large fracture process zone of variable size. The determination of the fracture energy of concrete has been difficult. Numerous papers address these problems (Bazant et al., 1983-1991; Chen et al., 1986,

1989; Cook, 1989; Giaccio, et al., 1993; Hillerborg, 1985; Landis et al., 1990; RILEM, 1985; Taylor et al., 1986). Some researchers have observed crack growth and damage and have built analytical models based on the principles of linear elastic fracture mechanics to model cracking (Taylor et al., 1986). It was suggested that a micromechanics based approach, similar to the 'slip theory' in metals, might be studied further (Bazant et al., 1983-85). Using fracture mechanics concepts, a method to calculate crack width for a monotonic loading was presented by Gerstle et al. (1992).

Some researchers have carried out numerical simulations of a center-cracked concrete specimen subjected to a step tensile pulse (Giaccio et al., 1993). Hillerborg, Modeer, and Petersson (1985) introduced a 'fictitious crack model' (FCM) which assumed that the zone at the tip of a crack is long and infinitesimally narrow, and this zone was characterized by a normal stress-versus-crack opening displacement curve, which was considered a material property.

Tension softening behavior in concrete had been predicted by some constitutive models (Bazant et al., 1988-91; Landis et al., 1989). The localization of the damage zone near a crack was also predicted to some degree by their models. This failure localization and size-effect of concrete for small specimens and the formulas to determine their fracture energies were also discussed, and a strain-averaging concept (later called 'nonlocal') was developed (Bazant et al., 1990). However, the other characteristics of concrete, pointed out in the previous section, as well as the effects of load reversals, have yet to be modeled by the fracture mechanics researchers successfully.

### **2.2.3. Papers on Statistical Mechanics**

A number of papers in the general area of Statistical Mechanics are relevant to this study in that many researchers have tried to quantify the various heterogeneous characteristics of concrete material by using Statistical Mechanics. Some have used statistical theories to develop constitutive modeling as an extension of their earlier work on

plasticity applied to metals (Bazant, 1991a; Chen 1986,1989; Chen, 1982,1988). These papers basically involve 'an estimate' of the failure probability of concrete and assume failure to be a sudden random event. The results from these approaches do not correlate well with experimental data, except for simple cases like uniaxial tension and compression, and hence these approaches are unsuitable for our purposes.

#### **2.2.4. Papers on Plasticity and Continuum Mechanics**

Engineers working in the area of Plasticity and Continuum Mechanics have also studied the response of concrete and predicted its cumulative damage due to fatigue loading. They have discussed the consequences of using different postulates (such as, Drucker's and Il'yushin's) from the theories of plasticity (Mizuno et al., 1992; Chen, 1986; Chen et al., 1990; Dragon et al., 1979; Drucker, 1950; Drescher et al., 1993; Il'yushin, 1961; Kupfer et al., 1969). Researchers (Dafalias, 1986; Ortiz, 1984; Stevens et al., 1992) employed plastic failure and damage theories from metals (Nadai, 1950) and applied them for concrete. Although these constitutive models required a modest number of constants (10), in general, they do not perform well at strain-softening and beyond.

#### **2.2.5. Papers on New Finite Element Formulation**

The majority of the current papers surveyed in this category had one broad objective: to develop a new type of an element to model a single crack (Brebbia, 1985; Cofer, 1992; Hibbit, 1993-94; Oliver, 1989; Schreyer, 1990; Taylor et al., 1986; Zienkiewicz, 1977, 1992). Krawczuk (1994) simulated crack propagation for point loads, and the algorithm used was based on Zienkiewicz's method (1992) for thin, non-cracked shell elements. Roelfstra et al. (1985) introduced fracture analyses based on discretization of the material into three component structures: aggregate, matrix, and aggregate-matrix interface. He termed these three structures combined as a 'mesoscale structure'. Nirmalendran et al. (1992) adapted this technique to model the energy distribution at the

forming microcrack. The above research was continued by Bolander et al. (1994) who employed an artificial neural network (Kosko, 1992; Masters, 1993) to track interfacial strength among grain boundaries of the concrete particles which were modeled by a lattice finite element structure. His research assumed all other properties and responses to be constant over the range of specimens examined and is only applicable for modeling a three-dimensional response under monotonic loading. Kawai et al. (1978) introduced the concept of rigid particles interconnected by flexible interfaces to model concrete response. Ghosh et al. (1996) extended this concept and used Voronoi polygons to model the geometry of each concrete particle. Each polygon formed a rigid finite element which gave satisfactory results only for two dimensional problems and under monotonic loading. Toi et al. (1993, 1995) extended Kawai's approach to model cracking. However, none of the noted papers have addressed techniques to initiate a crack gradually from an undamaged material. Additionally, element response to load cycling or strain rate effects is not addressed.

#### **2.2.6. Damage Assessment and Experimentation**

Researchers have tried to assess damage through experimental techniques for materials that are brittle and prone to cracking (Marshek et al., 1989; Mitchell et al., 1991; Matthews et al., 1993; SHRP Report, 1993). Notable among those techniques is Acoustic Emission (Matthews et al., 1993). Some researchers used improved laboratory procedures to measure characteristic properties of asphalt and concrete experimentally. These procedures have been discussed in detail with a lot of experimental data (Drescher et al., 1993; Landis et al., 1989; Matthews et al., 1993; Roque et al., 1992-94; Uzan et al., 1994; Van Dijk, 1975,1977; van Mier, 1984). Of particular interest, one investigation has studied the effect of truck tire inflation pressure and axle load on flexible and rigid pavement performance (Marshek, 1985a,1985b,1989). In general, these papers are test-oriented and do not analytically approach material modeling. However, they are good sources for

various material constants (e.g., elastic modulus, Poisson's ratio, density, etc.) as well as providing a means for verifying the analytical results in this dissertation.

### **2.2.7. Papers on Micromechanics**

Papers on Micromechanics (Bazant, 1985a and 1985b, 1988, 1990-1996) are the ones most relevant to constitutive modeling of concrete. The theories based on micromechanics take into account the granular heterogeneous nature of concrete and are based on the response at any point in concrete along all possible planes passing through that point. The Microplane Theory, as proposed by Bazant (1988), forms the basis for the micromechanics examination of concrete in this study. This theory has opened new frontiers in analytically formulating the brittle behavior of geomaterials (concrete, rock and ceramic).

The Microplane Theory calculates an actual response of concrete at a point strained along arbitrary orientations called Microplanes. This formulation is also versatile enough to capture discontinuities and heterogeneities associated with a composite material such as a multilayered reinforced pavement. Figures 2.1 and 2.2 show the typical features represented in the microplane formulation. Figure 2.1 shows the response to a cyclic loading. Figure 2.2 shows the nonlocal strain with mesh size effects.

It must be noted that a simulation of cyclic response is essential for damage prediction in concrete pavements. A well-defined cyclic loading scheme should have the rules defined for loading and unloading. It should also be able to capture progressive damage, strain softening and plasticity. Bazant's research has demonstrated all of those features. However, Bazant has not implemented his theory in a three dimensional finite element code or in any highway environment.

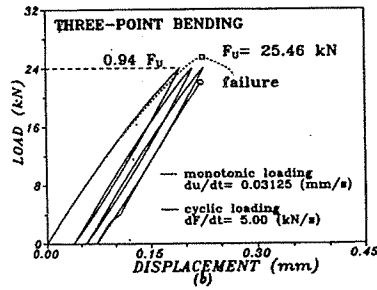


Figure 2.1 : Load-Displacement Curve before peak load (Bazant, 1992).

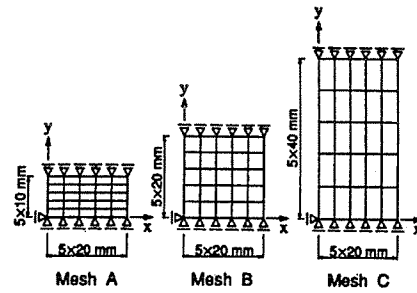


FIG. 2. Finite-Element Meshes for van Mier's (1974) Specimens

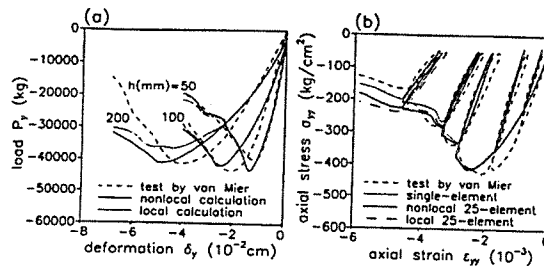


FIG. 9. (a) Comparison with van Mier's (1984) Tests on Effect of Height-to-Width Ratio; (b) Comparison with Cyclic Uniiaxial Compressive Test by van Mier (1984) (Nonlocal 25-Element Calculation, Local 25-Element Calculation and Single Element Calculation)

Figure 2.2 : Finite Element Meshes used (top) and van Mier's tests (van Mier, 1984) compared with analytical results from Bazant (1993b).

### 2.2.8. Papers on Vehicle Modeling

Papers on vehicle modeling are very important for understanding the dynamic interaction between a vehicle (truck) and the pavement. Work done by researchers at the University of Michigan Transportation Research Institute (UMTRI) is particularly

noteworthy (Cebon, 1993-96; Gillespie, 1992-93a; Goktan et al., 1995). The papers in this category have considered various issues including:

- The static load carried by each tire (Cebon, 1993).
- The dynamic variation of load at each tire (Gillespie, 1993a and 1993b) and spatial repeatability of the wheel load histories (Collop et al., 1996; Jacob, 1995).
- The nature of the pressure distribution (normal stress) arising from the total load (static and dynamic) which is applied to the surface under the tire (Cebon, 1993).
- In-plane forces which are applied to the surface in the form of shear stresses (Gillespie, 1992).
- Design of truck suspension components for stiffness and damping, and the speed dependencies on pavement response (O'Connor et al., 1996; Streit et al., 1995; Gillespie, 1992-93; Mitchell, 1991).
- Effect on the pavement due to the tire forces and reduction of stiffness for flexible pavements (Cebon, 1994,1996; Chatti et al., 1995; Papagiannakis, 1996).
- Damage potential of the multi-axle vehicles (Gillespie, 1993; Goktan, 1995).

Gillespie (1992-1993) used a rigid body planar model (Figure 2.3) with lumped masses connected by compliant linkages to represent the suspension. The results (Figures 2.4 and 2.5) reproduced from this work compare the differences between the measured and simulated values of axle force plotted against frequency values.

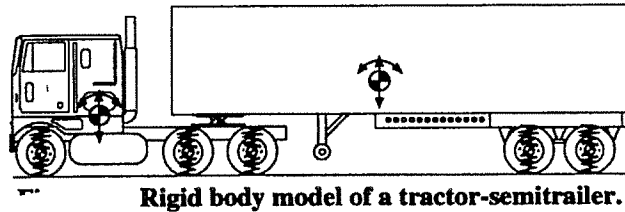
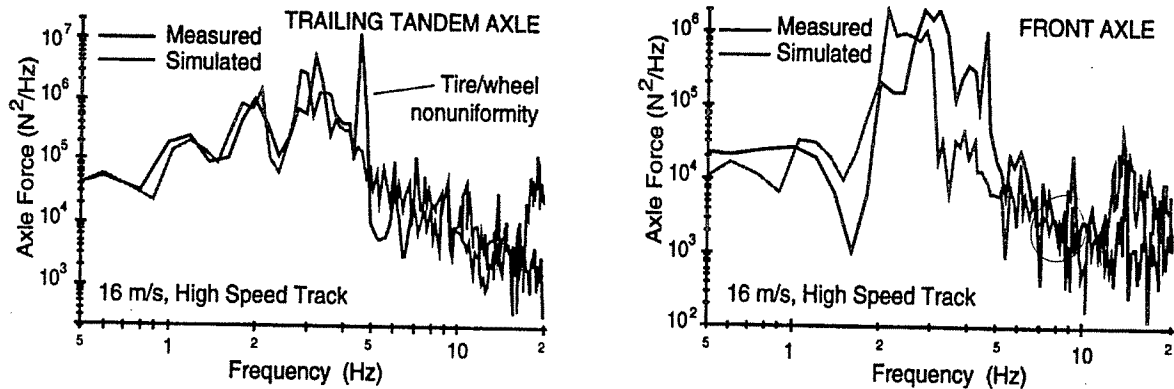


Figure 2.3: Truck Model (Gillespie, 1993).



Figures 2.4 & 2.5: Simulated Results (Gillespie, 1993).

The results from these papers are indicative of the successful simulation of the pitch plane model up to a range of axle-hop resonance. Some differences were due to the tire deformations, others were due to the pavement being treated as linear elastic and used mostly as a 'blackbox' (Goktan et al., 1995; Padovan, 1986a,b and c).

- Some researchers have also noted the damage susceptibility of the road materials to vehicle speed and to the frequency content of the applied loads (AASHO, 1962; Alpan, 1977; Battiato, 1977; Bhatti et al., 1994; Christison, 1978; Cryer et al., 1976; Eisenmann, 1975; Ferne, 1972; Hallquist et al., 1989,1995; Hardy et al., 1988,1993; Nazarian, 1989; Peattie, 1978; Sebaaly et al., 1988).

- Vehicle researchers have also discussed the variations in pavement layer thickness and material properties. An example of this variation in the properties from a special purpose test track: layer thicknesses-typically  $\pm 20\%$ , moduli-typically  $\pm 30\%$  and deflection under a standard load-typically  $\pm 25\%$ . They also discussed the nonlinear nature of pavement response (Gillespie, 1992; Jain, 1979; Lai, 1994; OECD, 1985).
- Two other approaches to estimate road damage due to dynamic tire forces are a) 'Road Stress Factor' (Eisenmann, 1975) and b) 'Whole Life Models' (Papagiannakis et al., 1996). 'Road Stress Factor' uses the assumption that road damage depends on the fourth power of the instantaneous wheel force. 'Whole Life Models' uses an empirical relationship between the wheel force and the change of road surface profile.

In summary, three remarks may be made about this category of papers. First, the researchers working in this area looked into pavement response from a vehicle point of view. Second, none of the above researchers could provide any technique for the development of a predictive tool to simulate dynamic pavement response and damage. Last, they however provided extensive test data on areas like prediction of influence function, and measurement of vehicle parameters (e.g., truck weight, size, suspension and other component characteristics, etc.) which could be used to develop analytical models.

### **2.2.9. Papers on Tire Modeling**

Notable work on viscoelastic tire modeling has been done by Padovan (1986a,b, c). The trend in the pavement community (Huang, 1993) has been to use circular or elliptical patches to represent the area of a moving vehicle-tire in contact with the pavement. Padovan's three part series of papers published in 1987 dealt with a more realistic approach to analytical tire modeling in which he developed a generalized finite element scheme to handle the steady and transient response of moving/rolling nonlinear tire. The solution strategy involved very complex mathematical functions with a series of operations at each

step. He modeled the tire with 20,000 elements and his extensive mathematical schemes, which involved numerous computations, had to be exercised on a supercomputer. His formulations involved parameters that needed extensive testing and bench marking for an environment similar to the highway's. Padovan's technique would thus be impractical for our specific use.

## **2.3. Status of Other Analytical Methods**

As the literature search has revealed, the status of technology in the area of concrete pavement modeling is still in its incipient stages. While there has been a wealth of work, the complex nature of its properties has precluded the development of a model to predict cyclic response and damage in pavement analytically. To follow, the available tools to perform such a study are summarized.

### **2.3.1. Commercial Arena**

The commercial codes available as analytical tools to model concrete as a structural material cover a broad range. Most of them are Finite Element Method based software (e.g., ANSYS, ABAQUS, NIKE3D, NISA, IDEAS, NASTRAN, DYNA3D, PROBE, SAP, COSMOS, ADINA etc.) that could provide commands or user interfaces to help an user build a structural model. However, even the most advanced and widely used large codes (e.g., ABAQUS, ANSYS and DYAN3D) have yet to provide a model of concrete or asphalt in its material library that could capture a realistic constitutive response of a pavement under dynamic loading, varying strain rates, or cyclic loading. Table 2.3 lists the relevant Finite Element Method based software that have been surveyed for this thesis.

| Codes     | Static | Transient | Harmonic | Buckling<br>Post and Pre |   | Fracture | Heat<br>Transf. | Notes       |
|-----------|--------|-----------|----------|--------------------------|---|----------|-----------------|-------------|
| Abaqus    | *      | *         | *        | *                        | * | *        | *               | Nonlinear   |
| Adina     | *      | *         | *        | *                        | * | *        | *               |             |
| Ansys     | *      | *         | *        | *                        | * | *        | *               | Diverse     |
| A-Sap     | *      | *         | *        |                          |   |          | *               | Soil        |
| Asas      | *      | *         | *        |                          |   | *        | *               | Fluid       |
| Aska      | *      | *         | *        | *                        |   | *        | *               |             |
| Beasy     | *      |           |          |                          |   |          | *               |             |
| Bersafe   | *      | *         | *        |                          |   | *        | *               |             |
| Castem    | *      | *         |          | *                        | * | *        | *               | Fluid       |
| Castor    | *      | *         | *        | *                        |   | *        | *               |             |
| Chalm     | *      | *         | *        | *                        |   | *        | *               | Transient   |
| Comet     | *      |           |          |                          |   | *        | *               |             |
| Cosmos    | *      | *         | *        | *                        | * | *        | *               |             |
| Dart      | *      |           | *        |                          |   |          | *               |             |
| Dial      | *      | *         | *        |                          |   |          | *               |             |
| Diana     | *      | *         | *        | *                        | * |          |                 | Cracking    |
| Dream     | *      |           |          | *                        | * |          |                 |             |
| Fasor     | *      |           | *        | *                        | * |          |                 |             |
| Felco     | *      | *         |          | *                        |   |          | *               |             |
| Fenris    | *      | *         | *        | *                        | * |          |                 |             |
| Fidap     | *      | *         |          |                          |   |          | *               | Buoyancy    |
| Flash2    | *      |           |          |                          | * |          |                 |             |
| Fluent    | *      |           |          |                          |   |          | *               | Fluid       |
| Lawpile   | *      |           |          | *                        |   |          |                 |             |
| Lisa      | *      | *         | *        | *                        | * |          |                 |             |
| Lusas     | *      | *         |          | *                        | * | *        | *               |             |
| Marc      | *      | *         | *        | *                        |   | *        | *               |             |
| Micas     | *      |           |          |                          |   | *        | *               | Nonlinear   |
| Mix       | *      |           |          | *                        | * |          |                 |             |
| Model     | *      |           |          |                          |   | *        | *               |             |
| Modulef   | *      | *         | *        |                          |   |          | *               | Hybrid      |
| Nastran   | *      | *         | *        | *                        | * |          | *               | Static etc. |
| Pafec     | *      | *         | *        | *                        |   | *        | *               | Seismic     |
| Patran    | *      | *         |          |                          |   |          |                 |             |
| Pecet     | *      |           |          |                          |   |          |                 |             |
| Prefem    | *      |           |          |                          |   |          |                 |             |
| Raft      | *      |           |          |                          |   |          | *               |             |
| Scia      | *      | *         | *        |                          |   |          | *               |             |
| Sesam     | *      | *         | *        |                          | * | *        | *               |             |
| Set, Star | *      | *         | *        |                          |   |          |                 | Concrete    |
| Statik    | *      |           |          | *                        |   |          |                 |             |
| Stdynl    | *      | *         | *        | *                        | * |          |                 |             |
| Strudl    | *      | *         | *        |                          |   |          |                 |             |
| Thafem    | *      |           |          |                          |   |          | *               | Phase Ch.   |
| Titus     | *      | *         | *        | *                        | * | *        | *               | Earthquake  |

Table 2.3: Survey of FEA based softwares in the commercial arena

PC based software is plentiful, but none predict fatigue or cracking accurately, as most assume a linear or nonlinear elastic behavior while using empirical or semi-empirical constitutive relationships. Some of the plasticity based codes (like ANACAP 95) use smear-cracking and a stiffness degradation approach. Such approaches have convergence problems especially in the post-peak softening range, as well as for cyclic loading. It must be again noted that strain softening, microcracking, rate, temperature, creep and size effects (Bazant et al., 1984) are some of the features that must be captured in modeling concrete response. The commercial programs, even though user-friendly, are not capable of modeling the initiation of cracking and accumulation of damage due to a time varying load. It is this cracking and damage prediction that is especially relevant to this thesis.

The methods of flexible highway pavement design can be classified into five categories: empirical methods with or without a soil strength test, limiting shear failure method, limiting deflection method, regression method based on road test and mechanistic-empirical method. Each of these approaches has their shortcomings as follows. The empirical methods (Porter, 1950) can only be applied to a given set of environmental, material, and loading conditions. The limiting shear method (Yoder and Witczak, 1975) is based on barely preventing shear failures. The limiting deflection method (Kansas State Highway Commission, 1947) does not work properly for cases where pavement failures are caused by excessive stresses and strains instead of deflections. The regression method (Hall et al., 1989) has design equations that can be applied only to the conditions at the road test site. The mechanistic-empirical methods (Huang, 1993) are still at a research stage.

There are a whole variety of small scale pavement computer programs prevalent in the highway community (e.g., KENSLAB, KENLAYER, VESYS, ILLI-SLAB, ILLI-PAVE, MICH-PAVE, SAP etc.). In general, the underlying methods use empirical relationships which operate in an elastic range. While any of these programs are valuable as a preliminary design tool, they have not succeeded in capturing the fatigue response

accurately. These computer programs thus fail to deal with phenomena like damage due to stress reversal, strain localization, size effects, etc. Moreover, they use Miner's rule (1945) based on a one-pass linear response under static monotonic loading to predict concrete damage, and hence they do not perform well.

### **2.3.2. Academic Arena**

The literature survey had also shown that among all the constitutive models used to represent concrete type heterogeneous material behavior, Bazant's Microplane Theory is the best among those that captures the essential characteristics like tri-axial response, cracking, strain softening, damage (mechanical and thermal), etc. for concrete and other geomaterials. However, this theory has yet to be applied to pavement modeling in any highway environment.

## **2.4. Justification for this Research**

Pavement is a multilayered, non-homogeneous anisotropic structure and understanding its response to vehicle loading behavior essentially involves understanding its structural characteristics. One of the most important structural materials used in the pavement today is concrete (PCC) and its response to vehicle loading, as seen from current research, is highly nonlinear (Gillespie, 1992; Goktan et al., 1995; Huang, 1993). This nonlinearity arises out from the inherent heterogeneity of the concrete material itself. Engineers have used pavement models to predict its behavior, but as our survey has shown, no good correlation exists today that has reproduced three-dimensional concrete response to a cyclic loading up to the peak-stress value or even a two-dimensional response beyond the post-peak strain-softening range.

The behavior of concrete could be different for different loading rates and also for different types of loading. In particular, the pavement is extremely damage prone to cyclic

loading, which accelerates fatigue and damage. If temperature gradients are considered, the strain sensitivity of concrete to cracking can worsen. The problem is further complicated when cracking is to be simulated in a three-dimensional stress state due to a dynamic traffic loading. To add to this problem, we recall that a highway pavement could actually be a multilayered material of varying thickness having joints (Jointed Plain) and reinforcements (Jointed Reinforced). Prediction of the damage response of concrete involves understanding the constitutive characteristics of the virgin concrete material itself. However, as mentioned earlier, experimentally measuring a pavement response is expensive, disruptive and not practicable, so analytical modeling is essential. This work employs a novel analytical approach based on Microplane Theory to capture the essential characteristics of concrete.

Simulation of a traffic loading, being inherently transient and nonlinear, is difficult. This loading on the highway is through the vehicle tires which deform when the tires load the pavement. However, good literature sources are available that have estimated the vehicle loading on the pavement (see Section 2.2.8). Thus, by combining the vehicle loading history from these sources with a (Microplane Theory based) pavement model, the response can be more efficiently predicted through analytical means.

Through analytical modeling, it is relatively simple to simulate jointed pavement. Thus the joint design can be guided with the above tool to determine the best joint parameters in a highway environment.

## **2.5. Summary**

In this chapter two objectives are fulfilled. First, a detailed literature search identified the need for a predictive tool in the area of pavement response modeling. The literature search was divided into nine different categories relevant to the modeling of the vehicle pavement interaction and the resultant damage. Second, the search identified the

Microplane Theory as the one best capable of capturing the material response of concrete. This theory has never been implemented in a 3-D finite element code or in any highway environment.

## Chapter 3. Microplane Theory

### 3.1. Introduction

The literature search in the last chapter identified Bazant's Microplane Theory to be the one best capable of capturing the concrete properties most important for modeling damage in highway pavement. Accordingly, in this research the Microplane Theory is employed to model concrete pavement response. This chapter presents the important features of this theory. The theory will be implemented for the study of pavement in later chapters.

### 3.2. Bazant's Microplane Theory

Bazant's Microplane Theory is based on representing the material's constitutive laws by a relation between the stress and strain components on planes of various orientations. These planes may be imagined to represent the damage planes or weak planes in the microstructure, such as contact layers between aggregate pieces in concrete. The history of the general approach underlying the Microplane Theory had been developed initially for plastic polycrystalline metals (Taylor, 1938). Bazant pursued the approach to develop his own formulation and coined the term 'Microplane Theory' in 1983 in application to geomaterials. His research has continued since then and here, his revised work published in the 1992-96 time frame is to be applied. The theoretical framework of the work is based on the three hypotheses given below.

*Hypothesis I*: The normal and shear (tangential) strains  $\epsilon_n$  and  $\epsilon_t$  on a microplane of unit normal are the resolved components of the macroscopic strain tensor  $\epsilon_{ij}$  in that direction, which implies that

$$\varepsilon_n = \varepsilon_{ij}n_i n_j \quad \text{and} \quad (3.2.1)$$

$$\varepsilon_{t_i} = \varepsilon_{ij}n_j - \varepsilon_n n_i. \quad (3.2.2)$$

Additionally, the normal strain is split into two parts, the (mean) volumetric part and the deviatoric part, which are expressed as

$$\varepsilon_v = \varepsilon_{kk} / 3 \quad \text{and} \quad (3.2.3)$$

$$\varepsilon_d = \varepsilon_n - \varepsilon_v. \quad (3.2.4)$$

*Hypothesis II:* Associated with the three strains  $\varepsilon_v$ ,  $\varepsilon_d$ ,  $\varepsilon_t$ , three corresponding stresses  $\sigma_v$ ,  $\sigma_d$ ,  $\sigma_t$  exist so that their respective products give directly the work done on a microplane. The stress-strain laws at this level are a set of relationships, defining the evolution of each of those three stresses as a function of the three microplane strains (and possibly their histories). The stress-strain laws can be written as

$$\sigma_v = F_v(\varepsilon_v), \quad (3.2.5a)$$

$$\sigma_d = F_d(\varepsilon_d), \quad \text{and} \quad (3.2.5b)$$

$$\sigma_t = F_t(\varepsilon_t) \quad (3.2.5c)$$

where F represents the functional relationship between stress and strain discussed in Appendix F and the subscript (*v, d or t*) represents the microplane component (volumetric, deviatoric or tangential).

*Hypothesis III:* The relationship between the microplane stresses  $\sigma_v, \sigma_d, \sigma_t$  and the microscopic stress tensor  $\sigma_{ij}$  is obtained by applying the principle of virtual work. The expression for the incremental macroscopic stress is then expressed as

$$d\sigma_{ij} = d\sigma_v \delta_{ij} + \frac{3}{2\pi} \int_{\Omega} d\sigma_d n_i n_j d\Omega + \frac{3}{2\pi} \int_{\Omega} \frac{d\sigma_{t_r}}{2} (n_i \delta_{rj} + n_j \delta_{ri} - 2n_i n_j n_r) d\Omega. \quad (3.2.6)$$

A salient feature of this model is that the computation of the stress corresponding to a prescribed strain increment of finite size is fully explicit.

The Microplane Theory uses a kinematic constraint which means that the microplane strains are equal to the resolved component of the strain tensor on the plane. This is opposed to a static constraint which means that the microplane stresses are equal to the resolved component of the stress tensor on that plane. The idea of static constraint was used in metals (Batdorf et al., 1949) and geomaterials (Pande et al., 1983). Bazant (1983) found that to represent the behavior of quasi-brittle materials such as concrete or rock, showing strain softening, a kinematic constraint was necessary.

The basic scheme for the computation of macroscopic stresses from the macroscopic strain is shown in the Table 3.2. As shown there, using the kinematic constraint, the given strain input is resolved into 3 types of component strains (volumetric, deviatoric and in-plane components). Microplane laws relate each component strain with a corresponding component stress. The principle of virtual work is then applied to combine the component stresses to generate a stress tensor.

|        | Macroscopic Level       |                                                  | Microplane Level                                                                            |
|--------|-------------------------|--------------------------------------------------|---------------------------------------------------------------------------------------------|
| STRAIN | $\epsilon_{ij}$ (input) | $\xrightarrow{\text{Kinematic Constraint}}$      | $\epsilon_v, \epsilon_d, \epsilon_{t_i}$<br>$\downarrow$<br>Microplane Laws<br>$\downarrow$ |
| STRESS | $\sigma_{ij}$ (output)  | $\xleftarrow{\text{Principle of Virtual Work.}}$ | $\sigma_v, \sigma_d, \sigma_{t_r}$                                                          |

Table 3.2: Macroscopic stresses from macroscopic strain

The relationship between the microplane stresses and strains are expressed as

$$\sigma_v = c_v \varepsilon_v, \quad (3.2.7)$$

$$\sigma_d = c_d \varepsilon_d, \text{ and} \quad (3.2.8)$$

$$\sigma_t = c_t \varepsilon_t \quad (3.2.9)$$

where  $C_v, C_d, C_t$  represent the volumetric, deviatoric and shear secant moduli, given by

$$C_v = C_v^o (1 - w_v), \quad (3.2.10)$$

$$C_d = C_d^o (1 - w_d), \text{ and} \quad (3.2.11)$$

$$C_t = C_t^o (1 - w_t). \quad (3.2.12)$$

In equations 3.2.10-3.2.12,  $w_v, w_d, w_t$  represent the volumetric, deviatoric and shear damage.

### 3.3. Damage Rule

Damage as expressed in the Microplane Theory, is inherent to the microplane constitutive laws. The degradation in the volumetric, deviatoric and secant moduli is expressed in terms of the damage variables as follows

$$\text{for } \varepsilon_v \geq 0; \quad w_v = 1 - \left( \exp - \left| \frac{\varepsilon_v}{a1} \right|^{p1} \right) \quad (3.2.13)$$

$$\text{for } \varepsilon_d \geq 0; \quad w_d = 1 - \left( \exp - \left| \frac{\varepsilon_d}{a1} \right|^{p1} \right) \quad (3.2.14)$$

$$\text{for } \varepsilon_d < 0; \quad w_d = 1 - \left( \exp - \left| \frac{\varepsilon_d}{a2} \right|^{p2} \right) \quad (3.2.15)$$

$$\text{for } \varepsilon_t \geq 0; \quad w_t = 1 - \left( \exp - \left| \frac{\varepsilon_t}{a3} \right|^k \right) \quad (3.2.16)$$

In equations, 3.2.13 to 3.2.16, the parameters  $p_1$ ,  $p_2$ ,  $a_1$ ,  $a_2$ ,  $a_3$ ,  $a_3^0$  and  $K_a$  are material constants, and  $a_3$  is expressed as

$$a_3 = a_3^0 + K_a \varepsilon_v. \quad (3.2.17)$$

The stress-strain curves for each microplane are path-independent as long as there is no unloading on the microplane. During each unloading and reloading, each microplane response is defined individually and these responses are path dependent. For further details on the material constants and their relevance to Microplane Theory, the interested reader is referred to Appendix F as well as the reference (Bazant, 1988-96).

### 3.4. Summary

In this chapter, the various features of Bazant's Microplane Theory are briefly explained. The constitutive laws for volumetric, deviatoric and in-plane components were discussed, and the damage rule defining the degradation of different component moduli in any microplane was stated as well. This chapter has been purposely concise, and the interested reader is referred to the numerous papers of Bazant for any additional information.

# **Chapter 4. Implementation of the Microplane Theory**

## **4.1. Introduction**

The focus of this research is simulating concrete pavement response to traffic loading. With that objective, the Microplane Theory, as described in the previous chapter, best describes the concrete material behavior under cyclic loading and in particular, can be applied to Portland Cement Concrete in the highways. However, this theory has neither been implemented in a 3-D finite element code nor has it been applied to modeling the highway. Accordingly, the first phase of the research revolves around the numerical implementation of the Microplane Theory in a finite element code. A computer program applying the Microplane Theory for this implementation in Fortran 77 is developed. This program is included in Appendix E. This chapter describes the various aspects of this numerical implementation. The next chapter will discuss the validation of the developed program with known test results.

## **4.2. Constitutive Implementation**

The constitutive implementation is carried out with the help of an user interface module which linked the Fortran subroutines written for this purpose, to the large scale finite element solver Abaqus (Hibbitt, 1994). The user interface module (called VUMAT) was programmed so that the constitutive calculations are performed following the developed numerical integration scheme at each element integration point, for each increment, and during each load step. Large scale nonlinear finite element codes like Abaqus have capabilities to interpret these interface modules so that users may introduce

their own constitutive model via Fortran 77 subroutines. It was necessary to numerically code the subroutine so that it would integrate the solution dependent state variables, stresses, energy measures, etc., to the end of the increment, and provide the Jacobian matrix  $\frac{\partial \Delta \sigma_i}{\partial \Delta \varepsilon_j}$  for use in the overall Newton scheme. The required number of material constants, as formulated in the Microplane Theory are introduced through this input module for use in the developed explicit program. Provisions for storage have been incorporated at each material calculation point for any number of solution dependent state variables. The interface of the developed program provided the state at the beginning of each increment and the kinematic solution at the end of the increment. The user module is then linked with the Abaqus Finite Element Solver to solve the equation in accordance with the developed numerical routine and to graphically represent the results (post-process). The steps involved in the implementation of the Microplane Theory are summarized below.

- The constitutive equation (3.2.6) below is rewritten, and expanded for different values of  $i$ , and  $j$  and the volumetric, deviatoric and in-plane contributions are separately incorporated into the developed algorithm. This is done at each integration point, depending on the type of 3-D finite element chosen. For example, for  $i = j$ , the contribution to the macroscopic stress tensor is only volumetric and deviatoric as the tangential contribution becomes zero.

$$d\sigma_{ij} = d\sigma_v \delta_{ij} + \frac{3}{2\pi} \int_{\Omega} d\sigma_d n_i n_j d\Omega + \frac{3}{2\pi} \int_{\Omega} \frac{d\sigma_r}{2} (n_i \delta_{rj} + n_j \delta_{ri} - 2n_i n_j n_r) d\Omega \quad (3.2.6)$$

- The strain tensor is to be computed from the Deformation Gradient. The Abaqus user module provides the deformation gradient at the start of each increment. So at each integration point of an element, the deformation gradient tensor (denoted by  $\underline{F}$ ) at the start of each increment is called by the developed numerical program.

The deformation gradient is then used to compute the strain increment  $\Delta \underline{E}$ , as described next. First, it is noted that the subscripts 'new' denotes the state at the end of an

increment and 'old' denotes the state at the beginning of that increment, so that we can express  $\Delta \underline{E}$  as

$$\Delta \underline{E} = \underline{E}_{\sim new} - \underline{E}_{\sim old} \quad (4.2.1)$$

First, the developed Fortran program calculates the Green deformation tensor given by:

$$\underline{C}_{\sim old} = \underline{F}_{\sim old}^T \quad (4.2.2)$$

where  $\underline{C}_{\sim old}$  is the Green Deformation Tensor at the beginning of any increment.

Then the Lagrange Strain Tensor at the beginning of any increment, is calculated as

$$\underline{E}_{\sim old} = \frac{1}{2}(\underline{C}_{\sim old} - \underline{I}) \quad (4.2.3)$$

Dropping the subscript 'old' we have from 4.2.3 and 4.2.2 :

$$\underline{E} = \frac{1}{2} \begin{bmatrix} F^2_{11} + F^2_{12} + F^2_{13} - 1 & F_{11}F_{12} + F_{12}F_{22} + F_{13}F_{23} & F_{11}F_{13} + F_{12}F_{23} + F_{13}F_{33} \\ & F^2_{12} + F^2_{22} + F^2_{23} - 1 & F_{12}F_{13} + F_{22}F_{23} + F_{23}F_{33} \\ & & F^2_{13} + F^2_{23} + F^2_{11} - 1 \end{bmatrix} \quad (4.2.4)$$

*SYMMETRY*

Similarly,  $\underline{E}_{\sim new}$ , the strain tensor at the end of the increment, is calculated as above from  $\underline{F}_{\sim new}$  at the end of same increment.

After the developed program has calculated the incremental strain tensor  $\Delta \underline{E}$  from equation 4.2.1, it resolves  $\Delta \underline{E}$  into  $\Delta \varepsilon_v$ ,  $\Delta \varepsilon_d$  and  $\Delta \varepsilon_t$  using the kinematic constraints (equations 3.2.1 - 3.2.4). The program employs the microplane constitutive laws (eqns. 3.2.7, 3.2.8, and 3.2.9) to calculate the corresponding volumetric, deviatoric and tangential incremental stress components ( $\Delta \sigma_v$ ,  $\Delta \sigma_d$  and  $\Delta \sigma_t$  respectively) according to the microplane flowchart shown in Figure 4.2. While calculating the various strains and stresses, the program performs various checks to assure the accuracy in the numerical scheme. These checks will be described in section 4.3.

The developed program also integrates equation 3.2.6 in accordance with hypothesis III, to return the incremental stress tensor re-written below from Chapter 3,

$$d\sigma_{ij} = d\sigma_v \delta_{ij} + \frac{3}{2\pi} \int_{\Omega} d\sigma_d n_i n_j d\Omega + \frac{3}{2\pi} \int_{\Omega} \frac{d\sigma_{tr}}{2} (n_i \delta_{ij} + n_j \delta_{ri} - 2n_i n_j n_r) d\Omega \quad (3.2.6)$$

The stress at a given integration point is then calculated by the developed program as:

$$\sigma_{ij_{new}} = d\sigma_{ij} + \sigma_{ij_{old}} \quad (4.2.5)$$

The microplane flow chart of Fig. 4.2 represents the numerical routine describing the Microplane Theory.

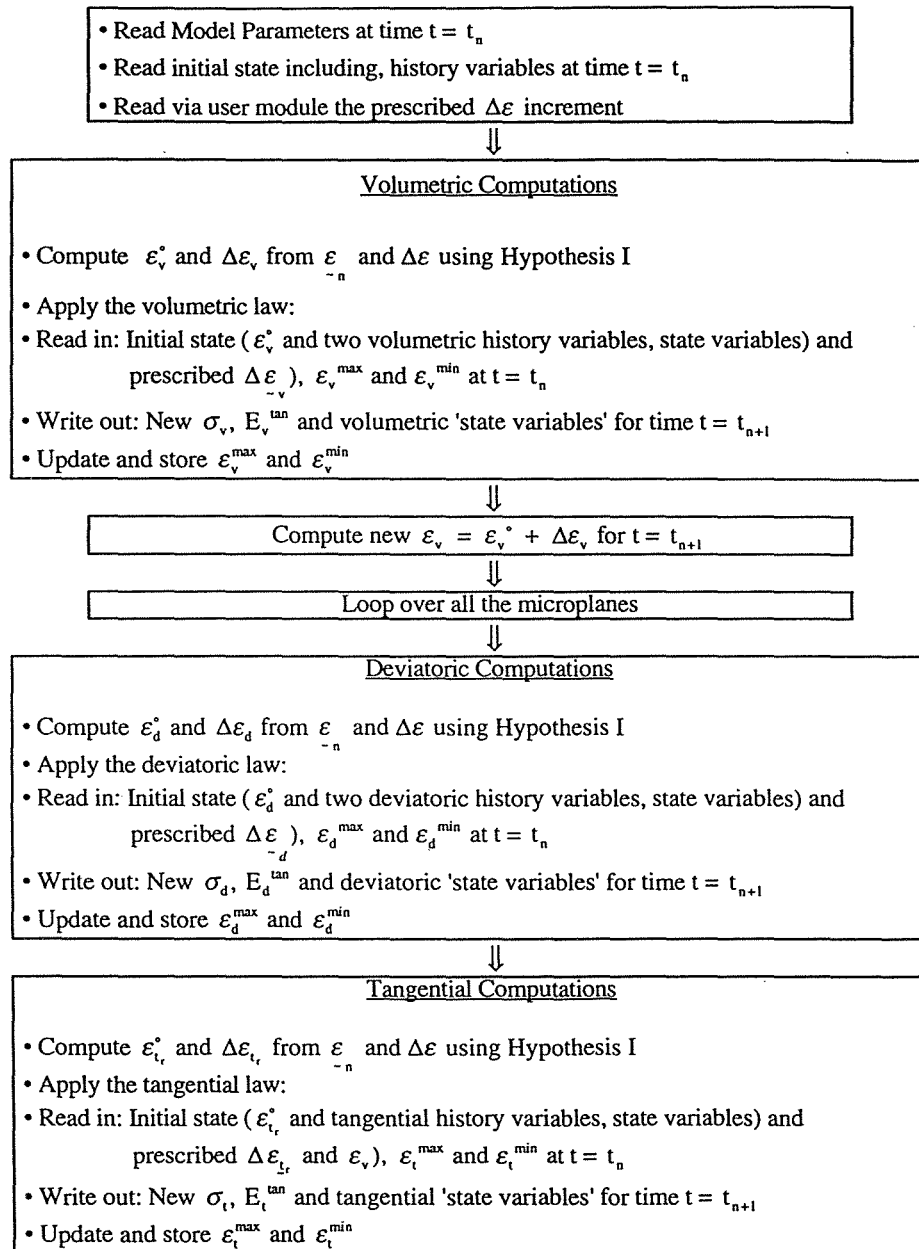


Figure 4.2: Flow Chart of Implemented Microplane Theory

## 4.2.2 Incremental Tangent Stiffness Matrix

Some discrepancies were encountered in the derivation of the incremental tangent stiffness matrix in Bazant's (1992) original paper. Accordingly, a detailed derivation has been performed and this is given in Appendix A. The corrected expression for the incremental tangent stiffness matrix is given as

$$D_{ijkl}^{\tan} = \frac{E^{\tan}}{3} \delta_{ij} \delta_{kl} + \frac{3}{2\pi} \int_{\Omega} E_D^{\tan} n_i n_j (n_k n_l - \delta_{kl} / 3) d\Omega + \frac{3}{2\pi} \int_{\Omega} \frac{H_{rs}^{\tan}}{4} (n_i \delta_{rj} + n_j \delta_{ri} - 2n_i n_j n_r) (n_k \delta_{sl} + n_l \delta_{sk} - 2n_k n_l n_s) d\Omega. \quad (4.2.5)$$

This equation was also used also to double-check the stress calculation as well as to see if at zero strain, the initial elasticity matrix of the material was returned.

## 4.2.3 Numerical Integration

The equations 3.2.6 and 4.2.5 have physical significance. They imply the summation of all the contributions from all microplanes passing through a point (integration point of a finite element) of interest. Thus, summing up all the deviatoric and tangential contributions from all the microplanes and adding them with the volumetric contribution (which is same for all microplanes) produce the stress response (eqn. 3.2.6) or the incremental tangent stiffness (4.2.5). The integrals in these equations refer to spherical integrals and the domain of the integral is the upper hemisphere represented by  $\Omega$ . These equations need to be integrated so that incremental stress tensor and incremental tangent stiffness tensor can be calculated at the end of any given load increment. Moreover, this integration needs to be performed at each element integration point, for every increment and for each load step. Therefore, an efficient integration scheme is necessary for the developed program.

To perform these integrations numerically, an integration scheme along the line of Bazant (1988a) is employed. The numerical integration formula may be written as a summation of the values of the function inside the integrals, evaluated at N integration points, and multiplied by their corresponding weights. The integrand can then be computed as

$$\int_s F(\boldsymbol{\varepsilon}) ds \approx \sum_{\alpha=1}^N \omega_{\alpha} [F(\boldsymbol{\varepsilon})]_{\alpha} \quad (4.2.6)$$

where  $F(\boldsymbol{\varepsilon})$  is the function of strain to be integrated for N integration points (microplanes).

Microplane integration can be carried out by means of a rectangular mesh in a plane, but such an approach is rather inefficient. One reason is that the integration points are wastefully crowded near the pole (Bazant, 1985b). Also, the functions that are smooth on the spherical surface near the pole may be unsmooth in the rectangular plane. Therefore, the appropriate integration formulas should be constructed directly for the surface of the sphere. The greatest efficiency is achieved with an uniform distribution of the integration points over the spherical surface. These distribution of points would result in a polyhedron which can be inscribed in a spherical space passing through the points. Many numerical methods have been established for such integrations and procedures have been written in books that utilize the orthogonal polynomials for this type of a distribution (Stroud, 1971). However, they are inaccurate for the post peak and strain softening region. For this research, a similar technique (Bazant, 1988a) is used.

The technique employed in the developed program uses the Taylor series expansions directly for the function values at the surface of the sphere, and relies on the computer to find the weights and point locations for which the degree of the error is maximized and the coefficient of the truncation term is minimized. In total, 21 points (microplane) are chosen. This choice is based on Bazant (1985b, 1988, 1996b) who has

shown that 21 integration points for a hemisphere are sufficient for such integrations, as increasing the number of integration points has little effect on the results.

Figure 4.1 shows the 42 points (marked by small circles) in a polyhedron, inscribed in an unit sphere and Figure 4.2 shows how those points would be distributed for a quarter of the sphere. The 42 points for the full model may be evident from the quarter model in Figure 4.4, remembering that some points (points along the edges) will be shared as they are common to the boundaries. There are 24 (3 points/quarter X 8 quarters/sphere) central points and 18 points on the boundary when calculated for the entire sphere. The direction cosines for a microplane passing through a point, is given by the unit normal vector connecting the origin to that point. Programming each of these directions in Fortran 77 to check the convergence error (Figure 4.3) is pertinent to the definition of a microplane and numerical implementation. At each integration point of the finite element describing PCC behavior, the response (e.g., stress) was checked for convergence. Additional tests as described below are used to ensure that the integration error is minimized and the response is stable.

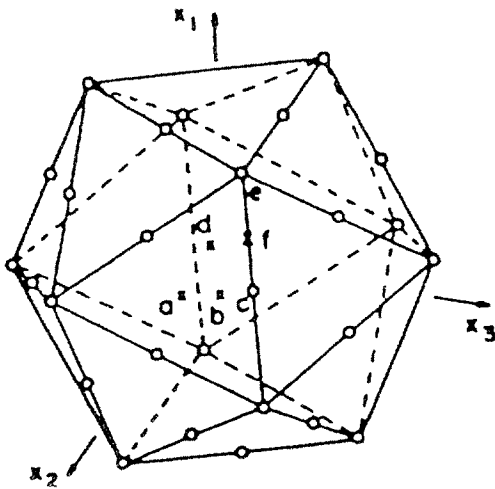


Figure 4.1: Microplane Directions (Full model)

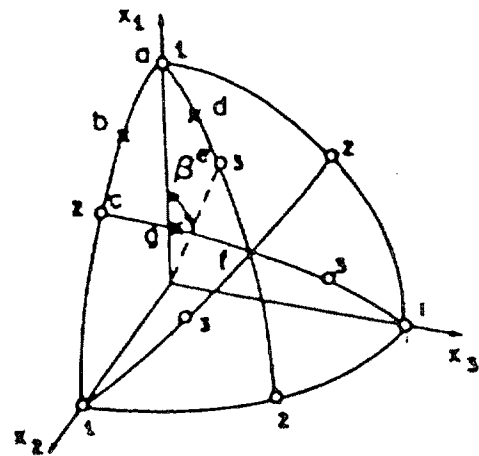


Figure 4.2: Quarter Model

- As the cyclic loading progresses the error between the maximum and minimum values of the stresses for any given value of a post peak strain is minimized for the equal weights chosen in different directions. The weights for those directions are incrementally varied in the computer until the error is steady (converges) and is minimized. Figure 4.5 shows the post-peak bifurcation error (denoted by the dotted lines) which differs from the experiments of Chen (1988) on PCC Concrete. This approach is a combination of the methods of Bazant (1992) and Chen (1988) and is efficiently utilized in our numerical algorithm for the first time in pavement modeling. The benefits of the approach are twofold. First, the convergence is achieved with respect to an actual PCC experimental curve and error minimization is performed through iteration on the weights assigned for each microplane direction. Second, by varying these weights until a converged response is reached, certain microplanes are automatically made weaker or stronger than the other, thus capturing the inherent concrete heterogeneity.

- The stress strain curves calculated through the integration method must remain the same when the set of integration points is arbitrarily rotated as a rigid body with respect to the material, while the applied stress is not rotated. This is obvious as the pavement stress response in reality is independent of the set of integration points chosen and any exception to that may be attributed to numerical error which has to be stabilized.

## Numerical Integration and Post-Peak Convergence Error

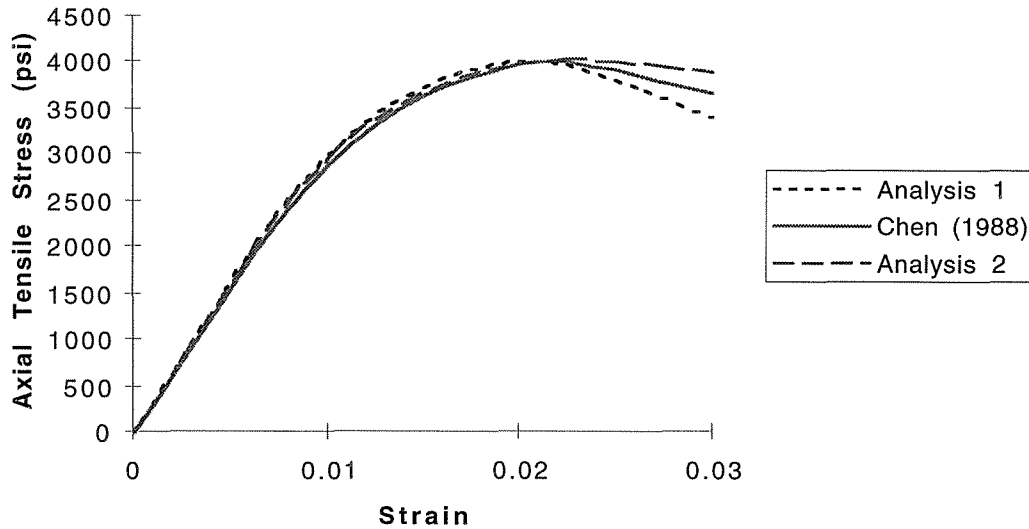


Figure 4.3: Numerical Convergence

- The maximum difference among the stress strain curves (shown by Analysis 1 and Analysis 2) in the post peak range for all such combinations of rotations is the measure of the error as shown by the post-peak bifurcation for PCC concrete in Figure 4.3.
- Convergence occurred when the curves represented by Analysis 1 and Analysis 2 (in Figure 4.3) merged into one curve and maintained a steady error with respect to the experimental result.

### 4.3 Program Checks

The author devised four further program checks to ensure that the response at each increment at each time step is well computed by the developed program as follows

1) The tangential strain is a vector with three components in space, but its direction always lies in the microplane of normal  $n_i$ . So for every microplane, the program checks that

$$\varepsilon_i n_i = 0.0 \quad (4.3.1)$$

is satisfied at every load increment.

2) The volumetric strain when added to the deviatoric strain components should give back the original strain tensor. Thus the deviatoric Strain must satisfy the following

$$(e_{ij}) = \varepsilon_{ij} - \varepsilon_v \delta_{ij}. \quad (4.3.2)$$

3) The volumetric, deviatoric and in-plane stress-strain relationships are plotted to ensure that they follow the constitutive relationship (equation 3.2.6) at the microplane level. This is a qualitative check on the trend of the microplane component response.

4) Checks are made to see if initially, at zero or low strain, the developed program returns the well-known elastic moduli matrix for isotropic elastic materials (Mellor et al, 1973).

That is

$$\begin{Bmatrix} d\sigma_{11} \\ d\sigma_{22} \\ d\sigma_{33} \\ d\sigma_{12} \\ d\sigma_{23} \\ d\sigma_{31} \end{Bmatrix} = \begin{bmatrix} A & B & B & 0 & 0 & 0 \\ B & A & B & 0 & 0 & 0 \\ B & B & A & 0 & 0 & 0 \\ 0 & 0 & 0 & C & 0 & 0 \\ 0 & 0 & 0 & 0 & C & 0 \\ 0 & 0 & 0 & 0 & 0 & C \end{bmatrix} \begin{Bmatrix} d\varepsilon_{11} \\ d\varepsilon_{22} \\ d\varepsilon_{33} \\ d\varepsilon_{12} \\ d\varepsilon_{23} \\ d\varepsilon_{31} \end{Bmatrix} \quad (4.3.3)$$

where,

$$A = \frac{E(1-\nu)}{(1+\nu)(1-2\nu)}, \quad (4.3.4)$$

$$B = \frac{E\nu}{(1+\nu)(1-2\nu)} \quad \text{and} \quad (4.3.5)$$

$$C = \frac{E}{(1 + \nu)} = 2G \quad (4.3.6)$$

must be satisfied at zero strain which occurs either when the virgin loading starts or after loading and unloading the strain is returned to a zero value.

From Bazant's Microplane Theory (Bazant, 1988) we have:

$$A = \frac{1}{15}(5C_v^0 + 4C_d^0 + 6C_t^0) \quad (4.3.7)$$

$$B = \frac{1}{15}(5C_v^0 - 2C_d^0 - 3C_t^0) \quad \text{and} \quad (4.3.8)$$

$$C = \frac{1}{5}(2C_d^0 + 3C_t^0). \quad (4.3.9)$$

Equating A from equations 4.3.4 and 4.3.7 and B from equations 4.3.5 and 4.3.8 and solving for  $\nu$  and E we have

$$\nu = \frac{(5C_v^0 - 2C_d^0 - 3C_t^0)}{(10C_v^0 + 2C_d^0 + 3C_t^0)} \quad \text{and} \quad (4.3.8)$$

$$E = (1 - 2\nu)C_v^0. \quad (4.3.9)$$

These above parameters are also checked by the developed program.

#### 4.4. Unloading and Reloading

It was outlined in the Microplane Theory, that the various microplanes undergo loading and unloading. The rule governing the unloading and reloading from the Microplane Theory (Bazant and Prat, 1988a, 1993) is given as

$$\varepsilon \Delta \varepsilon \geq 0.0 \quad \text{and} \quad (\varepsilon - \varepsilon^{\max}) (\varepsilon - \varepsilon^{\min}) \geq 0.0 \quad (4.4.1)$$

This rule means that if equation (4.4.1) holds true for a given microplane component in any microplane, then virgin loading occurs for that component. Alternatively, if it does not, then unloading and reloading occurs. To keep track of  $\varepsilon^{\max}$  and  $\varepsilon^{\min}$  and their incremental time histories for each component in each microplane, state variables are defined in the developed program. This allows the allocation of space at each material calculation point for solution of the dependent state variables. For 'n' number of microplanes, at least '8+3n' state variables are necessary (6 strain components, 2 components for volumetric stress, 2n components for deviatoric stress, and at least n components for tangential-in plane stress). As Abaqus does not store these history variables, they were programmed into the user subroutine (V)UMAT to interact with the Abaqus finite element code.

#### 4.5. Explicit vs. Implicit Integration Methods

The developed program implements the constitutive equations along with the relevant integration schemes within the finite element solver Abaqus. To obtain dynamic response, Abaqus uses direct integration methods to solve those equations at every increment for each time step, following the directives of the developed program. The direct integration methods could be implicit or explicit. A brief discussion follows to illustrate their differences.

In a finite element code, for every finite element, the work of external forces is equated to the work of internal, inertial, and viscous forces for any small kinematically admissible motion and that results in the following equation (Zienkiewicz, 1992)

$$\begin{aligned}
 & \int_{V_e} \{\delta u\}^T \{F\} dV + \int_{S_e} \{\delta u\}^T \{\Phi\} dS + \sum_{i=1}^n \{\delta u\}_i^T \{P\}_i \\
 & = \int_{V_e} (\{\delta \varepsilon\}^T \{\sigma\} + \{\delta u\}^T \rho \{\ddot{u}\} + \{\delta u\}^T \mathbf{K}_d \{\dot{u}\}) dV
 \end{aligned} \tag{4.5.1}$$

where,  $\{\delta u\}$  and  $\{\delta \epsilon\}$  are small arbitrary displacements and their corresponding strains respectively,  $\{F\}$  are body forces,  $\{\Phi\}$  are prescribed surface tractions (which typically are nonzero over only a portion of surface  $S_e$ ),  $\{P\}_i$  are concentrated loads that act at a total of  $n$  points on the element,  $\{\delta u\}_i^T$  is the displacement of the point at which load  $\{P\}_i$  is applied,  $\rho$  is the mass density of the material,  $K_d$  is a material-damping parameter analogous to viscosity, and volume integration is carried out over the volume  $V_e$ .

Using the displacement field  $\{u\}$  we have,

$$\{u\} = [N] [d], \quad (4.5.2)$$

$$\{\dot{u}\} = [N] [\dot{d}], \quad (4.5.3)$$

$$\text{and } \{\ddot{u}\} = [N] [\ddot{d}]. \quad (4.5.4)$$

where  $[N]$  is the shape function and the nodal degrees of freedom are denoted by  $[d]$ .

Combining equations 4.5.1 with 4.5.2-4.5.4, we have

$$[m] \{\ddot{d}\} + [c] \{\dot{d}\} + \{r^{int}\} = \{r^{ext}\} \quad (4.5.5)$$

For the assembled structure equation 4.5.5 becomes (Cook, 1989),

$$[M] \{\ddot{D}\} + [C] \{\dot{D}\} + \{R^{int}\} = \{R^{ext}\} \quad (4.5.6)$$

In direct integration, the above equation of motion is written at a specific instant of time,

$$[M] \{\ddot{D}\}_n + [C] \{\dot{D}\}_n + \{R^{int}\}_n = \{R^{ext}\}_n \quad (4.5.7)$$

where  $[M]$  and  $[C]$  are mass and damping matrices, taken as time independent, but in many problems, these may be nonlinear. The subscript  $n$  denotes time  $n\Delta t$  and  $\Delta t$  is the size of the time increment or time step,  $\{R^{int}\}_n$  is the internal force vector at time  $n\Delta t$  due to

straining of the material and in our case, it is a nonlinear function of  $\{D\}_n$ ,  $\{R^{ext}\}_n$  is the external force vector on the structure.  $\{R^{int}\}_n$  is obtained by assembling element internal force vectors  $\{r^{int}\}_n$  obtained from the equation

$$\{r^{int}\} = \int_{V_e} [B]^T \{\sigma\} dV \quad (4.5.8)$$

where  $[B]$  is the derivative of the shape function matrix.

The equation 4.5.8 is valid for both linear and nonlinear material behavior as the stress tensor  $[\sigma]$  could be a nonlinear function of strain and strain rate. However, for linearly elastic behavior,  $[\sigma]$  is given by

$$\{\sigma\} = [E] [B] [d] \quad (4.5.9)$$

where  $[E]$  is the elasticity matrix, and in that case, the equation 4.5.8 becomes

$$\{r^{int}\} = [k] [d] \quad (4.5.10)$$

where  $[k]$  is the element stiffness matrix and  $[d]$  nodal displacement. But, in our case  $[\sigma]$  describes the nonlinear stress response obtained from the Microplane Theory.

The direct integration methods for solving the above equation (4.5.7) can be classified as explicit or implicit. The methods that are explicit can be represented as :

$$\{D\}_{n+1} = f(\{D\}_n, \{\dot{D}\}_n, \{\ddot{D}\}_n, \{D\}_{n-1}, \dots) \quad (4.5.11)$$

while those that are implicit can be represented as:

$$\{D\}_{n+1} = f(\{D\}_n, \{\dot{D}\}_{n+1}, \{\ddot{D}\}_{n+1}, \dots) \quad (4.5.12)$$

Therefore, for explicit methods, as in our case,  $\{D\}_{n+1}$  is to be determined in terms of completely historical information consisting of displacements and time derivatives of displacements at time  $n\Delta t$  and before. In contrast, for implicit, the determination of  $\{D\}_{n+1}$  requires the knowledge of the time derivatives of  $\{D\}_{n+1}$ , which are unknown.

Additionally, for implicit schemes the structural stiffness matrix  $[K]$  has to be formed for each increment and  $\{R^{int}\}_n$  in equation 4.5.7 is replaced by matrices  $[K]$  and  $[D]$  as

$$\{R^{int}\}_n = [K] \{D\}_n \quad (4.5.13)$$

This involves decomposition of the stiffness matrix at each increment of the time step and that may be numerically difficult depending on the type of nonlinearity.

These methods are discussed in detail in many finite element books and the interested reader is referred to Cook (1989) and Zienkiewicz (1992) who have provided excellent treatments of this subject.

#### 4.6. Time Step Calculation

It is necessary to estimate the stable time increment in the model. The stable time increment (Time Step) is the smallest time taken to transmit a dilational wave across any of the elements in the mesh and is given by

$$\Delta t \approx \frac{L_{min}}{W_d} \quad (4.6.1)$$

where  $W_d$  the dilational wave speed, is defined for the developed program as

$$W_d = \sqrt{\frac{\lambda + 2\mu}{\rho}} \quad (4.6.2)$$

$$= \sqrt{\frac{5C_v + 4C_d + 6C_t}{15 * \rho}} \quad (4.6.3)$$

The number of increments is given by

$$n = \frac{T}{\Delta t} \quad (4.6.4)$$

where  $T$  is the total time period in the developed program.

The computer time involved in running a simulation using explicit time integration with a given mesh is directly proportional to the time period of the event (Hibbitt et al, 1994). The stability limit (ignoring damping) is written as

$$\Delta t \leq \min (L^{el} \sqrt{\frac{\rho}{\lambda + 2\mu}}) \quad (4.6.5)$$

where,  $L^{el}$  is the characteristic length associated with an element,  $\rho$  is the material density, and  $\lambda$  and  $\mu$  are effective Lamé's constants. Therefore, for the developed program, the number of increments is defined as

$$n \approx T \max \left( \frac{1}{L_{\min}} \sqrt{\frac{5C_v + 4C_d + 6C_t}{15 * \rho}} \right). \quad (4.6.6)$$

To reduce  $n$ , we can speed up the simulation compared to the time of the actual process, that is, we can artificially reduce the time period of the event  $T$ . This will introduce two possible errors. If the simulation speed is increased too much, the increased inertia forces will change the predicted response (in an extreme case the problem will exhibit wave propagation response). The only way to avoid this error is to choose a speed-up that is not too large. However, in certain instances like in a rate-dependent material problem, it may not be feasible to change the actual time period of the event being modeled.

## 4.7. Mass Scaling

As we note in the equation (4.6.6), artificially increasing the material density,  $\rho$ , by a factor  $f^2$  reduces  $n$  to  $n/f$ , in much the same manner as decreasing  $T$  to  $T/f$ . This concept is known as mass scaling and it is attractive because it allows us to treat rate dependent problems. This concept of mass scaling was used in our simulation. While modeling a concrete slab for example, the total weight of the slab in the numerical model was verified against the actual weight of the slab from concrete literature, and the additional weight used

for mass scaling to speed up the solution (reduce the number of increments) was lumped at the locations of least interest.

#### **4.8. Summary**

In this chapter, Bazant's Microplane Theory is implemented for the first time in a three dimensional finite element code. The implementation involved rearranging and defining the equations using continuum mechanics so that they could be numerically programmed. It involved checks on computations as well as assurance of stability. The program employed the implementation of suitable stable integration schemes (Section 4.2.2) for the user defined algorithm (Section 4.2.1). Additionally, for the material parameters chosen, the algorithm in the developed program was checked for minimum error between the analysis and literature data for PCC concrete. For an explicit formulation, the concept of mass scaling has also been introduced to speed up the solution process for modeling material response, and this type of an approach is novel for pavement response modeling.

# Chapter 5. Verification of the Numerical Model

## 5.1 Introduction

In Chapter 4, the Microplane Theory was implemented in a Fortran program. In this chapter, the simulated response using that program is verified with test data taken from the literature.

The constitutive laws in the Microplane Theory are general laws applicable to geomaterials (concrete, rock or ceramic) and involve a set of material parameters (Section 3.3) which depend on the constituents of the material. Depending on the method of production, they vary from concrete to concrete. To determine the values of those parameters for Portland Cement Concrete, the Taguchi Method (Roy, 1990) is used. This chapter deals with the application of the Taguchi Method and discusses its use in verifying the analysis. This chapter also discusses the various laboratory controlled tests that are successfully simulated for the purpose of validating the developed program. Finally, the developed program is checked for convergence.

## 5.2 Sensitivity Study

Bazant's Microplane Theory (1988-96) requires 14 or more (depending on which version of the Microplane Theory is applied) material constitutive parameters to describe volumetric, deviatoric and in-plane behavior of the geomaterials. Most of these parameters are inherent to Bazant's Microplane Theory only, and they vary from one type of concrete to another depending on the type of the mixture, aggregate size, moisture content, entrapped air as well as the method of production. Accordingly, they cannot be directly obtained from PCC literature. For our problem, we are specifically interested in parameter

values for Portland Cement Concrete (PCC). These parameters, which have already been discussed in Sections 3.2, 3.3 and Appendix F, are as follows:

- Elastic parameters:  $E$ ,  $\nu$ ,  $\eta_o$ ,
- Volumetric law parameters:  $a$ ,  $b$ ,  $p$ ,  $q$ ,  $a_1$  and  $p_1$ ,
- Deviatoric law parameters:  $a_2$  and  $p_2$ , and
- Tangential law parameters:  $a_3$ ,  $K_a$  and  $p_3$ .

Bazant (1988) had suggested a range of values for these parameters for geomaterials, and these can be used as starting values. Seven of these parameters stay the same for PCC and the rest which vary from one concrete to another are chosen for the Taguchi sensitivity study. With the help of this study, the values for the parameters were finally determined.

A finite element model as shown in Figure 5.1 is employed to provide data for the Taguchi sensitivity study. This model consists of 750 brick elements each with 8 nodes. At each integration point of every element, the constitutive characteristics are defined by the developed program. The minimum size of the element used is 0.102 m (4 in.). Two layers are used along the depth. Only a quarter of the model is shown in Figure 5.1. The full model spans 4.6 m (15 ft) in length and 3.7 m (12 ft) in width resembling the dimensions of a highway pavement slab. The model is supported by elastic spring elements (not shown in Figure 5.1), the end nodes of which are grounded. The properties of the springs are taken from Huang (1993). Symmetry boundary conditions are used at the ends of the slab. A pressure load is distributed along the 4 center elements. Altogether, 5 cycles of loading and unloading from a peak load value of 1.60E5 N (36,000 lb) to a zero value is carried out to obtain the response. Before proceeding further with the sensitivity study, it is first appropriate to discuss the Taguchi Method as it pertains to this research.

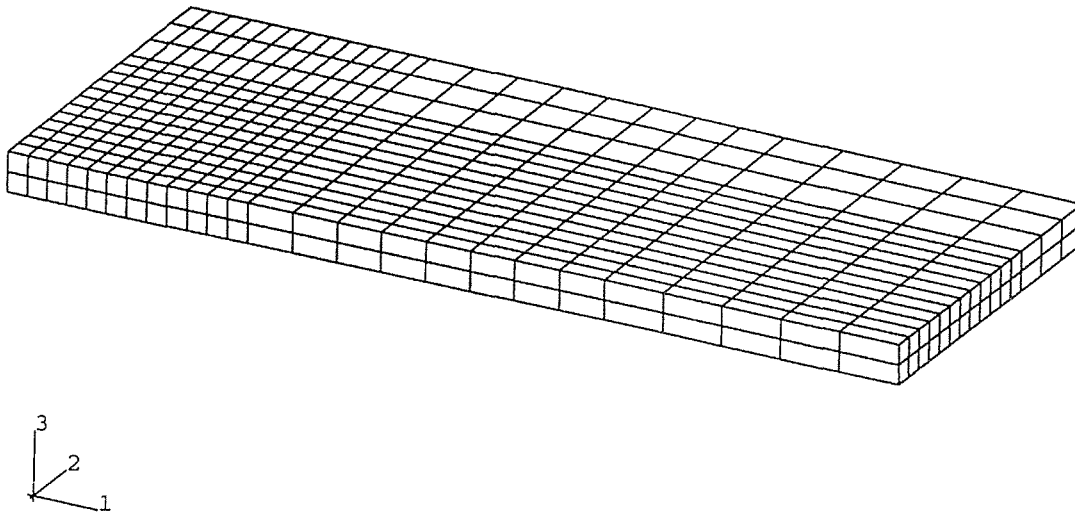


Figure 5.1: Finite Element Mesh (quarter model)

### 5.3 Taguchi Method and Its Application

Taguchi's Design of Experiments (Taguchi et al., 1987; Ross, 1988; and Roy, 1990) is applied when the objective is to determine the contribution of various factors that simultaneously control a desired result. In reality, these factors may occur with different sets of values and in all sorts of combinations among themselves to influence the result. Experiments can be designed for all possible combinations of these factors to study and rank such influence. This is known as Factorial Design or Design of Experiments (Fisher, 1951). However, as the number of factors and the values (known as 'levels' in the Taguchi Method) increase, the number of experiments required can get extremely large. For example, in a case involving seven factors and two levels, the total number of runs/experiments required for a factorial design will be 128 ( $2^8$ ), and this is known as 'full factorial design'. The advantage of the Taguchi Method is that it utilizes a partial factorial design. That is, a small set out of all possible combinations is selected in order to reduce

the number of required experiments in such a manner that accuracy is retained in predicting the contributions of the individual factors.

Taguchi Method involves a 2-step process. In the first step, this method clearly defines a way of conducting the experiments by the use of statistical tables, known as 'Orthogonal Arrays' (OA). The dimension of the OA depends on the number of factors and the level of information available for each factor. The second step uses the Analysis of Variation (ANOVA), a common method for statistical analysis (Ross, 1988; Roy, 1990), to examine the relative significance of each of the factors.

The initial range of values for the seven parameters are presented below in Table 5.3.1. The two levels denote the upper and lower end of the range of the values and is chosen from the literature (Bazant, 1992). An orthogonal Array  $L_8$  from Taguchi's Design of Experiments is used as shown in Table 5.3.2. The target response selected was tensile stress in the direction of travel at the bottom of the pavement layer and is shown in the last column of Table 5.3.2 for each of the 8 runs required in the array. Table 5.3.3 shows the average effect of the variables using Taguchi's  $L_8$  array. In Table 5.3.3, 'Sum 1' for any factor refers to the sum of the stress results for the runs which used level 1 values, 'Sum 2' refers to the same for the level 2 values and 'Avg. 1' and 'Avg. 2' refer to their corresponding average values. Based on Table 5.3.3, the average performance of the factors are computed using the Taguchi Method and is represented in Figure 5.2. This schematic figure is also known as Main Effects and it shows that two extreme cases are possible. In the first case, the factors combine to give the highest value of the target response (stress) and in the second case, the factors combine to give the lowest value of the response. In our case, a higher stress represents the worst situation with respect to damage growth, therefore the chosen combination of values are level 2 for E, level 1 for a1, level 2 for a2, level 1 for a3, level 1 for Ka, either level 1 or 2 for  $\eta_o$ , and level 1 for a (Figure 5.2). Let these values be termed as Base Values and we proceed to the next step ANOVA.

| Factors  | Variables                            | Values  |         |
|----------|--------------------------------------|---------|---------|
|          |                                      | Level 1 | Level 2 |
| E        | Elastic Modulus ( $\times 10^3$ psi) | 3000    | 4000    |
| a1       | Volumetric Parameter 1               | 0.0004  | 0.00005 |
| a2       | Deviatoric parameter 1               | 0.004   | 0.002   |
| a3       | Tangential Parameter 1               | 0.002   | 0.003   |
| Ka       | Tangential Parameter 2               | 0.0     | 0.1     |
| $\eta_o$ | Deviatoric parameter 2               | 0.5     | 0.8     |
| a        | Volumetric Parameter 2               | 0.005   | 0.006   |

Table 5.3.1: Factors used in The Taguchi Method

| E | a1 | a2 | a3 | Ka | $\eta_o$ | a | Stress Response ( $\times 10^3$ psi) |
|---|----|----|----|----|----------|---|--------------------------------------|
| 1 | 1  | 1  | 1  | 1  | 1        | 1 | .4435                                |
| 1 | 1  | 1  | 2  | 2  | 2        | 2 | .3944                                |
| 1 | 2  | 2  | 1  | 1  | 2        | 2 | .2969                                |
| 1 | 2  | 2  | 2  | 2  | 1        | 1 | .2362                                |
| 2 | 1  | 2  | 1  | 2  | 1        | 2 | .5771                                |
| 2 | 1  | 2  | 2  | 1  | 2        | 1 | .6260                                |
| 2 | 2  | 1  | 1  | 2  | 2        | 1 | .4412                                |
| 2 | 2  | 1  | 2  | 1  | 1        | 2 | .3357                                |

Table 5.3.2: Layout and Results

|          | Factors                                 | Sum 1 | Sum 2 | Avg. 2 | Avg. 1 | (Avg. 2 - Avg. 1) |
|----------|-----------------------------------------|-------|-------|--------|--------|-------------------|
| E        | Elastic Modulus (X 10 <sup>3</sup> psi) | 1.37  | 1.99  | .49    | .34    | .15               |
| a1       | Volumetric Parameter 1                  | 2.04  | 1.31  | .33    | .50    | .17               |
| a2       | Deviatoric parameter 1                  | 1.61  | 1.72  | .43    | .40    | .03               |
| a3       | Tangential Parameter 1                  | 1.76  | 1.60  | .40    | .44    | .04               |
| Ka       | Tangential Parameter 2                  | 1.71  | 1.66  | .42    | .43    | .01               |
| $\eta_o$ | Deviatoric parameter 2                  | 1.71  | 1.70  | .43    | .43    | .00               |
| a        | Volumetric Parameter 2                  | 1.75  | 1.61  | .40    | .44    | .04               |

Table 5.3.3: Average Effects of the variables

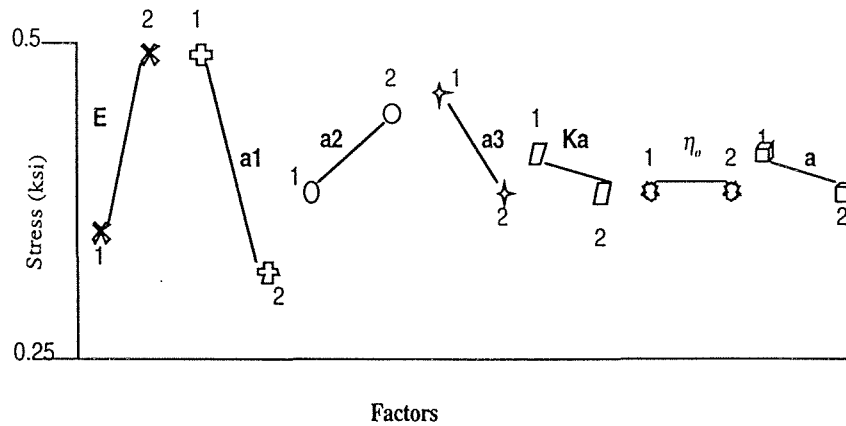


Figure 5.2: Main Effects

As a second step in the Taguchi Method, the Analysis of Variation (ANOVA) is employed. Following the steps outlined in the Taguchi Method (Appendix C), the percentage contribution of various factors are computed as shown in Table 5.3.4. The ANOVA provides a measure of sensitivity of the factors and determines the variability in the data. This ANOVA also establishes the relative significance of the individual factors and their interaction effects through a percent contribution value which is of interest here. The corresponding percentages for the factors are calculated using MINITAB and are shown in the last column of Table 5.3.4.

The sensitivity study identifies that the parameters  $a_1$ ,  $E$  and  $a_2$  change the stress response the most for a given change in their values. Therefore, iterations involving proportionate changes in  $a_1$ ,  $E$ , and  $a_2$  are made on the Base Values to reach the suggested trend of response (Bazant, 1992) shown in Figure 5.3.

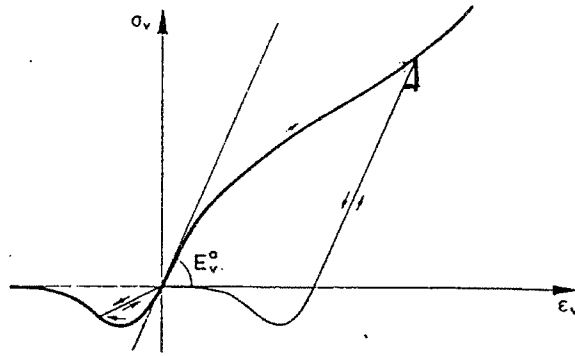
The responses are finally checked with the experimental data from the literature as will be described in Section 5.4. The final values used in the analyses are given in Table 5.3.5.

| Factors  | %    |
|----------|------|
| E        | 36.0 |
| a1       | 42.0 |
| a2       | 19.0 |
| a3       | 2.0  |
| Ka       | 0.1  |
| $\eta_o$ | 0.2  |
| a        | 0.2  |
| Error    | 0.5  |

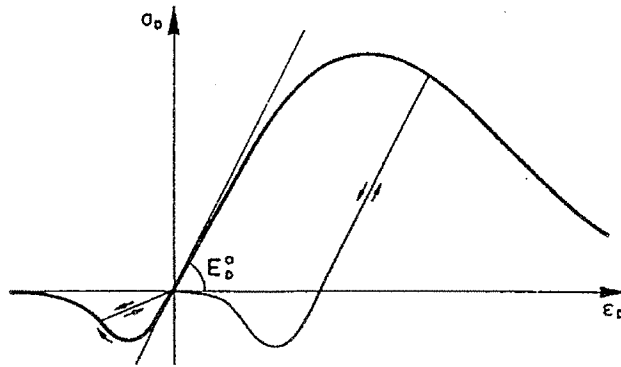
Table 5.3.4: ANOVA

| Parameters | Optimum Values    |
|------------|-------------------|
| E (psi)    | $4.0 \times 10^6$ |
| a1         | .0004             |
| a2         | .0025             |
| a3         | .0018             |
| Ka         | 0.0               |
| $\eta_o$   | 0.5               |
| a          | .005              |

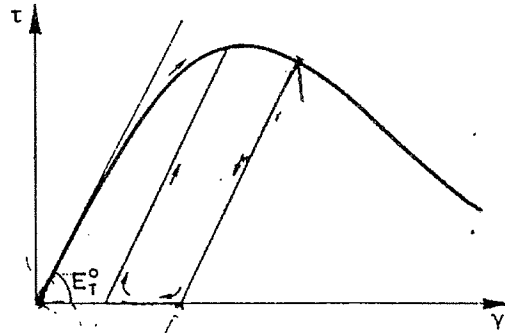
Table 5.3.5: Optimum Values



(a)



(b)



(c)

Figure 5.3: Microplane component curves from Bazant (1992); a) Volumetric, b) Deviatoric and c) Tangential stress-strain curves.

## **5.4. Verification of The Model**

The response obtained from the analysis using the chosen material parameter values is to be verified with a series of experimental tests and available data from the literature for PCC concrete in the following section. First, the analyses are verified on a single finite element and then on an assemblage of elements with multiple nodal degrees of freedoms. A number of runs simulating the laboratory tests are made and a few important and representative samples are discussed.

### **5.4.1. Uniaxial Tension**

A single solid brick element is generated using the developed program within Abaqus and the element is subjected to an uniaxial state of stress to match the experimental data of Kupfer (1969). Cofer (1992) had simulated the same experimental results analytically and using his guidelines the analysis is performed. The schematic arrangement of the loading is shown in Figure 5.4. The finite element had 2.54 cm (1 in) sides. To simulate the test conditions, the loading was applied through a prescribed displacement of  $12.7 \text{ E-}05 \text{ cm/s}$  ( $5.0\text{E-}05 \text{ in/s}$ ) at one end of the element. The other end of the element was kept fixed. The results comparing the literature and analysis are shown in Figure 5.5.

The results show a good overall correlation. The only difference seen in the curve is beyond the peak region. Strain-Softening (Cracking) occurs in that nonlinear region, and therefore, controlling the number of increments in those segments of the stress-strain curve of the analysis would give better results.

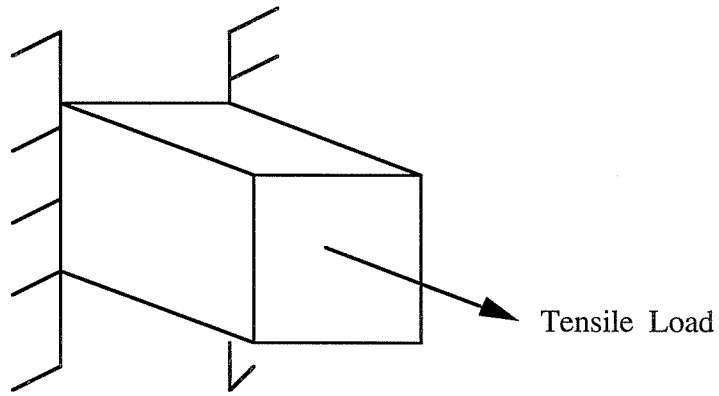


Figure 5.4: Uniaxial Tension

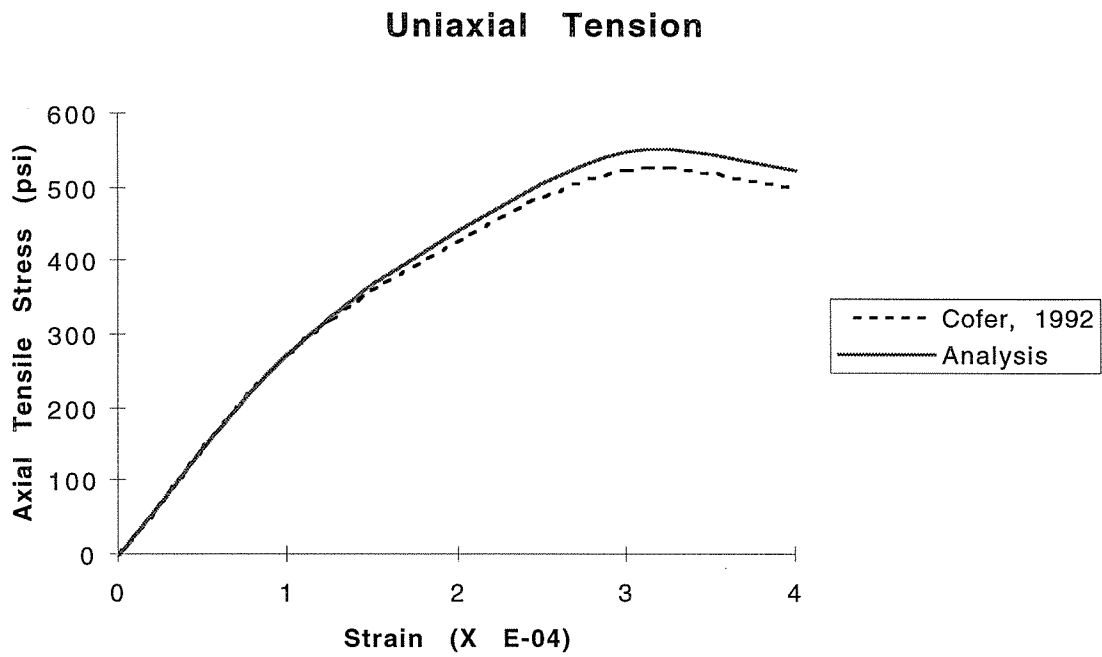


Figure 5.5: Analysis results for uniaxial tension test

### 5.4.2. Cyclic Compression

The single solid cube element having each side 2.54 cm (1 in) is tested here in uniaxial compression. First, it is tested for one cycle of loading beyond the softening range to match the experimental work by Hognestad (1995) which was later simulated by Bazant (1992). Then, the simulation in this research is further continued for 5 cycles of similar loading and unloading.

To start with, the solid element is held at one face and strained at the other. Following the guidelines of the numerical work by Bazant (1992), the simulation was performed. The uniaxial strain is first increased up to a value of .003 (beyond the peak). Then it is decreased to .001 and again increased to the final value of .004 all in load steps of .0002 in size. The amplitude of the strain cycle is applied such that it varies from the peak value to zero (unloading) as shown in Figure 5.6. The results from the finite element analysis are shown in Figure 5.7.

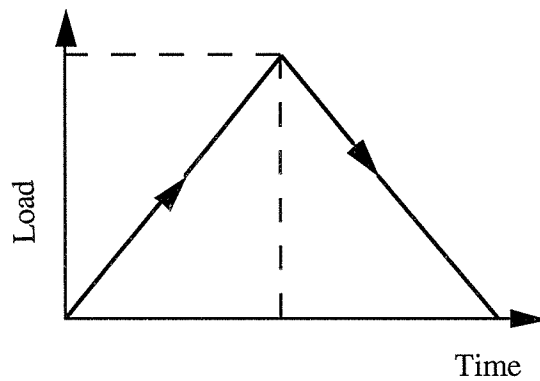


Figure 5.6: Cyclic Loop

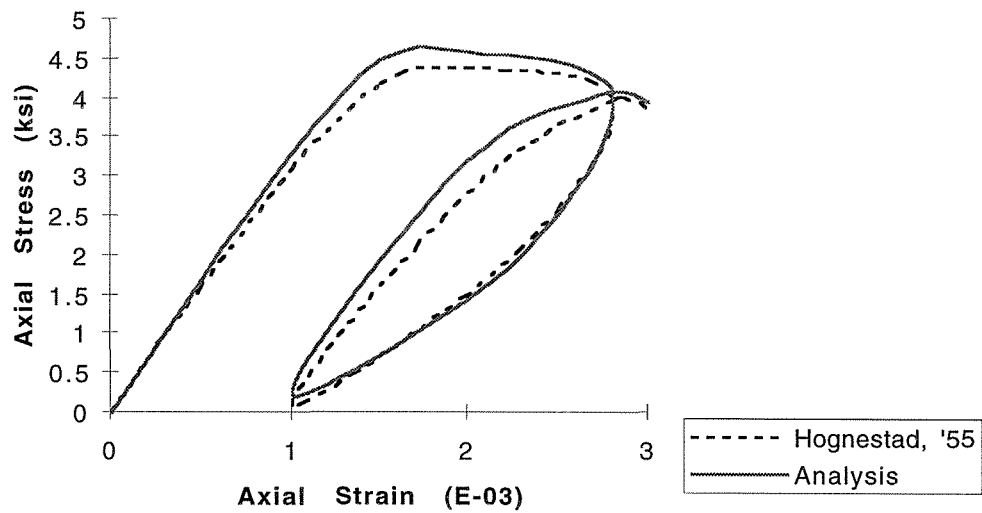


Figure 5.7: Post Peak and Hysteresis Loop compared

The results (Figure 5.7) show a reasonable correlation between the experimental and analytical data. The analysis is found to overpredict the experimental value by a small margin. One reason attributed is the lack of a better solution scheme to control the number of increments in the nonlinear part of the strain-strain curve beyond the peak value.

The same model is then further subjected to 5 cycles of loading and unloading in compression. First the numerical model is arbitrarily strained to values of 0.3E-3, 0.5E-3, 1.2E-3, 1.5E-3, 2.0E-3 and then unloaded to strain values of 0.2E-3, 0.3E-3, 0.4E-3, 0.6E-3, 0.7E-3 respectively. In absence of other test data, the results are compared with monotonic data from Bazant (1992). Figure 5.8 indicates the results obtained from the analysis using 5 of these loading-unloading cycles.

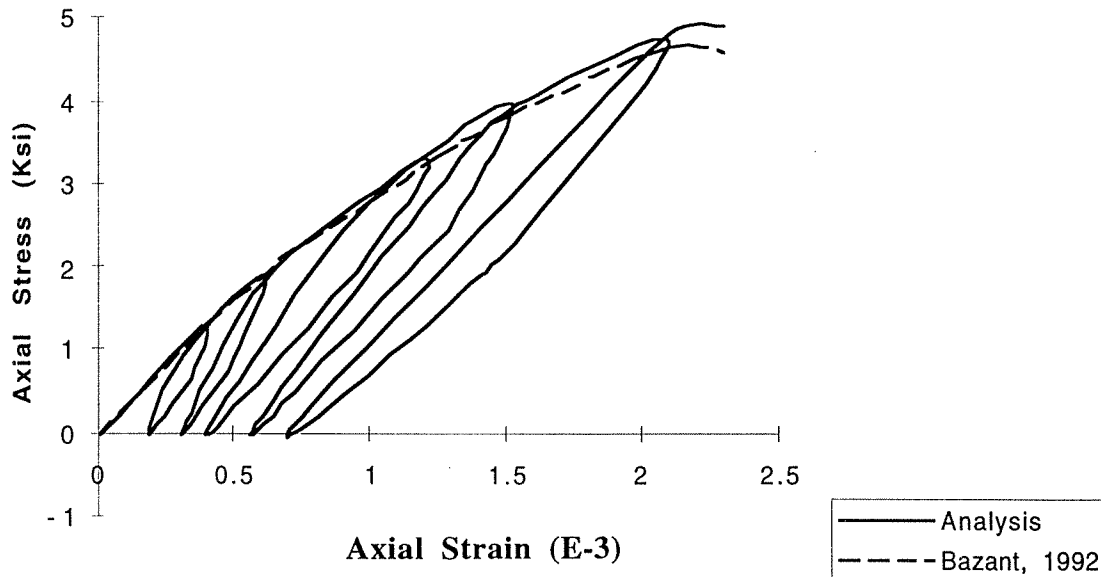


Figure 5.8: Cyclic Compression

The results showed that the monotonic curve enveloped the cyclic response. The solution converged and no numerical instability was noticed.

#### 5.4.3. Triaxial Test / Confining Pressure

Concrete properties depend on confining pressure. Confining pressure is defined by the lateral pressure equal to the average of the principal stresses in two directions (e.g. 1 and 2 direction) when loading is in the other direction (e.g. direction 3). Confining pressure subjects concrete to a triaxial stress state. In all the previous tests, zero confining pressure was assumed. There is no commercial program which can simulate concrete behavior under such a state beyond the softening region. This example demonstrates the capability of the developed program in simulating such a response.

In this test (Figure 5.9), a uniform pressure of 34.5 MPa (5000 psi) is applied in the 2 and 3 directions, and a constant uniaxial strain is applied in direction 1 as described in Bazant et. al. (1992). The loading in the finite element analysis is divided into two steps. The constant uniform pressure is applied in the first load step and the second load step is used to apply the uniaxial strain increment. The results are shown in Figure 5.10.

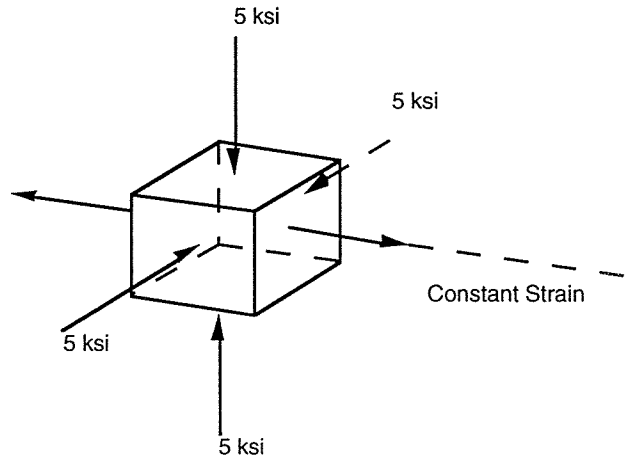


Figure 5.9: Triaxial Test

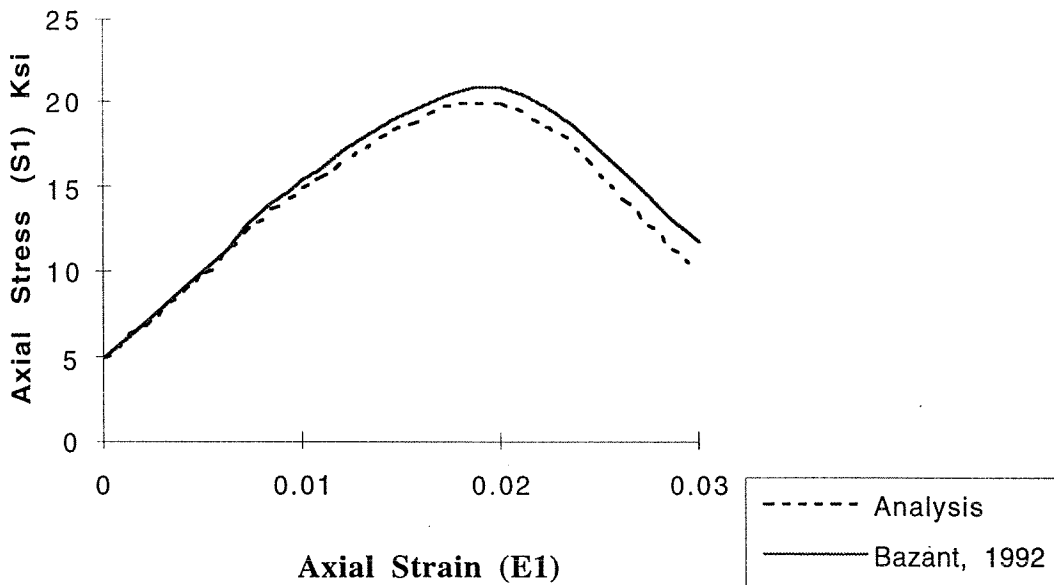


Figure 5.10: Triaxial Test Results

The results show a good correlation between the experimental and analytical data. The deviation observed beyond the post-peak region is attributed to the lack of a control of the number of increments in that region.

#### 5.4.4 Bending Test

In this case, an assemblage of elements is tested by simulating a bending test. The results here are compared with the test performed by Bazant and Ozbolt et. al (1992). The schematic diagram for the experiment is shown in Figure 5.11.

The specimen tested had dimensions 1.8 X .5 X .1 m (5.90 X 1.64 X 0.33 ft). In the analysis, solid elements are used to simulate the beam in three point bending. A mesh of uniform size elements, 5 in depth and 6 along the length are used. As the loading is symmetric about the vertical axis transverse to the length, half of the model with half the actual magnitude of the load is used and symmetry boundary conditions are used at the middle of the beam.

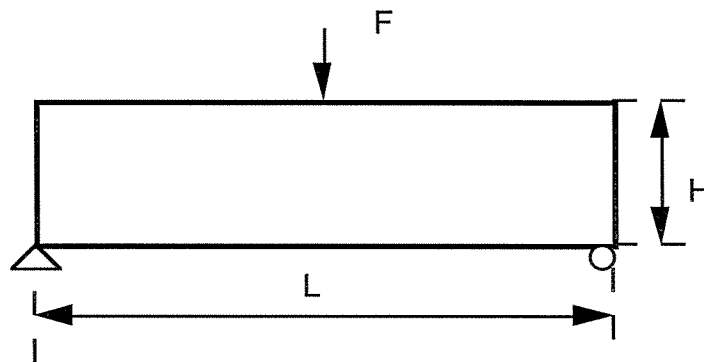


Figure 5.11: Three point bend test

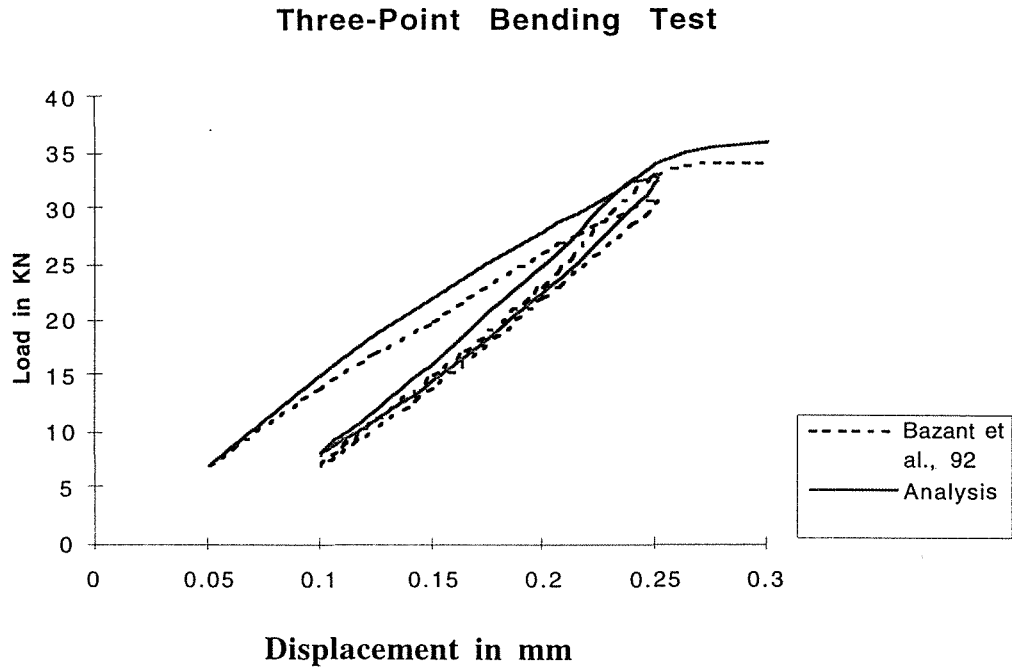


Figure 5.12: Three point bending test

The applied load is allowed to increase from 0 to 35 kN (7868 lb), while the maximum displacement increases from 0 to 0.30 mm (.01 in). Unloading is carried out from 0.25 mm to 0.1 mm (.008 in to .004 in) and that is followed by reloading back to 0.30 mm (.01 in). Figure 5.12 shows that the analysis results closely match the literature results. The initial difference between the two curves is attributed to a lesser number of increments in the analysis and this made the analysis almost linear in the region that precedes the start of the loop. In the post peak region, the difference is due to the average values of the parameters used as well as the coarse mesh used.

## 5.5. Taguchi Method Applied in Numerical Modeling

The previous tests validated the developed program with the laboratory controlled tests. It is now necessary to check the numerical sensitivity of the developed program with respect to the modeling factors like mesh density and loading rate. This is because, while

modeling the pavement response, optimum mesh size is required for the numerical solution to converge and arrive at the actual response, given the aggregate nature of concrete being modeled (Shah, 1991). It is necessary to determine the size of the finite elements to eliminate mesh dependencies and attain convergence. Also, the loading rate dependencies, if any, are to be determined as well. This dependency may arise in two ways. In a pavement environment, the rate of loading and unloading is dependent on the vehicle speed which may cause a particular strain rate. The speed of the solution in an explicit scheme may influence the strain rates as well (Cofer, 1992). Since these two aspects are linked, a study was conducted to determine the safe operating conditions for the developed program. The study involved mesh sizes, loading rates, and three other material parameters ( $a_1$ ,  $a_2$  and  $E$ ) which had the highest sensitivity in the previous study (Section 5.3).

### 5.5.2 Procedure

The values for the parameters referred to as factors in the study are listed in Table 5.5.1. Figure 5.13 show the differences between monotonic and cyclic loading. The peak equivalent vehicle axle load (designated by  $P_{max}$ ) was  $1.6E5$  N (36000 lb) and was allowed to ramp up from 0 for the monotonic loading. For the cyclic loading it is again unloaded from the peak value to zero.

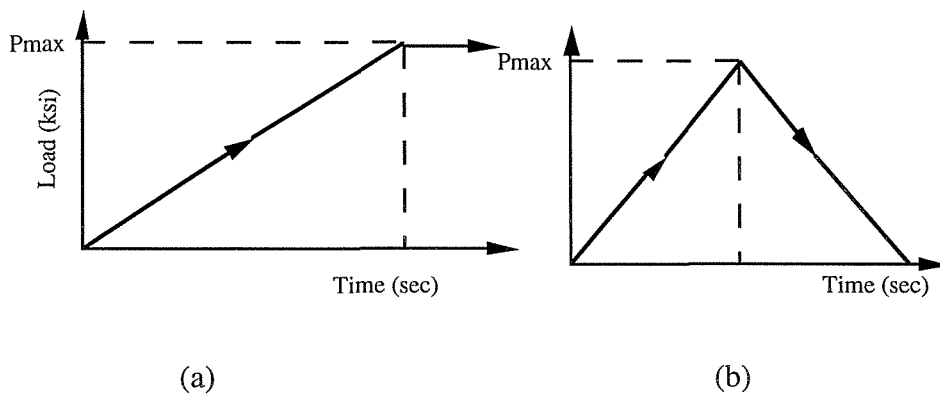


Figure 5.13: (a) Monotonic Load (b) Cyclic load

The axle load is assumed to act at the center of the contact patch represented by 4 finite elements at the center. The loading rate corresponding to a speed range of 48-96 km/hr (30-60 mph) is studied. The time T (in Table 5.5.1) is the time to load the center of the contact area of 0.3 m (144 in<sup>2</sup>) and is calculated from the speed of the vehicle. Two mesh sizes having 144 elements and 256 elements were considered in the analyses. The sensitivities of the solution are compared with the responses for the cases of monotonic and cyclic loading.

| Factor                           | Level 1                | Level 2                |
|----------------------------------|------------------------|------------------------|
| a1                               | .00005                 | .0004                  |
| a2                               | .001                   | .003                   |
| Modulus of Elasticity (E) in psi | 3000 X 10 <sup>3</sup> | 4000 X 10 <sup>3</sup> |
| Mesh Density                     | 144 Elements           | 256 Elements           |
| Duration of Load (Loading Rate)  | T / 2                  | T                      |

Table 5.5.1: Factors and their levels in Taguchi Method

### 5.5.3. Results

The results of the numerical sensitivity study are shown in Figures 5.14 and 5.15. The factors are arranged in order of decreasing sensitivity in Figure 5.14 which shows the results for monotonic loading. For cyclic loading (even in the softening region), the sensitivities of all factors are not significant enough to influence the convergence up to 5 cycles.

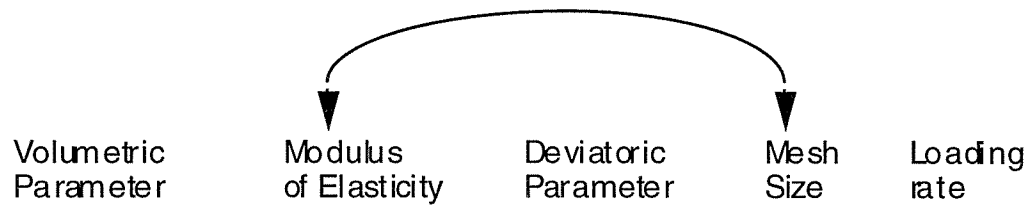


Figure 5.14: Numerical Sensitivity

After significant softening has occurred (beyond 5 cycles), it is seen that the factors arranged in the order of decreasing sensitivity are volumetric parameter, mesh size, deviatoric parameter, modulus of elasticity and loading rate. In contrast to monotonic loading, the order is the same except that switching of places occurs between the modulus of elasticity and the mesh size. In Figure 5.14, this switch is indicated by an arrow. To conclude this discussion on rate sensitivity, a further analysis is continued beyond 10 cycles, with Elastic Modulus, Mesh Density and Speed as the variables. Figure 5.15 shows the results from this study.

### Comparison Between Factors Influencing Pavement Response Modeling Under Cyclic And Monotonic Loading

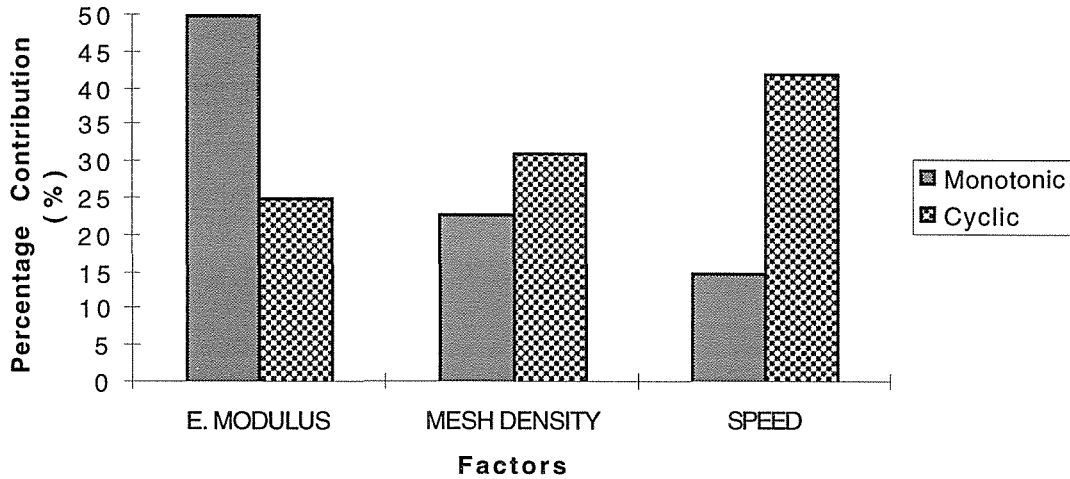


Figure 5.15: Comparison between cyclic and monotonic loading

Figure 5.15 shows that in the case of monotonic loading, the Elastic Modulus is the largest contributing factor in determining the maximum longitudinal stress. The mesh density is the next most important factor, followed by the strain rate effects. After 10 cycles in the post softening region, the pavement material undergoes both plastic deformation as well as a degradation in stiffness and is highly load rate sensitive. This rate sensitivity may be caused by the vehicle speed as well as numerical factors. It is therefore advised to run all the simulations at a controlled rate with a pre-determined number of increments after 10 cycles.

Such an effect has been supported by the experiments of Cofer (1992), and Cebon and Hardy (1994). A finer mesh avoids excessive strain localization and damage being confined to the width of the element, and hence a finer mesh (less than 3 times the aggregate size) becomes important as strain softening and progressive damage occurs on the pavement element under the load. In particular, the bottom of this element is in tension

and this state is immediately followed by a state of compression as the vehicle passes. Mesh Density is thus the next most important factor for cyclic loading.

Therefore, based on this study, as we have only gone up to 10 cycles in this dissertation, speed/rate sensitivity is considered insignificant, and therefore, it should not influence the stability of the numerical solution in this research. However, the mesh density may affect the solution and the next section is devoted to this issue.

## **5.6 Avoiding Mesh Dependence of the Numerical Solution**

It is known from the literature that concrete response may depend on the size of the finite element mesh as well as the size of the specimen used in the test. The researchers trying to simulate concrete response using finite element methods, have observed spurious mesh dependence of the response beyond the softening regime (Bazant et al., 1984, 1990; Cofer, 1992). This poses a problem in the post peak range of softening (cracking) when the response is simulated analytically (Shah et al., 1991). As reported in their work, the response computed gave errors due to the failure being localized to the width of the finite element used. They found that the width of the failure zone, which is known as the characteristic length, is a material property that must be ascertained through other methods. Additionally, they have concluded that by taking the element size to be about 1/3 of the characteristic length, the spurious mesh dependence can be removed (Bazant, 1993-95, Cofer, 1992). Otherwise, for arbitrary modeling, corrections using the Size Effect Law (Bazant et al., 1984) should be applied in the softening regime. This characteristic length was reported to be approximately 3-4 times the aggregate size (Bazant, 1987-88; Cofer, 1992). One notable paper (Shah, 1991) had also revealed that under cyclic loading, the coarse aggregate size determines the fatigue strength and life, and therefore, this size should be used in estimating this characteristic length. An average coarse aggregate size of 100 mm (4 in.) is usually found in concrete (Mehta, 1986). Therefore, for finite element modeling, the elements having dimensions in the vicinity of 100 mm (4 in.) or less should

be appropriate near the load. To verify this observation, analysis was performed and the results are shown in Tables 5.6.1 and 5.6.2.

To find the optimum mesh with respect to the maximum value of the target response (Longitudinal Stress denoted by S11), and the Damage Ratio (defined as the ratio of strain at fracture, to the longitudinal strain in the direction of travel) a short study was conducted. Damage ratio will be discussed in further detail in Chapter 6. The study used the same finite element model as discussed previously. Table 5.6.1 shows a synopsis of the results. Table 5.6.2 shows the converged mesh size with respect to the damage ratio. Also, 'mixed mesh' in the tables refers to a transition in element size from 100 mm (4 in) near the load to 300 mm (12 in) away from the load.

For the range of values held by the material parameters, the mesh dependence for element size as shown in Tables 5.6.1 and 5.6.2 is insignificant. So, for cyclic loading, 100 mm (4 in) element size was found to be satisfactory for up to 10 cycles of simulation as the developed program gave insignificant error. Moreover, for cases where response near the load is of interest, a mixed mesh may be more efficient.

| Mesh size (in) | S11 (X 10 <sup>3</sup> psi) |
|----------------|-----------------------------|
| 4              | 2.2                         |
| 6              | 2.3                         |
| 9              | 2.5                         |
| 12             | 2.5                         |
| Mixed Mesh     | 2.3                         |

Table 5.6.1: Numerical Sensitivity Study 1

| Element Size | Damage ratio |
|--------------|--------------|
| 4            | .70          |
| 6            | .67          |
| Mixed Mesh   | .60          |

Table 5.6.2: Numerical Sensitivity Study 2

## 5.7. Summary

In this chapter, Taguchi's orthogonal arrays were applied to determine the relative contribution (sensitivity) of material parameters (used in volumetric, deviatoric and in-plane constitutive laws) to obtain a numerically correct pavement response (longitudinal stress). This helped in the selection of appropriate parameter values to match the constitutive curves (volumetric, deviatoric etc.) for the PCC material used in highways.

Then, the analysis results were verified with known laboratory controlled experimental results.

Finally, a sensitivity analysis was performed to study the performance of the developed program and to determine the stable operating region for the analysis. It was shown, that for up to 10 cycles and for a vehicle speed ranging from 48-96 km/hr (30-60 mph), the solution is numerically stable for a mesh size of 100-150 mm (4-6 in.) near the load.

# **Chapter 6. Pavement Response Modeling**

## **6.1. Introduction**

In the previous chapter, the developed program was verified with the laboratory controlled tests. In this chapter, first, the methods applied to model a foundation are discussed and a pavement model is built. The pavement response is then verified with the results from the literature as well as with dynamic truck test data. A notion of qualitative damage is introduced and progressive damage distribution is represented on a slab of a plain concrete pavement. Finally, as damage caused by excessive tensile stress (in the direction of travel) is critical to the pavement design and maintenance, a sensitivity study of various pavement design parameters is carried out with respect to the same stress response. The study identifies for the first time, the relative contribution of various pavement design parameters to an increased level of stress and cumulative damage for a highway pavement.

## **6.2. Foundation Modeling**

In a highway, a layer of concrete pavement slab is supported by one or more layers of foundation maintaining a proper load transfer between the layers. Even though the main focus of this research is to determine the dynamic response of a given concrete slab, the foundation structure, which is of secondary interest, is also a necessary component in a highway structure. It is to be modeled with proper material properties and stiffness so as to capture the load transfer between the layers of foundation and the concrete pavement. For representing a foundation structure analytically, there are three types of foundation models in use, namely solid, liquid and layer. The foundation in our

research is modeled with linear springs having appropriate stiffness using the principles of a liquid foundation and this is discussed in Subsection 6.2.2. The solid foundation is briefly described in Subsection 6.2.3, as in one of the examples from the literature with which our analytical results are validated, has employed a solid foundation. The third type of a foundation, the layer foundation, is only briefly discussed for the purpose of completeness. A relationship between a solid and liquid foundation is also discussed (Subsection 6.2.4), such that any of these two foundation models (liquid and solid) can be interchanged for the conveniences of simulation, as will be demonstrated in Subsection 6.4.1.

### 6.2.2. Liquid Foundation

Liquid foundations have been used for most of the finite element computer programs, and they are based on Westergaard's theory (Huang, 1993). The deformation of the foundation can be modeled by placing the slab over an infinite number of springs and allowing the total volume of displacement to be proportional to the total load applied. The stiffness of the total foundation is defined by

$$k = p / w \quad (6.2.1)$$

where  $k$  is known as the modulus of subgrade reaction (Huang, 1993);  $p$  is the unit pressure, or force per unit area; and  $w$  is the vertical deflection.

Figure 6.2.1 shows the discretization of the liquid foundation under a rectangular concrete pavement element with a length  $2x$  and width  $2y$ . A replacement of a large number of springs under the element is done by identical springs at each of the four corners. For each spring, the force is equal to the unit pressure multiplied by the area  $xy$ . From the above equation  $p = kw$ , or the force at node  $i$ ,  $F_{w_i}$ , is related to the deflection at node  $i$ ,  $w_i$ , by

$$F_{w_i} = kxy w_i. \quad (6.2.2)$$

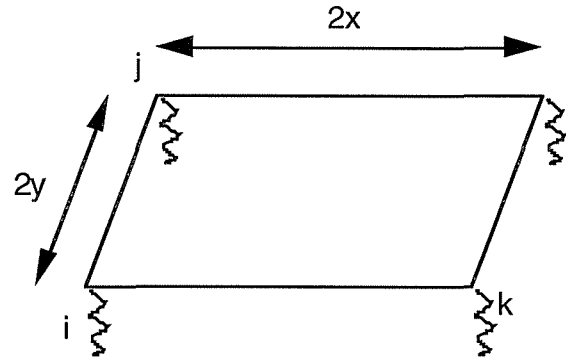


Figure 6.1: Pavement element discretization

It is to be noted that multiplying the modulus of subgrade reaction by the corresponding area of an element gives the spring constant. Equation 6.2.2 for the liquid foundation, is employed for modeling the foundation stiffness in this research. The foundation throughout this dissertation, has been modeled as a set of linear springs connected between each element corner node and a fixed node (ground node) vertically below it.

### 6.2.3. Solid Foundation

For a solid foundation, the deflection at any nodal point depends not only on the force at the node itself, but also on the forces at all other nodes. The solid foundation is also called a Boussinesq foundation as Boussinesq's (1888) equation for surface deflection is used for determining the stiffness matrix as given by the equation

$$w_{ij} = \frac{P_j(1 - \nu_f^2)}{\pi E_f d_{ij}} \quad (6.2.3)$$

where  $w_{ij}$  is the deflection at node  $i$  due to a force at node  $j$ ,  $P_j$  is the force at node  $j$ ,  $\nu_f$  is the Poisson's ratio of the foundation,  $E_f$  is the elastic modulus of the foundation, and  $d_{ij}$  is the distance between nodes  $i$  and  $j$ .

The program KENSLABS with which our analysis results are compared, is based on a solid foundation as described by equation 6.2.3.

#### 6.2.4. Layer foundation

Burmister's (1943,1958) layered theory is used to form the flexibility matrix of a layer foundation. Since this was not pertinent to our work, it is not further discussed but only mentioned here for the sake of completeness.

#### 6.2.5 Relationship between solid and liquid foundation

In one of the analyses to follow (in section 6.4.1), it will be found useful to relate the k value (modulus of subgrade reaction) for a liquid foundation to the elastic modulus  $E_f$  and Poisson's Ratio  $\nu_f$  of the solid foundation for a given slab thickness h. For that purpose, the following relationship between solid and liquid foundations will be used (Huang, 1993).

$$k = C \left( \frac{E_f}{E} \right)^{1/3} \frac{E_f}{(1 - \nu_f^2)h} \quad (6.2.4)$$

In the above equation E is the elastic modulus for concrete and C is a constant, whose value ranges from 114 to 258 kN/m<sup>3</sup> (0.42 to 0.95 lb/in<sup>3</sup>) depending upon the material constituents of the foundation. *K ranges*

### 6.3. Pavement Modeling

A finite element model of a pavement is built using the pre-processor module in Abaqus. Unless otherwise specified, the lane width used for all the analyses, is 3.6 m (12 ft) and the length of the concrete slab modeled for simulation ranges from 4.6 m to 9.1 m (15 to 30 ft). A pavement slab length of 4.6 m (15 ft) is used where the instantaneous response under the load (the maximum tensile stress) is of major concern.

A slab length of greater than 4.6 m (15 ft) is considered where response at various locations which are further away from the load are of interest (as in subsection 6.4.3). The pavement slab thickness used is in the range of 0.2 to 0.25 m (8 to 10 inches).

### **6.3.1. Finite Element Mesh**

For simulating the pavement behavior, 8 noded brick elements (C3D8 elements in Abaqus) are used. At each integration point of the element, constitutive laws, as calculated from the previously developed program (Chapter 4), are introduced and the PCC constitutive calculations are performed. The finite element mesh for the each model used in the analysis consists of a finer mesh of 0.1 m (4 in) under the load and a coarse mesh of .3 m (12 in) is used farthest away from the load. Two layers of elements are used to model the concrete slab thickness throughout the analysis.

### **6.3.2. Boundary Condition and Loads**

A set of linear elastic springs representing the foundation stiffness is connected at the four bottom corner nodes of each element. Fixed boundary conditions are used at the node on the lower end (grounded end) of the spring. Symmetric boundary conditions are applied at the ends of the slab.

Different types of loading from quasi-static to dynamic are used in the analyses depending on the test being verified or simulated. They will be discussed individually on a case by case basis.

## **6.4. Verification of Pavement Response**

In Chapter 5, the developed program was verified with the lab-controlled tests. To verify the capabilities of the program in simulating an actual pavement response, the analysis needs to be validated with tests in a highway environment as well. For that

reason, the response from the analyses are verified with 3 tests in this section. The first of these tests simulates the static response and the other two simulate dynamic response. These tests are performed to verify the techniques used in modeling the pavement, the foundation, and the material properties used to simulate the dynamic response.

#### **6.4.1. Static Test**

The first pavement response test is a static problem taken from literature (Huang, 1993). In this case a large concrete slab 7.3 m X 7.3 m X 0.2 m (24 ft X 24 ft X 8 in) was created. An elastic modulus of  $68.9E6$  N/sq. m (10,000 psi) and a Poisson's ratio of 0.4 was used for the PCC concrete material. A 40034 N (9000 lb) static wheel load with a contact pressure of 517 kN/sq. m (75 psi) is applied at the center of the slab.

Two commercial programs, KENSLABS and KENLAYER (Huang, 1993), widely used in the highway community, are chosen to calculate the response with the above properties first. Then, the developed program is used to compute the static response for the same model. The simulation is run quasi-statically and the same material and boundary conditions are used for all three programs (KENSLABS, KENLAYER and the developed program). Both KENSLABS and KENLAYER use a solid foundation whereas our simulation uses a liquid foundation. To calculate the equivalent spring stiffness for the liquid foundation to substitute for the solid foundation used in KENSLABS and KENLAYER, equation 6.2.4 is employed.

The concrete slab is divided into rectangular finite elements and because of symmetry, a quarter model as shown in Figures 6.2 and 6.3 (a and b) is used. The same mesh is used in all the programs. The circles in Figure 6.2 denote the springs representing the foundation. The deformed plot for the quarter model is shown in Figure 6.3b. It is noted that only in this problem, large elements (with sizes larger than 6 in) are used in areas under the load. This is done to match the similar mesh sizes already in use

in KENSLABS and KENLAYER and thus avoid the mesh dependency of the solutions.

Table 6.4 shows a comparison of the results.

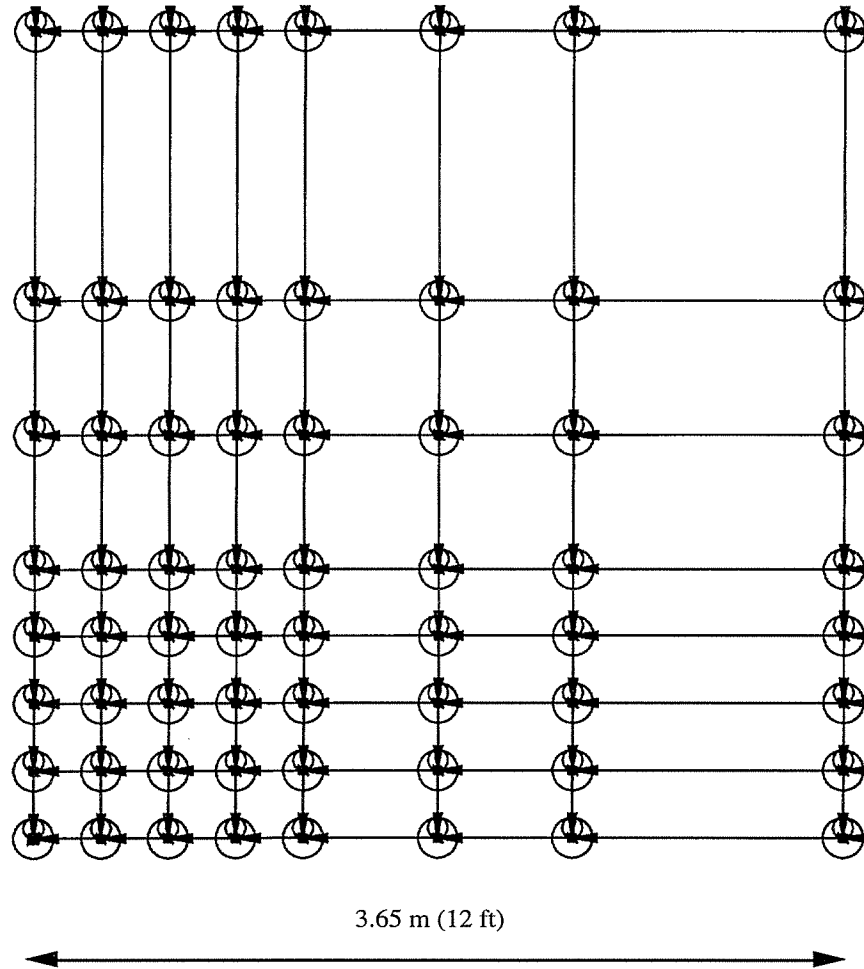
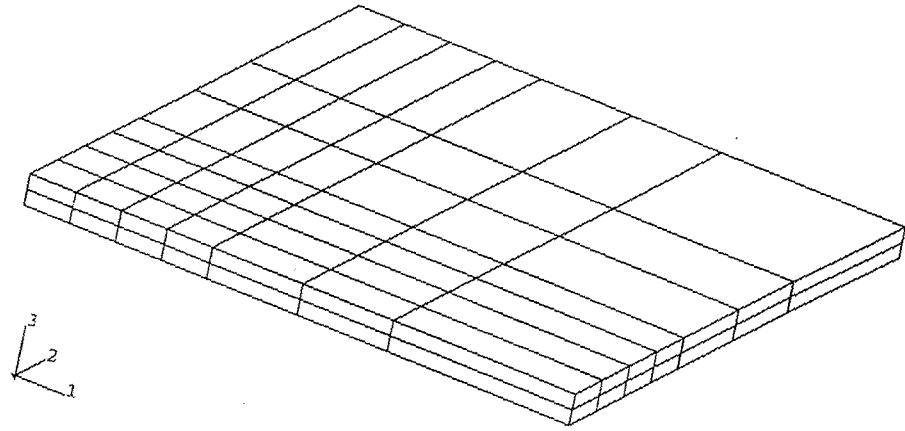
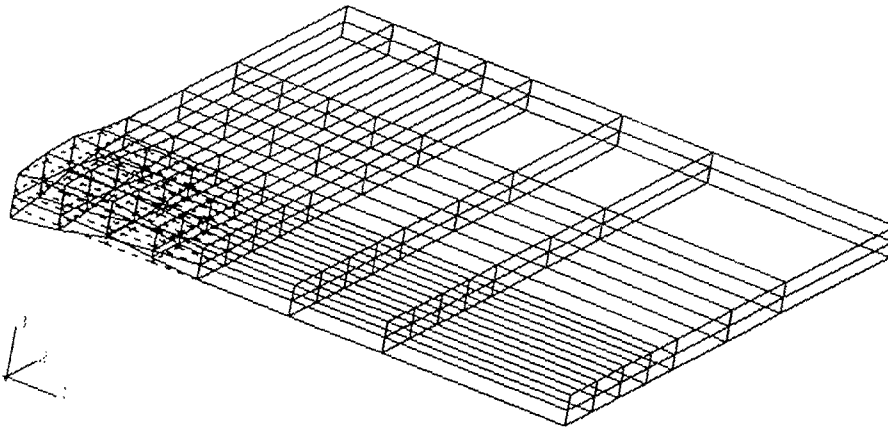


Figure 6.2: Finite Element Mesh of the quarter model used in the analyses



(a)



(b)

Figure 6.3: (a) Undeformed shape and (b) Deformed shape of the quarter model

|                      | Max. Deflection<br>(inches) | Min. Deflection<br>(inches) | S11<br>(X 10 <sup>3</sup><br>psi) | S22<br>(X 10 <sup>3</sup><br>psi) |
|----------------------|-----------------------------|-----------------------------|-----------------------------------|-----------------------------------|
| KENSLABS             | 0.009                       | 0.005                       | 0.170                             | 0.170                             |
| KENLAYER             | 0.010                       | 0.005                       | 0.200                             | 0.200                             |
| Developed<br>Program | 0.008                       | 0.005                       | 0.200                             | 0.200                             |

Table 6.4 : Comparison of the simulated response with available programs

The results show that the analytical response from the developed program compares very well with the commercial programs, KENSLABS and KENLAYER. The longitudinal stress (in the direction of travel) is denoted by S11 and the lateral stress (transverse to the direction of travel) is denoted by S22 and Developed Program refers to the analyses performed in this research using our developed program.

The deflection and stress results obtained by using the commercial programs and the Developed Program are in the same range. The results show that even for static problems, the developed program can predict the same range of results as the commercial programs.

#### 6.4.2. Influence Function

The Influence Function is defined as the relationship between the pavement response determined at a point of interest for a set of given positions of the axle load. It represents the variation in response as a wheel gradually approaches a point in the

pavement, reaches it and then and moves away from it. Usually, the Influence Function is expressed as a plot of Stress/Axle Load vs. Tire Position at a given point. In all the previous research work, the influence function was calculated from a linear static model of the pavement. To obtain a dynamic response from those analyses, dynamic factors were used (Gillespie, 1992) or the collocation method was applied (Cebon, 1996) to convert the response from static to dynamic. These approaches have resulted in considerable errors when compared with experimental data.

To demonstrate the capability of our program, the analysis is simulated with the test data from Gillespie (1992). The length of the pavement slab modeled was chosen to be 4.6 m (15 ft) for the concrete pavement simulated in the test. A quarter model with symmetry conditions at the ends is used for the analysis. In the test, an equivalent single axle load 160,135 N (36,000 lb) was distributed by an actual contact area of 0.04 sq. m (64 square inches) of the tire. For the simulation, a force of 40,033 N (9000 lb) is used on the quarter model and is distributed on four finite elements (16 sq. in.) at the corner, as this load is equivalent to a 160,135 N (36000 lb) load on the full model. The stiffness of the foundation is calculated as described in Section 6.3 and is based on the average homogeneous foundation properties.

Figure 6.4 shows the deflection basin under a loaded wheel (Gillespie, 1992). The bottommost layer under the wheel is in a state of tension. As concrete is weak in tension, the tensile stress response in that layer is of utmost concern as it affects the pavement life. The response (longitudinal stress at the bottom denoted by S11) at various points in the pavement is plotted. Figure 6.5 shows the simulated basin of deformation for the quarter model. The stress response per unit axle load is shown in Figure 6.6.

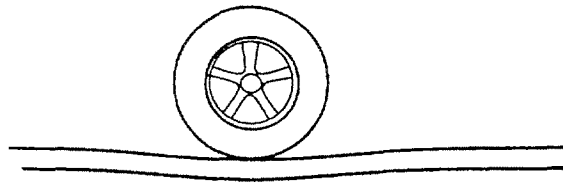


Figure 6.4 : Deflection basin under a loaded wheel

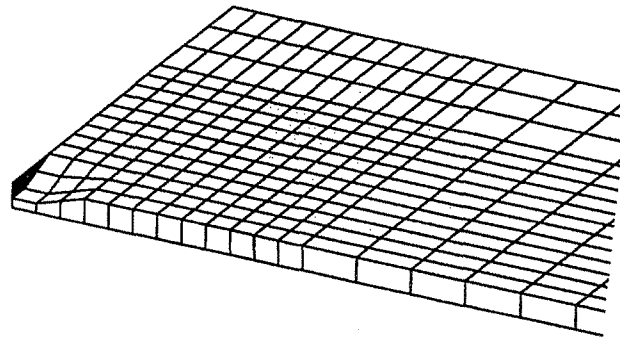


Figure 6.5: Simulated deflection basin under wheel load

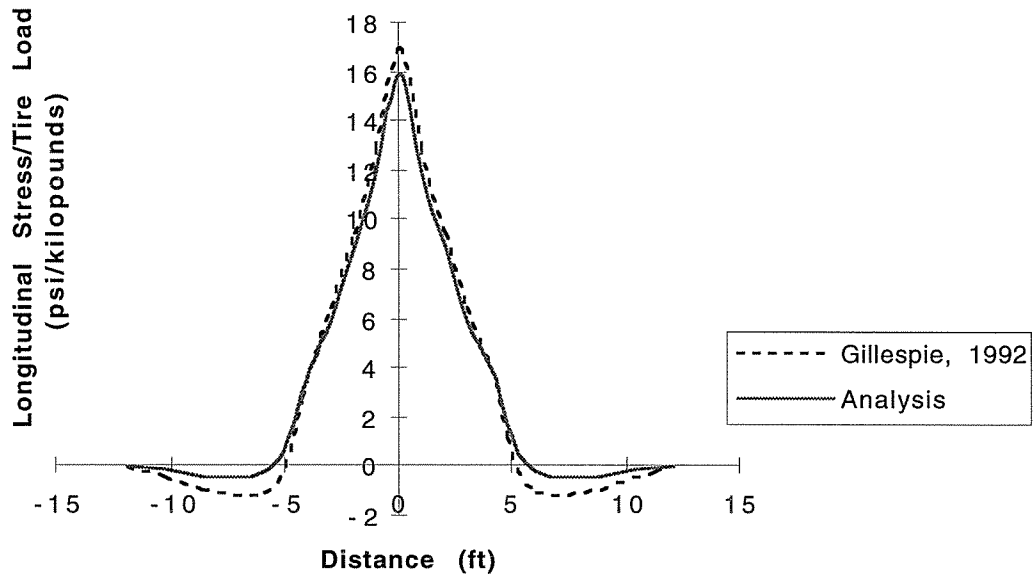


Figure 6.6: Rigid Pavement Influence Function. Longitudinal Stress at fixed point normalized with respect to tire load as a function of tire position relative to the fixed point.

The results show a good correlation between the experimental and the analytical data. The differences between the two results are at the peak stress as well as at about 5 ft removed from the wheel location in the compressive stress region. The discrepancies in the peak stress could be due to the difficulties in modeling the actual distribution of the applied load to match the experiment. While the actual load in the experiment was distributed over a certain area, the analysis used equivalent areas and loads. This anomaly in distribution of the load on an area could cause a different localized nature of stress in that area of a concrete layer, causing the peak tensile stress to differ. The discrepancies in the compressive stress is attributed to the difference in foundation characteristics between the actual test and that used in this simulation.

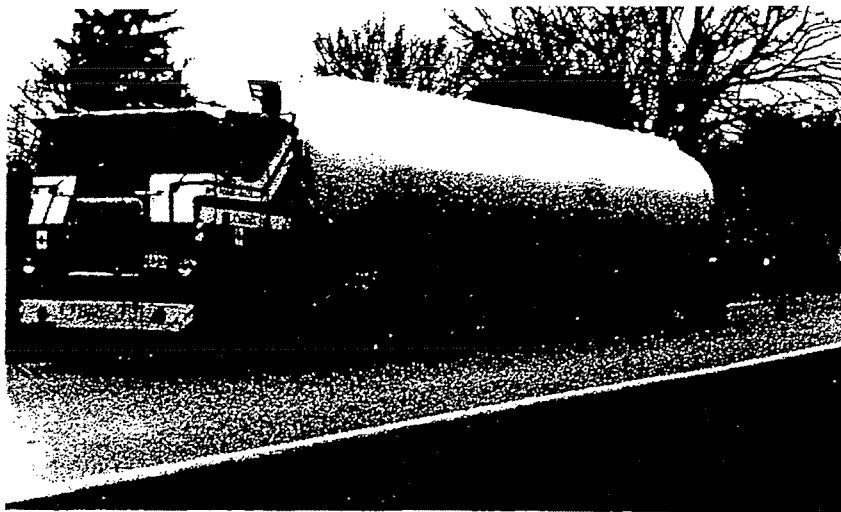
### 6.4.3. Canadian Truck Test

So far, we have predicted the pavement response (stress) in areas at or near the load. The load applied has been an equivalent single axle load applied at the center of a concrete slab, distributed on a tire-pavement contact area represented by finite elements. A quarter model of a concrete slab having symmetric boundary conditions at the ends sufficed for those analyses. This type of an analysis has given an instantaneous response of the pavement with respect to an equivalent single axle load for a given point and the amplitude of response has been found to diminish as the axle position has moved away from the load. This was demonstrated in the influence function approach in the previous example (Section 6.4.2). This approach is very useful when damage or cyclic behavior is to be studied and the progressive damage due to a single axle load is to be tracked in the highway. More of these applications will be discussed in the next Subsection. To further demonstrate the capability of our developed approach, a pavement response due to the dynamic motion of a multi-axle truck will be simulated in this subsection.

The loading and other relevant information for this Truck Test is given in Figure 6.8. A finite element mesh 3.7 m X 15.2 m (12 ft X 50 ft), with the same mesh size and properties as before, is created. The mesh is shown in Figure 6.10. The foundation is modeled by linear elastic springs with appropriate spring constants to simulate the load transfer from the foundation. The mesh, which is longer than the previous models, is created to accommodate the length of the 5-axle truck during the dynamic simulation. The experimental data has been provided by the Federal Highway Administration and the actual testing was performed at Ohio University in 1995 and 1996 (El-Gindy, 1996).

In the finite element model, the respective axle loads are applied on equivalent areas of elements. The multi-axle truck is shown in Figure 6.7. The loading applied in the test is shown in Figure 6.8 and the distribution of axle load employed in the simulation is shown in Figure 6.9. The loading ramps up from a zero value to the

maximum amplitude at the center of the tire contact area as indicated in Figure 6.9. The load transfer between the axle and the pavement occurs simultaneously for all the five axles in a given time calculated from the vehicle speed. The times marked by  $t_1$ ,  $t_2$ ,  $t_3$ ,  $t_4$  and  $t_5$  represent the time taken to load the center of the tire-pavement contact areas for the first to the fifth axle respectively. The other test conditions are shown in Figure 6.8. Figure 6.11 isolates the narrow strip of fine mesh under the load out of the finite element model and shows the undeformed plot of the strip on top and the local deformation contour plot at the bottom. Figure 6.11 shows the instantaneous deflection results comparing the simulation against the field test data.



National Research Council Canada Test Vehicle

Figure 6.7: Canadian Truck Test Description



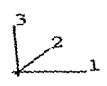
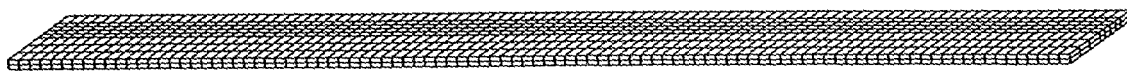


Figure 6.10: Finite Element Mesh

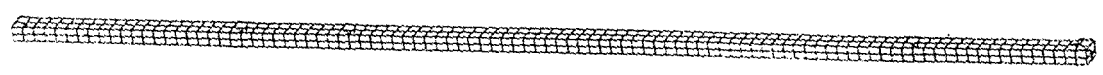
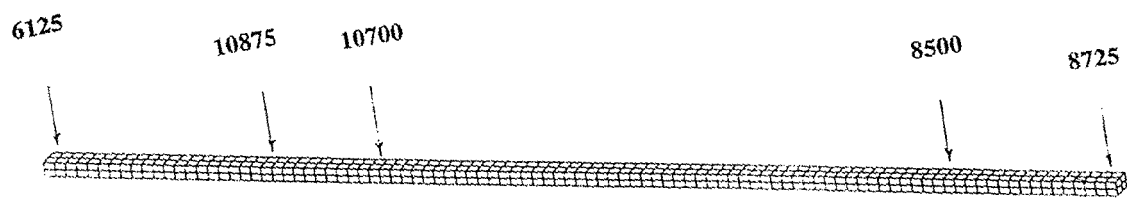


Figure 6.11: Narrow strip of the pavement under load

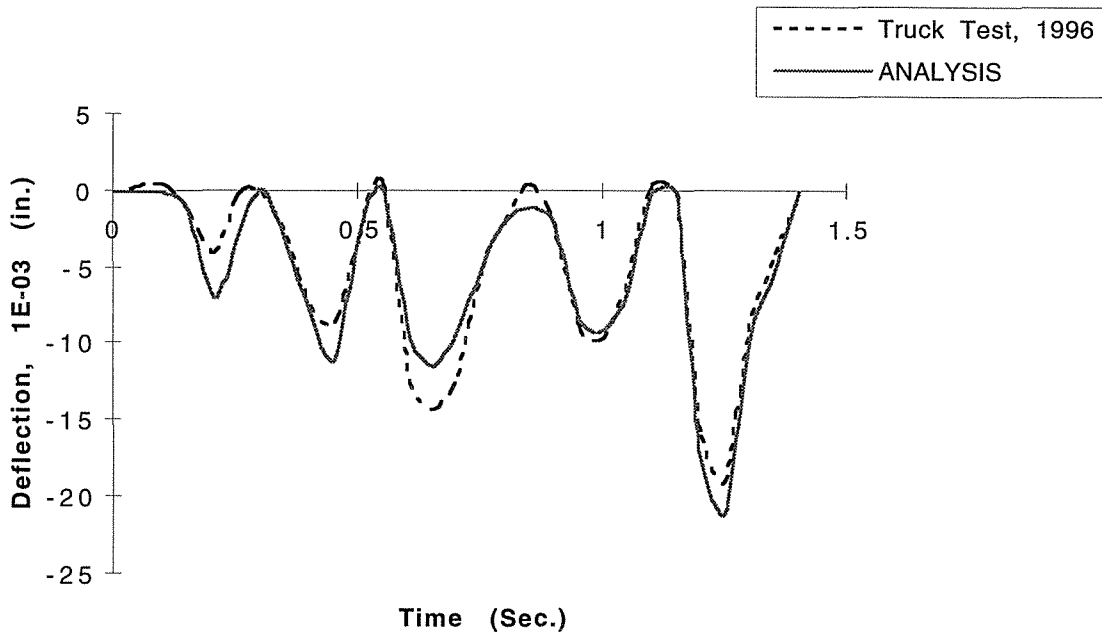


Figure 6.12: Dynamic Truck Test Simulation

Figure 6.12 shows a good correlation between the test results and analysis. In the absence of many accurate data (like foundation stiffness, contact area) the mean values from the literature (Gillespie, 1992-93; Goktan et al., 1995; Huang, 1993) were used. The differences in the peak loads could be due to the differences in the loading areas causing different localized stresses between the analysis and the test. The difference in the positive segments of the deflection curve could be attributed to that differences in the foundation stiffness as only average values for foundation stiffness were used in the analyses. As we will see in the sensitivity study in Section 6.5, the influence of the axle load on the loading area is significant, and this has to be taken into account when distributing the pressure load from the tires in order to accurately simulate the responses at the peaks.

## **6.5. Damage Distribution**

One of the key objectives of the research is to qualitatively predict the trend of damage in a concrete pavement slab. It is relevant to mention here that in the Microplane Theory which was implemented in the developed program, damage is intrinsic to its basic formulation. The developed program based on this theory keeps track of the cumulative damage (Section 3.3) for the deviatoric and in-plane components in each microplane. State Variables have been defined in the developed program for this purpose and the new values of these variables representing the direction and magnitude of material degradation is computed at each increment. These computations are taken into account in generating the final stress response. So the response at the end of any cycle is the net response taking into account all the microplane damage and deformation accumulated at the end of that cycle. To sum up, the current state of damage is implicit in the calculated response.

### **6.5.1. Damage Ratio**

As discussed earlier, damage is calculated internally in the developed program and is estimated indirectly by studying the stress (or strain) response. However, to visualize damage directly, a damage distribution parameter is defined. From previous research (Gillespie, 1992), it is known that in concrete pavements, the bottommost layer directly under the wheel is in a state of maximum tension and is the area most prone to cracking. This tensile stress in the direction of travel, is the critical response because when it reaches a threshold value, it causes cracking and damage at the bottom of the pavement.

In the developed program, cracking is modeled as tensile strain softening. We have shown and verified in Chapter 5 that with the progress of strain softening, the stress response calculated by the developed program, is fairly accurate even in the post

peak region. Thus, the damage ratio at any cycle is defined as the ratio of peak strain (denoted by 'ef') beyond which fracture due to softening (cracking) starts, to the tensile strain in the direction of travel (denoted by 'e1'). The idea behind this is to give a qualitative indication of the progressive damage with the number of cycles.

Thus Damage Ratio, which is defined in the developed program, abbreviated as SDV (stands for State Damage Variable) is expressed as:

$$SDV = \frac{ef}{e_1} \quad (6.5.1)$$

where ef is the threshold value of strain in the longitudinal direction where visible fracture starts and is obtained from the experimental work of Chen, 1988. Also, e<sub>1</sub> is the current value of strain in the longitudinal direction obtained from the analysis. A SDV value of 1.0 or more indicates that damage due to cracking has already started and a value of less than 1.0 indicates fracture is yet to occur. This Damage Ratio indicates how far the cracking (which starts at the peak value of strain) has to go to reach a state of visible fracture.

### **6.5.2. Pavement Model**

The finite element model used for the damage analysis consisted of a pavement slab of 4.6 m (15 ft) in length and 3.7 m (12 ft) in width. The finite element model of the pavement used for the analysis is same as that used previously in section 6.4.3 and is shown in Figure 6.14. A finer mesh was used near the load and a coarser mesh further away from the load as before. The boundary conditions and pavement material parameters remain the same as earlier. The loading first consisted of 5 cycles and then continues to 10 cycles. Each cycle had a load going from a zero value to a chosen peak value of 160,135 N (36,000 lb) as shown in Figure 6.13. In Figure 6.13, P<sub>max</sub> is the equivalent single axle load and t, which is the duration of loading on a contact area, is calculated from the vehicle speed. The truck axle load and parameters are taken from

Huang (1993) and Gillespie et al. (1992). The instantaneous damage distribution is indicated in Figures 6.15 and 6.16.

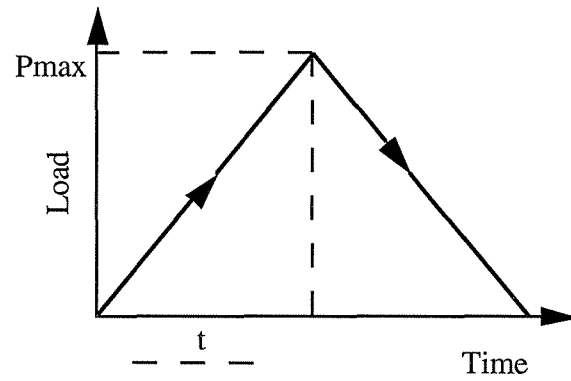


Figure 6.13: One loading cycle

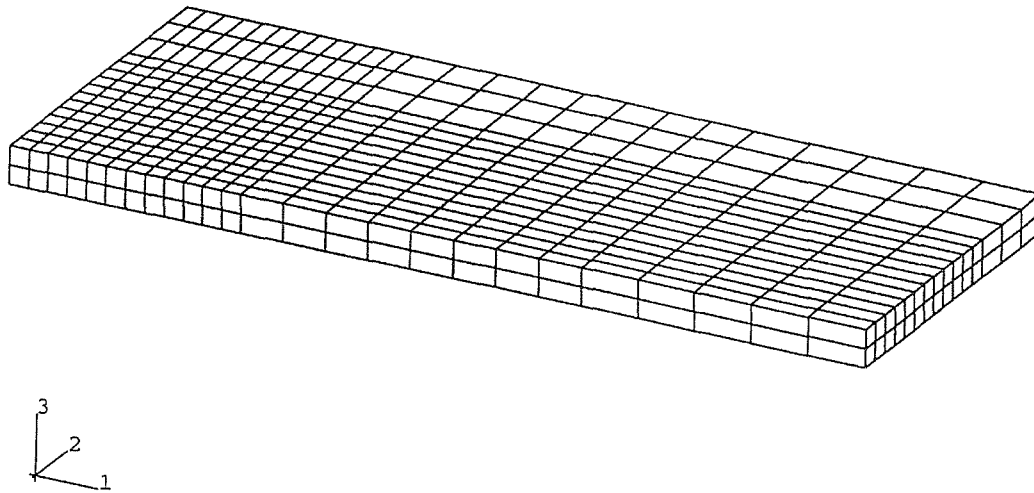
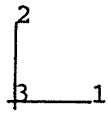


Figure 6.14: Finite Element Mesh



| SDV118 | VALUE     |
|--------|-----------|
| 0      | +2.35E-05 |
| 1      | +4.11E-04 |
| 2      | +7.89E-04 |
| 3      | +1.18E-03 |
| 4      | +1.57E-03 |
| 5      | +1.96E-03 |
| 6      | +2.35E-03 |
| 7      | +2.73E-03 |
| 8      | +3.12E-03 |
| 9      | +3.51E-03 |
| 10     | +3.90E-03 |
| 11     | +4.29E-03 |
| 12     |           |

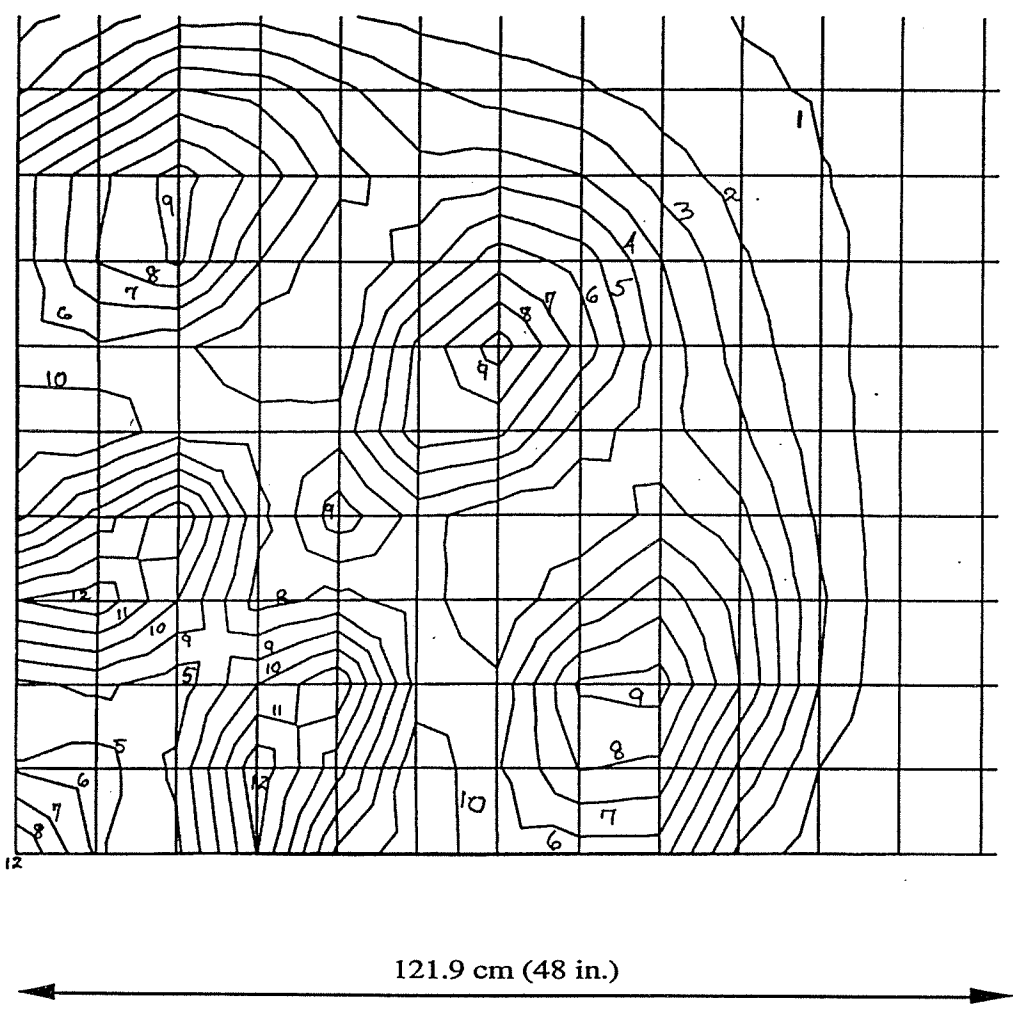
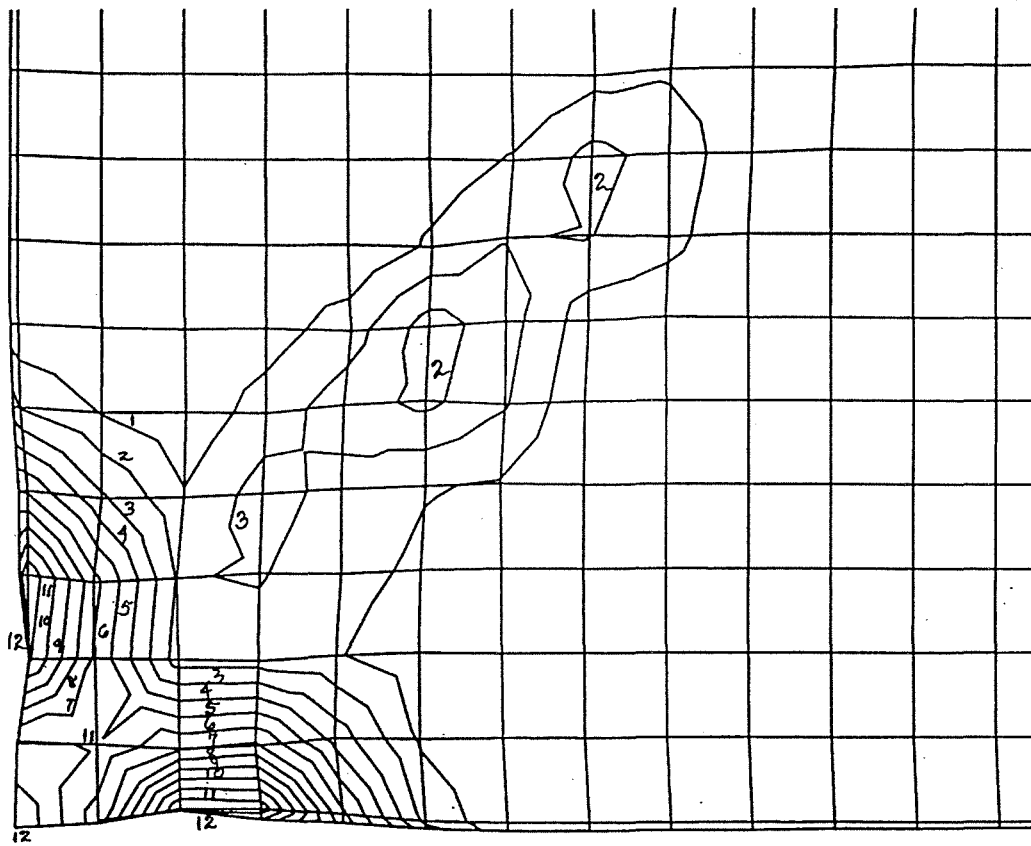
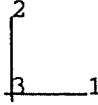


Figure 6.15: Instantaneous Damage Distribution after 5 cycles

| SDV118 | VALUE     |
|--------|-----------|
| 0      | +6.49E-02 |
| 1      | -1.10E-01 |
| 2      | -1.96E-01 |
| 3      | -2.62E-01 |
| 4      | -3.27E-01 |
| 5      | -3.93E-01 |
| 6      | -4.59E-01 |
| 7      | -5.25E-01 |
| 8      | -5.90E-01 |
| 9      | -6.56E-01 |
| 10     | -7.22E-01 |
| 11     | -7.87E-01 |
| 12     |           |



121.9 cm (48 in.)

Figure 6.16: Instantaneous Damage distribution after 10 Cycles

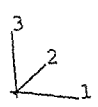
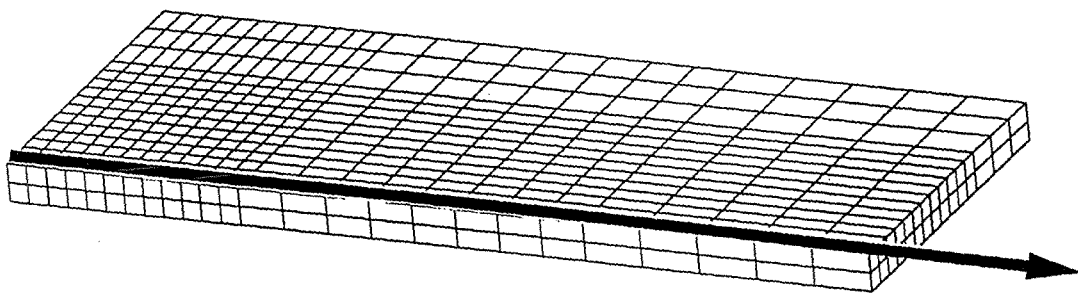


Figure 6.17: Extrapolated damage distribution along the vehicle path

The loading is carried out by repeating the cycle (Figure 6.13) at the corner of a quarter model (which is same as the center of a full model). This is supposed to represent the effect of the cyclic axle load at points near the load as a vehicle repeatedly passes over a certain area of the pavement. This is because the effect was found to be maximum at locations under the load from the influence function approach described earlier.

In the developed program, the state variables kept track of the history of stresses and strains in all microplanes up to 10 cycles. In total, 118 state variables were defined. The state variable for Damage (named as SDV-118 in Figures 6.15 and 6.16) calculated the damage ratio for each element to quantify damage. The bottom layer was identified to be the one having the most damage. Only a quarter of the slab is shown in Figures (6.15 and 6.16). These Figures show the instantaneous damage distribution for the bottom layer of the pavement.

The plots show that at any instant the damage is maximum under the load and increases from 0 to 10 cycles. Two things are noticeable in the plots. First, the instantaneous picture shows that the damage gets concentrated (indicated by damage contour lines numbered 10-12 with SDV values of 0.6 and higher) and narrowed at the corner of the quarter model (center of the full model), under the load with an increase in the number of loading cycles. In other words, the damage gets more severe under the load. Second, the damage ratio increases and approaches the fracture value of 1.0, with an increase in number of cycles and this increases in a nonlinear fashion. These plots however give an instantaneous picture for the instant when the load is at the corner of the quarter model (center of the full model). As the load moves, the locations of maximum damage move along with the load in the direction of travel and for vehicles traveling over the entire length, the damage gradually ends up being the maximum along the line of travel (that is, along the end for the quarter model or along the centerline for the full model). This fact is corroborated by experimental data (Gillespie, 1992 and

Cebon, 1993). Figure 6.17 shows the extrapolated distribution as the vehicle load has traveled over the pavement.

### **6.5.3. Damage Sensitivity Study**

The damage due to a tensile state of stress or strain response at the bottom layer of a slab of concrete pavement under the axle load, increases with each cycle and initiates cracking and fracture in the highways. There are factors that influence this response and cause damage. Highway engineers need to consider these factors for highway design and maintenance. There are factors on the vehicle side as well as on the pavement side to be discussed within the scope of this research.

On the vehicle side, the axle load is an important factor. The Damage Distribution analysis shown in the previous Section (6.5) was performed with respect to an equivalent single axle load. For a multi-axle truck, the distribution of load varies from axle to axle. This variation in axle loading influences the instantaneous distribution of stresses at the bottom layers. Additionally, in a multi-axle vehicle, the load is transferred to the pavement via the tires. Because of the different axle loads and tire conditions (e.g. tire pressure, age of the tire on different axles, tread etc.), the tire-pavement contact area will vary as well as the axle load.

On the pavement side, pavement thickness is a variable which the designers can change depending on the optimum structural and financial constraints dictated by project requirements. This slab thickness varies from one place to another. Moreover, depending on the process of manufacturing, the properties of the concrete material varies and the elastic modulus varies also. Finally, the characteristics of the foundation on which the pavement slab is placed can vary from one highway to another, and this can be a variable also influencing fatigue induced damage.

To sum up, for continuous concrete pavements, there are 5 parameters of importance in the design of a pavement slab (Gillespie, 1992). They are axle load, tire-

pavement contact area, pavement thickness, elastic modulus of the PCC, and the foundation stiffness.

A Taguchi sensitivity study was conducted to identify the relative contribution of these various parameters to a high value of tensile stress ( $\sigma_{11}$ ) in the direction of travel which is the primary cause of cumulative damage. The analysis was run for five complete cycles in the same manner as in the previous section. Table 6.6.1 shows the factors used in the Taguchi Method. The layout and results are shown in Table 6.6.2. Table 6.6.3 shows the average effect of the variables using Taguchi's  $L_8$  array. In Table 6.6.3, 'Sum 1' for any factor refers to the sum of the stress results for the runs which used level 1 values, 'Sum 2' refers to the same for the level 2 values and 'Avg. 1' and 'Avg. 2' refer to their corresponding average values. Figure 6.18 shows the same effects of Table 6.6.3 in a graphical form. For example, the line E1-E2 spans the maximum length along the vertical stress axis showing its maximum influence on longitudinal stress (tensile stress at the bottom of the layer, under the applied load).

| Symbols | Factors                               | Level 1<br>Values | Level 2<br>Values |
|---------|---------------------------------------|-------------------|-------------------|
| P       | Magnitude of the load<br>(kilopounds) | 36                | 27                |
| A       | Tire Contact Area (sq. in.)           | 64                | 48                |
| t       | Foundation Thickness (in.)            | 8                 | 6                 |
| K       | Foundation Stiffness                  | 0.20              | 0.15              |
| E       | Young's Modulus                       | 4.0E-3            | 3.0E-3            |

Table 6.6.1: Factors used in the Taguchi Method

Using the Taguchi method, once the Orthogonal Array is set up, Analysis of variation (ANOVA) is performed with respect to a cyclic loading. This ANOVA establishes the relative significance of the individual factors and the interaction effects. Following the previously outlined steps, we have the percentage contribution of various factors represented in Table 6.6.4.

| (1)<br>Axle Load<br>P | (2)<br>Contact Area<br>A | (3)<br>P*A | (4)<br>Pavement<br>Thickness<br>t | (5)<br>Found.<br>Stiffness<br>K | (6)<br>A*t | (7)<br>Elast.Mod<br>E | Stress<br>$\sigma_{11}$ |
|-----------------------|--------------------------|------------|-----------------------------------|---------------------------------|------------|-----------------------|-------------------------|
| 1                     | 1                        | 1          | 1                                 | 1                               | 1          | 1                     | .8                      |
| 1                     | 1                        | 1          | 2                                 | 2                               | 2          | 2                     | .4                      |
| 1                     | 2                        | 2          | 1                                 | 1                               | 2          | 2                     | .6                      |
| 1                     | 2                        | 2          | 2                                 | 2                               | 1          | 1                     | .7                      |
| 2                     | 1                        | 2          | 1                                 | 2                               | 1          | 2                     | .6                      |
| 2                     | 1                        | 2          | 2                                 | 1                               | 2          | 1                     | .6                      |
| 2                     | 2                        | 1          | 1                                 | 2                               | 2          | 1                     | .6                      |
| 2                     | 2                        | 1          | 2                                 | 1                               | 1          | 2                     | .4                      |

Table 6.6.2: Layout and Results

|   | Factors                  | Sum 1 | Sum 2 | Avg. 2 | Avg. 1 | (Avg. 2 - Avg. 1) |
|---|--------------------------|-------|-------|--------|--------|-------------------|
| 1 | Axle Load (P)            | 2.5   | 2.2   | .625   | .55    | .075              |
| 2 | Contact Area (A)         | 2.4   | 2.3   | .6     | .575   | .025              |
| 3 | Interaction 1 (P*A)      | 2.2   | 2.5   | .54    | .625   | .085              |
| 4 | Pavement Thickness (t)   | 2.6   | 2.1   | .65    | .525   | .125              |
| 5 | Foundation Stiffness (K) | 2.4   | 2.3   | .6     | .575   | .025              |
| 6 | Interaction 2 (A*t)      | 2.4   | 2.2   | .61    | .55    | .06               |
| 7 | Young's Modulus (E)      | 2.7   | 2.0   | .675   | .5     | .175              |

Table 6.6.3: Average Effects of the variables

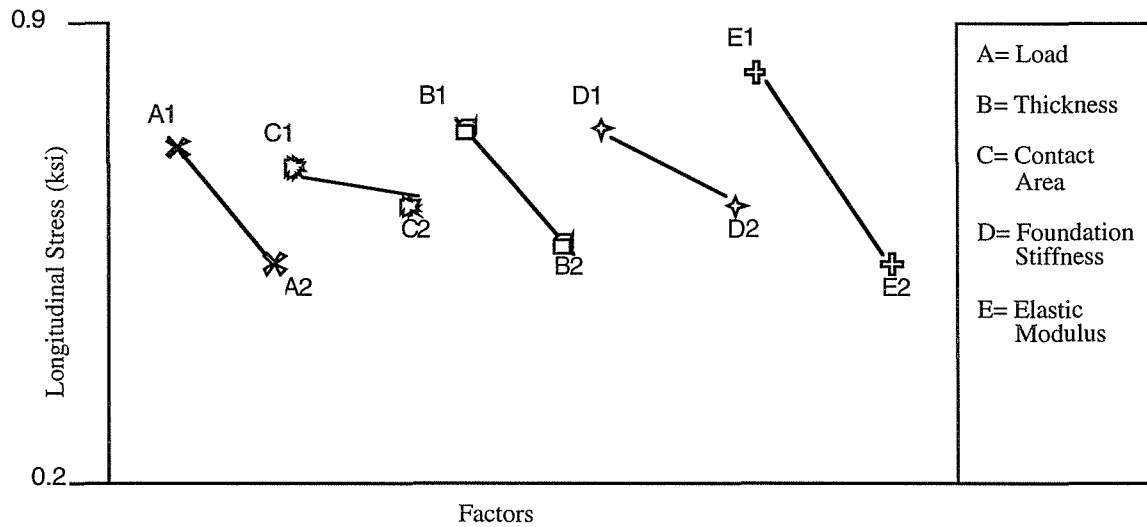


Figure 6.18: Main Effects in Cyclic Loading

| Factors                 | P (%) |
|-------------------------|-------|
| Load Magnitude          | 10    |
| Contact Area            | 1     |
| Interaction 1           | 8     |
| Thickness               | 24    |
| Foundation<br>Stiffness | 1     |
| Interaction 2           | 0     |
| Young's Modulus         | 48    |
| Other                   | 7     |
| Total                   | 100   |

Table 6.6.4: ANOVA Table (Cyclic Loading)

Table 6.6.4 shows that the elastic modulus has the greatest effect. That is, the degradation in stiffness is most sensitive to the elastic modulus. The thickness of the slab has the next most significant effect. The magnitude of the load and the interaction 1 (the combined effect of the load acting on a small or large contact area) have the next greatest influence on the tensile response. A large load applied on a smaller area increases the stress response and the probability of damage.

As seen from the above tables, the stress response was rather insensitive to the foundation stiffness as stress is very localized and changing the foundation stiffness uniformly under the pavement does not cause a major effect. The Table 6.6.5 summarizes the relative importance of the parameters.

| For Damage Growth                                          | Cyclic Loading                                                                                                                |
|------------------------------------------------------------|-------------------------------------------------------------------------------------------------------------------------------|
| Arranged in<br>Decreasing order of<br>influence of factors | Young's Modulus<br>Pavement Thickness<br>Equivalent Vehicle Load<br>Tire-Pavement Contact Area<br>Stiffness of The Foundation |

Table 6.6.5: Relative Importance of parameters to damage growth

## 6.6. Summary

In this chapter, first a concise description of the principles used in modeling the pavement and its supporting foundation was given. The response from the developed program was then validated with both problems from the literature (Subsection 6.4.1) as well as actual dynamic tests (Sections 6.4.2 - 6.4.3).

The course of damage in a slab of concrete pavement layer is then predicted. A qualitative damage growth from zero to five and up to ten cycles of dynamic loading was determined. This was represented in the instantaneous damage plots describing the state of accumulated tensile strain with respect to the strain at fracture. The factors responsible for accelerating damage was highlighted with the aid of a sensitivity approach.

Prior to this work, no numerical model was in existence that could accurately predict dynamic pavement response or even qualitatively predict the directional growth of damage in plain concrete pavements. The numerical approach developed in this work provides a valuable tool to guide designs by emphasizing a scientific basis for consideration of the specific factors that can trigger a high degree of tensile stress and cumulative damage in a pavement.

The work in this dissertation has been limited to ten cycles of loading due to available computational resources. However, the approach is directly applicable for predicting the performance of a pavement due to a large number of loading cycles, and only requires, the use of additional computer resources. Based on the rapid improvements in computer technology, such resources should be readily available in the not too distant future. Accordingly, this work has tremendous potential to impact the design of pavement in the future.

# Chapter 7. Joint Design

## 7.1. Introduction

So far in this dissertation, the response of a plain concrete pavement has been discussed. However, in the highways, the concrete pavements may have joints and these joints can be either transverse or longitudinal joints with or without reinforcements. The focus of this chapter is the design and analysis of Transversely Jointed Pavements. This chapter discusses the sensitivities of the various pavement joint parameters with respect to the tensile stress at the bottom of the pavement using the Taguchi Method. Additionally, using our numerical approach, a method of calculating joint stiffness, which is an useful parameter in pavement joint design, is implemented. Predicting the dynamic response of a jointed pavement is novel and this response has never been simulated before under dynamic loading.

## 7.2. A Typical Joint

Joints are designed in concrete pavements to prevent premature cracking. Among the four types of joints (contraction, expansion, construction, and longitudinal) in common use in the highways, our focus is the contraction joint. Contraction joints are basically a type of transverse joint designed to relieve tensile stresses in concrete. The important parameters in this type of a joint design are i) Joint width, ii) Depth of the dowels in the joint, iii) Dowel spacing, and iv) Dowel diameter.

Figure 7.1 describes the specifications for a typical contraction joint. Along with the joint parameters, slab length is a parameter of importance. The currently practiced rule of

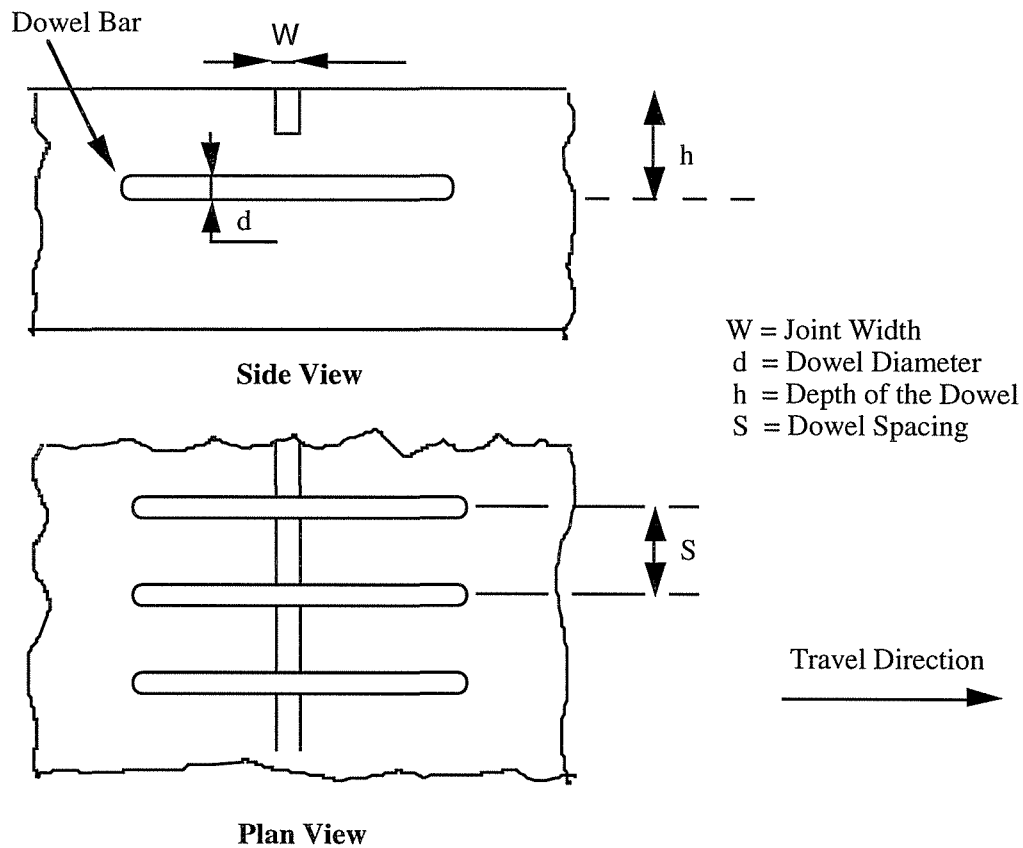


Figure 7.1: A typical Joint

thumb (Huang, 1993) is to use a joint spacing which is 24 times the slab thickness. AASHTO (1986) guidelines specify that the slab length should not to exceed 1.25 times its width for designing these types of joints. These starting values are used in our approach.

### 7.3 Pavement Response Under Dynamic Loads

To simulate traffic loading on the pavement, a time-varying dynamic load is applied on the jointed concrete pavement and the response of the pavement joint is studied.

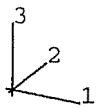
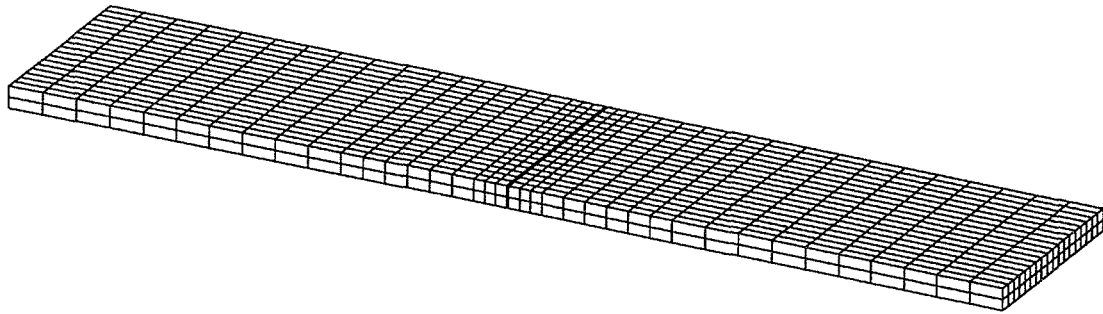


Figure 7.2: Finite Element Model of the Jointed Pavement

The pavement is modeled with brick type 8 noded finite elements, and the foundation with spring elements as before. The finite element mesh is shown in Figure 7.2. The joint simulated in our model is doweled, and it is modeled by beam elements connecting the brick elements on either side of the joint. The beam elements are placed at the middle of the pavement thickness. The dowel dimensions are calculated as discussed in Section 7.4. The set of bottom nodes of the two slabs on either side of the joint, are rigidly connected to each other representing load transfer through the slabs due to aggregate interlocking at the bottom (Huang, 1993).

To simulate the load transfer from the vehicle onto the pavement, the area representing the pavement-tire contact patch is represented on the jointed plain concrete pavement by an equivalent amount of element surface area on top, distributed equally on the elements which are on located on both sides of the joint. Loading, in the form of distributed pressure is allowed to gradually build up from 0 to 160,135 N (0 to 36,000 lb) on this surface area, representing the wheel-pavement contact patch, and the

amplitude ramps up to the peak value and then decreases down to zero to complete a cycle. The duration of the loading ( $t$ ) has been calculated from the tire-load contact patch length and vehicle speed. Load vectors are then longitudinally moved (along the direction of travel) to the next set of finite elements to represent the vehicle passing over the joint. An explicit algorithm as discussed in Subsections 4.5-4.7 is employed for the analysis. Before continuing the analysis any further, appropriate dowel dimensions are chosen from the considerations as described in the next section.

## **7.4. Dowel Design**

Dowels transfer the load across a transverse joint in two adjoining slabs. Design of dowels is still based on experience (Huang, 1993). The Portland Cement Association (PCA 1975,1991) have provided recommendations for selecting dowel parameters like diameter, spacing and length etc. These recommendations are based on a conservative estimate and Appendix D includes a table summarizing the data. To begin the analysis, the recommended values are selected.

When calculating the minimum diameter of the dowels, it is noted that the contraction joints are assumed to withstand the tensile stresses occurring as a result of the volume change in concrete due to factors like decreases in temperature, etc. The concrete moves to the center from both ends causing the doweled joint to be in tension. The frictional stresses developed between the concrete slab and the subgrade oppose the motion of the slab as shown in Figure 7.3. The minimum dowel diameter required can be calculated from this assumption (Huang, 1993).

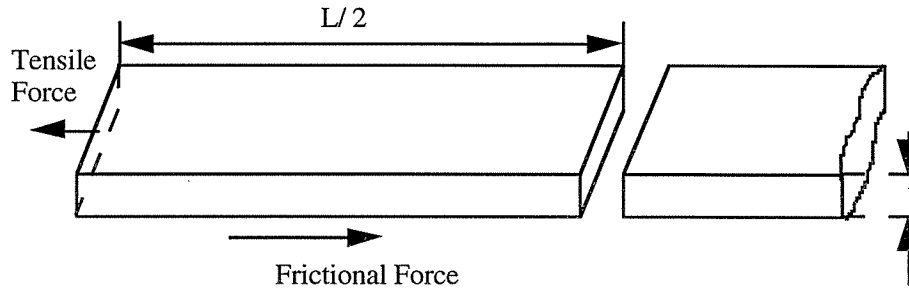


Figure 7.3: Pavement slab under tension

Therefore, equating frictional force per unit width of the slab to the tensile force ( $\sigma_c t$ ):

$$\gamma_c t \mu \frac{L}{2} = \sigma_c t \quad (7.4.1)$$

or,

$$\sigma_c = \frac{\gamma_c L \mu}{2} \quad (7.4.2)$$

where:  $\gamma_c$  = Unit weight of concrete,  $t$  is the pavement thickness,  $\mu$  is the average coefficient of friction,  $L$  is the slab length,  $\sigma_c$  is the stress in the concrete,  $\sigma_a$  is the allowable stress in the steel, and  $A_s$  is the cross section of steel required/per unit width. When (steel ) dowels are used, it is assumed that they carry the tensile stresses  $\sigma_s$ , so if  $A_s$  is the steel cross section area per unit width, then by replacing  $\sigma_c t$  by  $A_s \sigma_s$  above, we have:

$$A_s = \frac{\gamma_c t \mu L}{2 \sigma_s} \quad (7.4.3)$$

For a 3.6 m (12 ft ) wide slab, the minimum cross section required for the steel dowels to satisfy the thermal requirements is then calculated from eqn. 7.4.3 to be 2.0E-4 m<sup>2</sup> (0.35 in<sup>2</sup>).

We chose 2.4 E-4 m<sup>2</sup> (0.375 in<sup>2</sup>), a value close to the calculated value from Appendix D, and with this starting value, the design requirements under a traffic load is studied. The effect of dowel spacing on peak longitudinal tensile stress which causes cracking, will also be analyzed to guide dowel design.

## **7.5. Jointed Pavement Response**

The simulation is carried out through a two step process. The first part of the simulation is for the instant when the vehicle is directly over (hitting) the joint and the second step is the instant when the vehicle is passing over it. In both the cases, dowel spacing is varied from 0.3 m to 0.9 m (1 ft to 3 ft) and the longitudinal response at the bottom of the pavement is calculated. The two cases are discussed below.

### **7.5.1 Loading Onto The Joint**

In the first step, the resultant single axle load is distributed over a loading area on the joint modeled by a group of three dimensional brick type finite elements whose constitutive law at each integration point, is defined by our developed program. The program, as discussed in Chapter 5, is based on the Microplane Theory. Because of the presence of the joint, the pressure is scaled so that the product of the pressure and the contact area gives the equivalent load of 160135 N (36,000 lb). The finite element mesh used here is same as described in Section 7.3 (Figure 7.2). The deformed plot (longitudinal cross sectional view) is shown in Figure 7.4. The results are shown in Table 7.5.1. For clarity, deformation is magnified in the plot.

### **7.5.2 Loading Adjacent To The Joint**

Here the instant when the vehicle has just passed over the joint and is on the area next to the joint is simulated. This case, as we will see in section 7.8, will be used to calculate the stiffness of the joint. The deformed plot (longitudinal cross sectional view) is shown in Figure 7.5. The results are represented in Table 7.5.2.

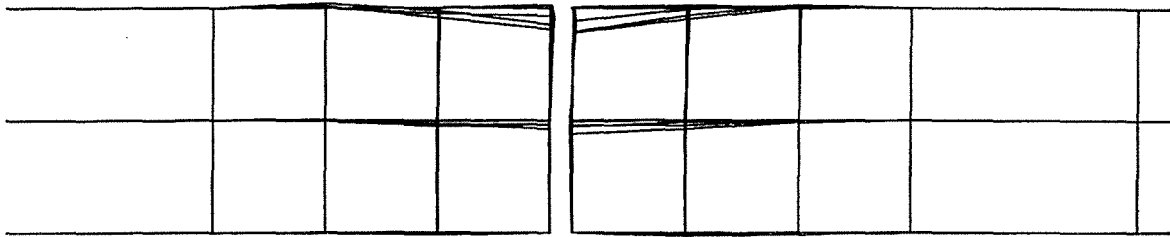


Figure 7.4: Deformed plot: Loading on the joint

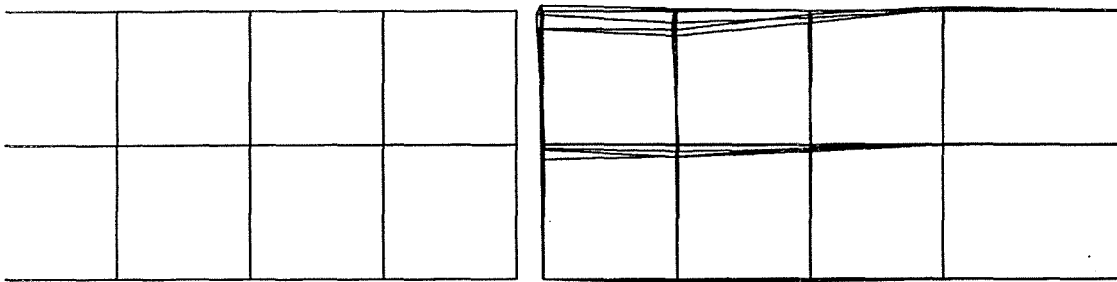


Figure 7.5: Deformed Plot: Loading next to the joint

| RESPONSE UNDER CYCLIC LOADING |                          |            |               |      |      |
|-------------------------------|--------------------------|------------|---------------|------|------|
| Response Calculated           |                          |            | Dowel Spacing |      |      |
|                               |                          |            | 1 ft          | 2 ft | 3 ft |
| In<br>Concrete<br>Pavement    | Peak Stress (psi)        | Tensile    | 15.0          | 17.0 | 17.0 |
|                               |                          | Shear      | 5.0           | 6.0  | 6.0  |
|                               | Max. Deflection<br>(E-4) | Under Load | 2.9           | 3.1  | 3.1  |
| In Steel                      | Dowel Force (psi)        | Near Load  | 556           | 562  | 562  |

Table 7.5.1: Load On The Joint

| RESPONSE UNDER CYCLIC LOADING |                          |            |                       |      |      |
|-------------------------------|--------------------------|------------|-----------------------|------|------|
| Response Calculated           |                          |            | Average Dowel Spacing |      |      |
|                               |                          |            | 1 ft                  | 2 ft | 3 ft |
| In<br>Concrete<br>Pavement    | Max. Stress (psi)        | Tensile    | 16.0                  | 16.6 | 16.6 |
|                               |                          | Shear      | 9.62                  | 9.63 | 10.0 |
|                               | Max. Deflection<br>(E-4) | Under Load | 4.3                   | 4.4  | 4.4  |
| In Steel                      | Dowel Force (psi)        | Near Load  | 11                    | 12   | 13   |

Table 7.5.2 : Loading Next to the Joint

### 7.5.3. Discussion

The following points can be noted here:

- First, with an increase in the dowel spacing from 0.6-0.9 m (2-3 ft), the maximum tensile stress in concrete does not change after the end of one cycle for either of the cases analyzed.
- As the vehicle passes over the joint, the longitudinal (tensile) stresses at the bottom of the pavement are lower than when the vehicle is directly over the joint (hitting the joint), as the load transfer to both sides of the joint is facilitated by a direct loading of the joint. The longitudinal tensile stresses decrease slightly when the vehicle has already passed over the joint. This effect is verified from the experimental observations of Gillespie (1993a,b) and Huang (1993).
- The shear stresses in concrete at the bottom increase when the vehicle is next to the load as compared to that case when vehicle is directly above it.
- The deflections increase only slightly with an increase in dowel spacing. This is observed both when the loading is directly over the joint as well as adjacent to it. However, the deflection increases by more than 25 % when the loading is next to the joint as compared to the instant when vehicle directly hits the joint. The shear forces in concrete also increase by a similar margin. For, calculating joint stiffness, as will be done later, the deflections are taken into account for the instant when loading is next to the joint, fully on one slab.
- The dowels are assumed to take the tensile stresses, and the cross-sectional forces through them only increase marginally with an increase in dowel spacing and decrease considerably as the vehicle passes from one slab to the other.

- The study can be extended to 10 cycles of traffic loading as the vehicle passes from one cycle to the other using the same approach.

## **7.6. Taguchi Sensitivity Study**

A sensitivity study to identify the critical joint design parameters for a jointed pavement under cyclic loading is performed. Table 7.6.1 summarizes the conditions examined which influence the design. The values are selected based on the following points.

- Both the longitudinal stress (along the direction of travel) and the dowel section force are higher when the vehicle hits the joint. So loading directly on the joint represents the worst scenario.
- An increased dowel spacing is desirable from a cost savings point of view, so the two cases of 0.6 m (2 ft) and 0.9 m (3 ft) spacing are studied.
- Joint width varies from 2.5 to 20.3 mm (0.1 in to 0.8 in) with 20.3 mm (0.8 in) being the worst case.
- A dowel diameter of 20 mm (0.75 in) was chosen for our study from Appendix D.
- Dowel Depth to start with was chosen as half the pavement thickness.

The results of the sensitivity analysis involved eight sets of runs and are tabulated in 7.6.2. In all the tables, S11 refers to the maximum tensile stress in concrete and SF1 is the cross-sectional force in the dowel.

| Factors        | Level 2 (in) | Level 1 (in) |
|----------------|--------------|--------------|
| Joint Width    | .8           | .5           |
| Dowel Diameter | .75          | .5           |
| Dowel Spacing  | 3            | 2            |
| Dowel Depth    | 4            | 2.7          |

Table 7.6.1: Pavement Factors

| Case No. | Taguchi Orthogonal Array ( $L_8$ ) |            |             |             | Results                   |                  |
|----------|------------------------------------|------------|-------------|-------------|---------------------------|------------------|
|          | Joint Width                        | Dowel Dia. | Dowel Spac. | Dowel Depth | S11 ( $\times 10^3$ psi ) | SF1 (kilopounds) |
| 1        | 1                                  | 1          | 1           | 1           | 2.14                      | 0.867            |
| 2        | 1                                  | 1          | 1           | 2           | 1.76                      | 0.506            |
| 3        | 1                                  | 2          | 2           | 1           | 2.69                      | 1.385            |
| 4        | 1                                  | 2          | 2           | 2           | 2.04                      | 0.735            |
| 5        | 2                                  | 1          | 2           | 1           | 2.00                      | 0.56             |
| 6        | 2                                  | 1          | 2           | 2           | 1.53                      | 0.331            |
| 7        | 2                                  | 2          | 1           | 1           | 2.47                      | 1.02             |
| 8        | 2                                  | 2          | 1           | 2           | 1.71                      | 0.601            |

Table 7.6.2: Results from the Analyses

The next step involved is the calculation of the statistical analysis of variation (ANOVA). The commercial software Minitab (1992) is used. The results are listed in Table 7.6.3.

| Factors        | P (%) |
|----------------|-------|
| Joint Width    | 10    |
| Dowel Diameter | 26    |
| Dowel Spacing  | 1     |
| Dowel Depth    | 60    |
| Error          | 3     |
| Total          | 100   |

Table 7.6.3: ANOVA Calculation

## 7.7. Discussion of the Results

The ANOVA Table 7.6.3, shows that the dowel depth is the most important factor in controlling pavement joint design. The bottom layer of the pavement is in tension. Lowering the dowels (increasing dowel depth), puts the dowels in the layer of pavement to take up tensile load, thus lowering longitudinal stress by transferring the load on the other slab and increasing pavement life. Dowel geometry (diameter, cross section) is the second most important factor affecting a build up of the longitudinal stresses in cyclic loading. Joint width is the next most important factor. An increase in joint width decreases load transfer. The fact that dowel spacing is insignificant should be

judged in the context that dowel spacing was changed from 0.6 m to 0.9 m (2 ft to 3 ft). Earlier it was recognized in Table 7.5.2, that the longitudinal (tensile) stress increases with the decrease in dowel spacing. This is due to reduced load transfer from one slab to another, until a spacing of 0.6 m (2 ft) is reached at which point the change in magnitude of the longitudinal stress becomes steady. Accordingly, increasing dowel spacing does not contribute significantly.

## 7.8. Joint Stiffness Study

The stiffness of a joint can be calculated from the dynamic analyses presented in Section 7.5. A dowel spacing of 0.6 m (2 ft) is chosen and the same load is distributed dynamically on the elements next to the joint as before. This represents the case when the vehicle has just crossed the joint and is now completely on one slab as in Section 7.5. Following the definition of Huang (1993), the stiffness of a joint can be represented by a shear spring constant  $C_w$  and a moment spring constant  $C_\theta$  as,

$$C_w = \frac{F_s}{\Delta U} \quad (7.8.1)$$

where  $C_w$  is the shear spring constant of the joint,  $F_s$  is the average shear force per unit length of the joint and  $\Delta U$  is the difference in deflections between the two slabs. The moment spring constant  $C_\theta$  is defined as

$$C_\theta = \frac{M}{\Delta\theta} \quad (7.8.2)$$

where  $M$  is the moment per unit length of the joint and  $\Delta\theta$  is the difference in rotations between two slabs.

The procedure to calculate the joint stiffness is similar to that performed by Chou et al. (1978, 1982) and Huang (1993). The vertical shear forces are measured at the two end nodes of each dowel represented by a beam element, and the mean value of those

shear forces per unit length of the joint is calculated. The vertical deflection is measured at each end of the dowel element and the mean value along the length of the joint is obtained from the results to calculate  $\Delta U$ . The shear spring constant is then calculated from equation 7.8.1.

The moment spring constant is calculated in a similar fashion. However, the moment per unit length of the joint between the two slabs is found to be insignificant and hence the moment spring constant is found to be close to zero. This is corroborated by the research of Ball and Childs (1975) and Huang (1993).

The results from the analyses are compared with the theoretical results based on the work of Huang (1993). The shear spring constant is represented by the following equation

$$C_w = \frac{1}{S_b \left( \frac{z}{GA} + \frac{2 + \beta z}{2\beta^3 E_d I_d} \right)} \quad (7.8.3)$$

where  $S_b$  is the dowel spacing,  $z$  is the joint width,  $E_d$  is the elastic modulus of the dowel,  $I_d$  is the moment of inertia,  $G$  is the shear modulus and  $A$  is the area of the dowel. Also,  $\beta$  is given by the equation

$$\beta = \sqrt[4]{\frac{Kd}{4E_d I_d}} \quad (7.8.4)$$

where  $K$  is the modulus of dowel support, a constant whose mean value is 245.25 GN/m<sup>3</sup> (0.9E06 lbs/in<sup>3</sup>), and  $d$  is the diameter of the dowel. Thus, using the appropriate numbers, the theoretical value of the shear spring constant is calculated using equation 7.8.3 as shown

$$C_w = \frac{1}{24 \left( \frac{0.8}{11 \times 10^6 \times 0.44} + \frac{2 + 0.7 \times 0.8}{2 \times 0.7^3 \times 30 \times 10^6 \times 0.015} \right)} \text{psi} \quad (7.8.5)$$

or, 
$$C_w = \left( \frac{1}{24(0.165 + 8.2928)10^{-6}} \right) \text{psi} \quad (7.8.6)$$

This finally gives,  $C_w$  to be equal to 33.96 MN/m<sup>2</sup> (4926 psi) and this value is listed in Table 7.8.

|                   | $C_w$ (X 10 <sup>3</sup> psi) | $C_\theta$ (lb/deg) |
|-------------------|-------------------------------|---------------------|
| Theory            | 4.926                         | ~ 0.0               |
| Developed Program | 4.436                         | ~ 0.0               |
| Difference (%)    | 9.0                           | 0.0                 |

Table 7.8: Joint Stiffness Comparison

The results from the Developed Program are compared with the theory in Table 7.8. The results show a good comparison between the theory and the analysis using the Developed Program. The theory uses the average values of the material constants like the modulus of dowel support (K), and equivalent static axle loading. The difference could be attributed to that as well as the dynamic nature of loading employed in the Developed Program. However, the approach used in this research is a superior one for the following two reasons.

First, the theory is not expected to give accurate results for a pavement subjected to dynamic loading as the underlying theory is based on static consideration (Huang, 1993). Second, it can be concluded from equation 7.8.6, that the deformation of concrete actually determines the spring constant of the joint as the term relating to the deformation of dowel is 9.4 E-4 m/N (0.165 in/lb) while that relating to the

deformation of concrete is  $473.5E-4$  m/N (8.293 in/lb). Thus, the micromechanics based approach used in the Developed Program is better at capturing concrete characteristics. Accordingly, the stiffness computed using this approach is expected to be more accurate.

## **7.9. Summary**

In this chapter, the response of a transversely jointed pavement was studied. The analysis was broken down into two cases. First, the vehicle (represented by an equivalent axle load) being directly over the joint and the next being the vehicle passing over the joint. The relative differences in the responses of the two cases were illustrated for the first time using simulations.

The transverse joint analyzed was also doweled and the various dowel parameters which are important in designing transverse joints were discussed with a Taguchi sensitivity study. For the first time, the contributions of these parameters in influencing a dynamic response is detailed by the use of an analytical program developed in this research. The dowel depth is the most critical parameter contributing to the level of stress in the jointed pavements. The various cases illustrated in this chapter could be extended to a variety of loading and transverse joint descriptions.

## **Chapter 8. Conclusions and Recommendations for Future Research**

### **8.1. Contributions of this Thesis**

At the beginning of Chapter 1, the need for studying a concrete pavement behavior under traffic loading was recognized. It was pointed out that the prediction of a pavement response through analytical means was more efficient. A literature survey was conducted and it showed a dearth of analytical models available both in the academic and commercial arena (Chapter 2), that could predict a dynamic response accurately.

The literature search also identified the Microplane Theory (Chapter 3) as the one best suited to capture the typical features of concrete. But that theory had never been implemented before in a highway environment. Accordingly, the Microplane Theory was implemented in a developed program for the first time in a 3-D finite element code in Chapter 4. The results from the developed program were verified with known results, both experimental and analytical, from the literature in Chapter 5.

The approach developed in this research was then used to simulate dynamic loading of pavement successfully. In particular, the analysis correlated well with dynamic test data from the Canadian Truck Test conducted in Ohio (Section 6.4). The model was exercised first for 5 cycles and then up to 10 cycles of loading and the pattern of response was characterized (Chapter 6). The progressive damage for a pavement slab was qualitatively estimated and its distribution due to cyclic loading was represented in contour plots (Section 6.5) showing damage in different areas of the pavement layer. This has never been simulated before. Specifically, the damage growth from 5 to 10 cycles in the bottom layer of the pavement was compared and was characterized by an increase in the value of damage ratio as well as by a concentration in the distribution of damage under the load.

A sensitivity study identified the sensitive parameters in pavement critical to the longitudinal stress causing damage (Section 6.5). This could be used as a novel tool to guide the design of plain concrete pavements. It was determined that the elastic modulus is the most significant parameter followed by pavement thickness, vehicle load, contact area and the foundation thickness.

Finally, in Chapter 7, a jointed pavement was studied and the dynamic response of a pavement, as the axle passes over the joint, was broken down into two phases. The first phase response was categorized as 'loading on the joint' and the next phase as 'loading next to the joint'. The responses in both were analyzed to understand the mechanism of load transfer through the joints, under dynamic loading per cycle of single axle loading. This was followed by a sensitivity study that classified and ranked the sensitive joint parameters according to their damage potential. Finally, a novel method of calculating joint stiffness was described. It was determined that this approach developed in this research is a method superior to the available methods in the literature and could be used as an useful tool to guide joint designs in the highways.

The above examples demonstrated the various capabilities of the developed state-of-the-art-approach and no other existing code can perform similarly in guiding a pavement design. This is a major contribution for the following reasons. First, this is the first time that the Microplane Theory, which is applicable to any type of geomaterial (concrete, ceramic and certain metal-matrix composites), has been implemented in a 3-D finite element code using a novel unified approach (based on employing the nonlinear finite element constitutive implementation, spherical integration schemes, Taguchi method, experimental data and the principles of continuum mechanics). Second, in the area of modeling pavement response analytically, this research captures the actual nonlinear pavement response under dynamic loading more accurately. The previous researchers have employed simplified linear models with hypothetical factors to account for the wide margins of variation between the analysis and test data. Third, prior to this

work, no analytical code existed today that could provide the response of pavement under dynamic or cyclic loading. Fourth, this approach is novel as no other code can even predict any preliminary damage distribution, even qualitatively, for any number of cycles. Also, using the developed unified approach, one can predict the relative importance (sensitivity) of the various parameters in pavement design. Finally, this work has employed the developed approach to better understand the design of joints under dynamic and cyclic loading.

This work has the potential to significantly affect the manner in which future pavement performance and redesign is accomplished. It should also be noted that this research can be easily extended to predict pavement life under large number of cycles through the use of more powerful computers.

## **8.2. Future Research**

The one area that needs further research is the extrapolation of the response from a small number of cycles to a large number of cycles to predict pavement life. As it currently stands, there is no means of rapidly and effectively predicting pavement life by either experimental or analytical methods. In this research, the pavement response up to 10 cycles was obtained. The numerical obstacles that came in the way of extrapolating the response to a large number (million or so) of cycles is beyond the scope of this research and can be summarized as follows:

- Beyond 10 cycles, the numerical error increases significantly. This error can be attributed to factors that are associated with the peculiarities of concrete like the Size Effect and Crack Branching which become significant for higher number of cycles beyond the softening regime. Further information about the nature of the crack, crack tip geometry, energy release rate etc., and the type of constituents used in the concrete, are necessary to account for the nonlinearities in the response. Adaptive meshing techniques

are necessary to remesh the cracked areas as the damage becomes confined to the width of the element (Cofer, 1992, 1996) close to the state of fracture (Damage Ratio  $\approx 1$ ).

- The numerical simulation generates large amount of data with each iteration. This is because for the type of formulation employed, many time-history variables need to be stored and updated at each memory location, at each iteration, and for each time step. This generates a huge amount of data even after a few cycles. In this study, computer resources have been quite limited, thus allowing only the low number of cycles. If we remember that pavement life is in millions of cycles and a large number of iterations are inevitable, we recommend the use of a supercomputer currently, and expect that a large number of cycles will be more easily simulated in the not too distant future as the computer technology rapidly grows.

- Experimental Data for one pass is available but not for a small number of intermediate passes (say 10 or 20 or 100). This is because of the practical difficulty in tracking the micro-level crack growth rate as it progresses in each cycle. Therefore, we recommend that crack growth rate be tracked at specific locations under controlled loading conditions in the highway.

- When it comes to obtaining the experimental data from pavements, it is found that the majority of the data available in the literature is after the damage has already occurred at or near the end of pavement life. This is because the pavement life is in the range of 2 to 4 years and it is not practicable to track the progressive damage by impeding the traffic for any long period of time. Therefore, we recommend that more road tests be undertaken to record data for intermediate numbers of cycles.

- The Size Effect also cause problems in laboratory testing. This explains the scatter of data seen in the literature (Huang, 1993). The Size Effect implies that after a large number of cycles, different types and sizes of concrete exhibit different responses. We recommend further research on Size Effects specific to the PCC material used in a highway environment.

- For the numerical method, a nonlinear scheme is employed at the beginning, to track progressive damage. But the type of material nonlinearity changes as we move from a low-cycle to a high cycle fatigue, well beyond the cracking (softening) regime. In other words, a different type of a numerical scheme is necessary after a certain number of cycles have been completed. We therefore recommend a unified numerical scheme that can handle both types of nonlinearity be researched.

# Bibliography

AASHO Road Test, Report 5, 'Pavement Research', Highway Research Board, Special Report 61E, Washington D.C., 1962.

*ABAQUS Manuals* (1994). Hibbitt, Karlsson and Sorensen, Incorporated, RI.

Aifantis, E. (1984). 'On the microstructural origin of certain inelastic models', *Journal of Engineering Materials and Technology*, 106, 326-330.

Alpan I, (1977). 'The speed effect in Pavement deflection', *Acta Technica*, Vol. 85, No 1-2, pp. 11-28.

Askeland, D. (1993). The Science and Engineering of Materials, PWS-Kent Publishing Company, Boston.

Ball, C. G. and Childs, L. D. (1975). 'Tests of Joints for Concrete Pavements', Bulletin RD026.01P, Portland Cement Association.

Balmer, G. (1949). 'Shearing Strength of concrete under high triaxial stress-computation of Mohr's envelope as a curve', *Structural Research Laboratory Report* No. SP-23, Denver, Colorado.

Barsom, R. (1977). Fracture and Fatigue Control in Structures, Prentice Hall Publications.

Batdorf, S. B. and Budianski, B. (1949). A mathematical theory of plasticity based on the concept of slip. *National Advisory Committee for Aeronautics (N. A. C. A.)*, Technical Note No. 1871, Washington, DC.

Battiato, G. (1977). 'Viscoelastic deformations in a two layered paving systems', *Trans. Res. Rec. 640 TRB*, 34-38.

Bazant, Z. P. and Oh, B. H. (1983). 'Crack band theory for fracture of concrete', *Materiaux et Construction* 16 (93), 155-177.

Bazant, Z. P. and Cedolin, L. (1983). 'Finite Element Modeling of Crack Band Propagation', *Journal of Structural Engineering*, 109(1), 69-72.

Bazant, Z. P. and Oh, B. H. (1984). 'Size effect in blunt fracture: Concrete, Rock, Metal', *Journal of Engineering Mechanics*, ASCE 110(4), 518-535.

Bazant, Z. P. and Oh, B. H. (1985a). 'Microplane model for progressive fracture of concrete and rock', *Journal of Engineering Mechanics*, ASCE 111(4), 559-582.

Bazant, Z. P. and Oh, B.H. (1985b), 'Efficient numerical integration on the surface of a sphere,' *Zeitschrift fur Angewandte Mathematik and Mechanik (ZAMM)*, Leipzig, Germany.

Bazant, Z. P. and Pijaudier-Cabot, G. (1987). 'Nonlocal Damage Theory', *Journal of Engineering Mechanics* , 113(10), 1512-1533.

Bazant, Z. P and Prat. P.C. (1988a). 'Microplane model for brittle plastic material', *Journal of Engineering Mechanics*, ASCE, 114(10),1672-1688.

Bazant, Z. P. and Prat, P.C. (1988b). 'Microplane Model for brittle plastic material: II. Verification' *Journal of Engineering Mechanics*, ASCE, 114(10), 1689-1702.

Bazant, Z. P. (1988). 'Stable States and Paths of Structures with Plasticity or Damage.' *Journal of Engineering Mechanics*, 114(12), 2013-2034.

Bazant, Z. P. (1990). 'Nonlocal Microplane Model for Fracture, Damage and Size Effect in Structures' *Journal of Engineering Mechanics*, ASCE, 116(11), 2485-2505.

Bazant, Z. P. and Mazars, J. (1990). 'France-U. S. Workshop on Strain Localization and Size Effect due to Cracking and Damage, *Journal of Engineering Mechanics*, 116(6), 1412-1424.

Bazant, Z. P. and Ozbolt, J. (1990). 'Microplane model for cyclic triaxial behavior of concrete', *Structural Engineering Report*, Dept. of Civil Engineering, Northwestern University, Evanston, IL.

Bazant, Z. and Kazemi, T. (1991). 'Size dependence of concrete fracture energy determined by RILEM work-of-fracture method', *International Journal of Fracture*, 1212-1238.

Bazant, Z. P. and Pijaudier-Cabot, G. (1991). 'Cracks interacting with sections or fibers in composite materials', *Journal of Engineering Mechanics*, 117(7), 1611-1629.

Bazant, Z. P. (1991a). 'Statistical Size effect in quasi-brittle structures; II nonlocal theory', *Journal of Engineering Mechanics*, 117(11), 2623-2640.

Bazant, Z. P. (1991b). 'Why continuum damage is nonlocal-micromechanics arguments', *Journal of Engineering Mechanics*, 117(5), 1070-1085.

Bazant, Z. P., Carol, I. and Prat, P. (1992). 'New explicit microplane model for concrete: theoretical aspects and numerical implementation', *Journal of Solids and Structures*, Vol. 29, 1173-1191.

Bazant, Z. P. and Ozbolt, J. (1992). 'Microplane model for cyclic triaxial behavior of concrete', *Journal of Engineering Mechanics*, 118(7), 1365-1386.

Bazant, Z. P. and Hasegawa, T. (1993a). 'Nonlocal microplane concrete model with rate effect and load cycles I: General formulation', *Journal of Materials in Civil Engineering*, 5(3), 372-393.

Bazant, Z. P. and Hasegawa, T. (1993b). 'Nonlocal microplane concrete model with rate effects and load cycles. II: Application and verification', *Journal of Materials in Civil Engineering*, 5(3), 394-409.

Bazant, Z. P. and Jirasek, M. (1994). 'Nonlocal Model Based on Crack Interactions: A localization Study', *Journal of Engineering Mechanics*, 116, 256-259.

Bazant, Z. P. (1994). 'Nonlocal Damage Theory Based on Micromechanics of Crack Interactions', *Journal of Engineering Mechanics*, 120 (3), 593-617.

Bazant, Z. P. (1995a). 'Modulus of Rupture: Size Effect Due To Fracture Initiation in Boundary Layer', *Journal of Structural Engineering*, Vol. 121, No. 4, April , 739-746

Bazant, Z. P. (1995b). 'Scaling of Quasi-brittle Fracture and the Fractal Question', *Journal of Engineering Materials and Technology*, Vol. 17, October, 361-367.

Bazant, Z. P. (1996a). 'Microplane Model For Concrete. I: Stress-Strain Boundaries and finite Strain', *Journal of Engineering Mechanics*, Vol. 122(3), March, 245-262.

Bazant, Z. P. (1996b). 'Microplane Model For Concrete. II: Stress-Strain Boundaries and finite Strain', *Journal of Engineering Mechanics*, Vol. 122(3), March, 254-262.

Bhatti, M.A., Stoner, J.W. and Hingtgen, J. (1994). 'Simulation of Dynamic Loads From Different Vehicle Configurations', *Heavy Vehicle Systems, Special Series, Int. J. of Vehicle Design*, Vol. 1, No. 4, pp. 396-416.

Bolander, J. E., Ebihara, T. and Hikosaka, H. (1994) et al. 'Evaluating Concrete Mesoscale Properties using Neural Networks', Proceedings of the Third materials Engineering Conference, ASCE, pp. 475 - 482.

Brebbia, C. A. (1985). Finite Element Systems: A Handbook, Springer-Verlag Publications.

Boussinesq, J. (1885) *Application des Potentials a l'etude de l'equilibre et du Movement des solids elastiques*, Gauthier-Villars, Paris.

Burmister, D. M. (1943) , 'The general theory of stresses and displacements in layered soil systems', Journal of applied physics, Vol. 16, 84-94, 126-127,296-302.

Burmister, D. M. (1958) , 'Evaluation of Pavement Systems of the WASHO Road test by layered systems method ', Bulletin 177, Highway Research Board, pp. 26-54.

Cebon, D. (1993). 'Interaction Between heavy Vehicles and Roads.' *Society of Automotive Engineers* , SP-931, 81p.

Cebon, D. and Hardy, M. (1994). 'Importance of Speed and Frequency in Flexible Pavement Response.' *Journal of Eng. Mechanics*, 120(3), 463-82.

Cebon, D., Green, M. and Cole D. (1994). 'Effects of Vehicle Suspension Design on Dynamics of Highway Bridges.' *Journal of Structural Engineering* 121(2), 272-281.

Collop, A.C., Cebon, D., and Cole, D. J. (1996) 'Effects of spatial repeatability on long term flexible pavement performance', Proceedings of the Institution of Mechanical Engineers, Part C: Journal Of Automobile Engineering, Vol. 210, pp 97-110.

Cebon, and Collop A. D. (1996). 'Stiffness reductions of flexible pavements due to cumulative fatigue damage.' *Journal of Transportation Engineering* 122(2), 131-138.

Chatti, K. and Yun, K. K. (1995). 'Dynamic Analysis of Multi-Layered Pavement Systems Under Moving Loads.' *SAE International*, No. 952635, pp. 41-47.

Chen, E. P.(1986). 'Continuum damage mechanics studies on the dynamic fracture of concrete', *Proceedings, Cement-Based composites: Strain Rate effects on fracture, materials research society symposium*, Vol. 64, Materials Research Society, Pittsburgh, PA, 63-67.

Chen, Er-Ping (1989). 'Dynamic brittle fracture analysis based on continuum damage mechanics', *Fracture Mechanics: Perspectives & Directions (Twentieth Symposium)*, ASTM (STP) 1020, 447-458.

Chen, W. F. (1982). *Plasticity in reinforced concrete*. McGraw-Hill, New York, N.Y.

Chen, W.F., and Han, D (1988). *Plasticity for Structural Engineers*. Springer-Verlag.

Chen, W.F., and Mizuno, E. (1990). *Nonlinear analysis in soil mechanics-Theory and implementation*. Elsevier, Amsterdam, The Netherlands.

Christison, J. (1978). 'In situ measurements of strains and deflections in a full depth concrete pavement', *Proc. Assoc. Asphalt Paving Tech.*, 47, 398-430.

Chou, Y. T. and Huang, Y. H. (1978). 'Discussion on Finite Element Analysis of Jointed or Cracked Pavements', *Transportation Research Record 671*, Transportation Research Board, pp, 17-18.

Chou, Y. T. and Huang, Y. H. (1982). 'A Finite Element Analysis for Concrete Pavements', *Proceedings, International Conference on Finite Element Methods*, Shanghai, China, pp. 348-353.

Cofer, W. (1992). 'Implementation of the nonlocal microplane concrete model with an explicit dynamic finite element program', *Applied Mechanics Review*, 45(3), S132-S139.

Collop, A. C., Cebon, D., and Cole, D. J., 1996, 'Effects of Spatial Repeatability on Long-Term Flexible pavement performance,' *Proceedings of the Institution of mechanical Engineers, Part C: Journal of Automobile Engineering*, Vol. 210, pp. 97-110.

Cook, R. D. (1989). *Concepts and Applications of Finite Element Analysis*, John Wiley and Sons Publications.

Cryer, B. W., Nawrocki, P. E., and Lund, R. A. (1976). 'A Road Simulation System for Heavy-Duty Vehicles.' *Society of Automotive Engineers*, Paper No. 760361, 13 p.

Dafalias, Y. F. (1986). 'Bounding Surface Plasticity I, Mathematical Foundation and Hypo-Plasticity.' *J. of Engineering Mechanics.*, ASCE 112(9), 966-987.

Dragon, A. and Mroz, Z. (1979). 'A continuum theory for plastic brittle behavior of rock and concrete' *International Journal of Engineering Science*, 17, 121-137.

Drescher, A., Kim, J., and Newcomb, D. (1993). 'Permanent deformation in Asphalt Concrete', *Journal of Materials in Civil Engineering*, 5(1), 112-127.

Drucker, D. C. (1950). 'Some implications of work hardening and ideal plasticity', *Applied Math. and Mech.*, 7(4), 411-418.

Eisenmann, J. (1975). 'Dynamic wheel load fluctuations - road Stress', *Strasse und Autobahn*, 4, 123-128.

El-Gindy, M. (1996), Personal Communication, Center for Surface Transportation Technology, National Research Council of Canada, Ottawa, Canada, K1A0R6.

Ferne, B. (1989). 'Private Communication', TRRL, 6 April 1989.

Ferrari, P.(1972). 'Calculation of the deformation caused by vehicles to flexible pavements, *Proc. of Conf. Struct. Design on Asphalt Pavements*, Univ. of Mich., 382-398.

Fisher, R. A. (1951). Design of Experiments, Edinburgh, Oliver & Boyd.

Gerstle, W., Dey, P. and Prasad, N. (1992). 'Crack growth in flexural members-A fracture mechanics approach', *ACI Structure Journal*, 89(6), 617-625.

Ghosh, S. and Moorthy, S. (1996). 'A model for analysis of arbitrary composite and porous microstructures with voronoi cell finite elements', *International Journal For Numerical Methods In Engineering*, Vol. 39, 2363-2398.

Giaccio, G. (1993). 'The fracture Energy of High Strength Concretes', *Materials and Structures*, 26, 381-386.

Gillespie, T. D., Karamihas, S., Cebon., D., Sayers, M., Nasim, M., Hansen, W., Ehsan, N. (1992). 'Effects of heavy vehicle characteristics on pavement response and performance', *National Cooperative Highway Research Program*, Trans. Res. Board, Report No. 1-25(1), UMTRI, MI,.

Gillespie, T. D. and Karamihas, S. (1993a). 'Characterizing the road damaging dynamics of truck tandem suspensions', *SAE International Meeting*, Detroit, MI, November 1-4, 137-144.

Gillespie, T. D. and Karmihhas, S. M. (1993b). 'Characterizing trucks for dynamic load prediction', *International Journal of Vehicle Design*, 1(1), 3-19.

Gillespie, T. D. (1993). 'Effects of Heavy-Vehicle Characteristics on pavement response and Performance.', *National Cooperative highway research program* , Report no. 353, 126 p.

Goktan, A and Mitschke, (1995). 'Road Damage Caused By Heavy Duty Vehicles', *Int. J. of Vehicle Design*, 16(1), 54-70.

Gorge, W. (1984). 'Evaluation of research reports concerning the influence of commercial vehicle development and design on the road fatigue, International Road Trans. Union, Geneva.

Goto, Y. (1995). 'Localization of Plastic Buckling Patterns Under Cyclic Loading', *Journal of Engineering Mechanics*, Vol. 121, No 4, 493-501.

Gyenes, L., Mitchell, C. and Phillips, S. (1994). 'Dynamic Pavement Loads and Tests of Road Friendliness for Heavy Vehicle Suspensions', *Heavy Vehicle Systems, International Journal of Vehicle Design*, 1(4).

Hall, K. T. (1989). 'Rehabilitation of Concrete Pavements, Vol. 3, Concrete Pavement Evaluation and Rehabilitation System', Report No. FHWA-RD-77-8, Federal Highway Administration.

Hallquist, J. and Whirley, R. G. (1989). *DYNA3D User's Manual*, UCID-19592, Rev. 5.

Hardy, M. S. and Cebon, D. (1988). 'The response of a flexible pavement to moving dynamic load', *Proc. Int. Acoustics*, Vol. 10, Part 2.

Hardy, M. S and Cebon, D. (1993). 'The response of continuous pavements to moving dynamic loads', *J. Engr. Mech. ASCE*, 119(9), 1762-1780.

Hawkins, J. Y., and Kobayashi, A. (1991). ' Numerical simulation of mode 1 dynamic fracture of concrete', *Journal of Engineering Mechanics*, 117(7), 1595-1609.

Hibbitt, H. (1993). 'Nonlinear Solid Mechanics', *Finite Element in Analysis and Design*.

Hillerborg, A. (1985). 'Fictitious crack model', *Materials and Structures*, 18 (106), 291-296.

Huang, Y. (1993). Pavement analysis and design, Prentice - Hall, New Jersey.

Hognestad, E., Hanson, W., and Newmann, B. (1955), 'Concrete stress distribution in ultimate strength design', *J. Am. Concrete Inst.* 52(4), 455-477.

Il'yushin, A. A. (1961). 'On the postulate of plasticity', *Journal of Applied Math. and Mech.*, 25(3), 746-752.

Ishihara, K. (1967). 'The theory of viscoelastic two -layered systems...in the pavement design', *Proc. Sec. Int. Conf. on Struct. Design of Asph. Pavements*, Univ. of MI, Ann Arbor, 245-254.

Jacob, B, (1995). 'Spatial Repeatability of Impact Forces on A Pavement and Multi-Sensor WIM \_ Research Element 5 of the OECD IR6 DIVINE Project,' *Road Transport technology, Proceedings of the Fourth International Symposium on Heavy Vehicle Weights and Dimensions*, Vol. 4, pp. 273-279.

Jain, S. (1979). 'Stochastic principles..', *J. Inst. of Engr. (India), Civ. Engr.*, 59, 214-218.

Kansas State Highway Commission, 1947. *Design of Flexible Pavement Using the Triaxial Compression Test*, Bulletin 8, Highway Research Board.

Kawai, T. (1978). New discrete models and their application to seismic response analysis of structures. *Nuclear engineering and Design*, 48, 207-229.

Kosko, B. (1992). *Neural Networks and Fuzzy Systems*. Prentice-Hall, Inc., Englewood Cliffs, NJ, 449 pp.

Kotsovos, M. D. and Newmann, J. B. (1978). 'Generalized stress-strain relations for concrete.', *J. of Eng. Mechanics.*, ASCE 104(4), 845-856.

Krajcinovic, D., and Fanella, D. (1986). 'A micromechanical damage model for concrete', *Engineering Fracture Mechanics* , 25(5/6), 585-596.

Krajcinovic, D., and Sumarac, D. (1987). 'Micromechanics of the damage processes', *Continuum damage mechanics, theory and applications*, D. Krajcinovic and J. Lemaitre, eds., Springer Verlag, Berlin, Germany, 135-194.

Kupfer, H., Hilsdorf, H. K., and Rusch, H. (1969). 'Behavior of concrete under biaxial stresses.' *J. ACI* , 66(8), 656-666.

Krawczuk, M. (1994). 'Rectangular shell finite element with an open crack', *Finite Elements in Analysis and Design*, 15, 233-253.

Lai, S. (1994), 'Probabilistic Solution for viscoelastic layered systems', *Intl. Conf. on Stat. and Probability*', 1, 390-401.

Landis, E., and Ouang, C. Shah, S. (1989). *Fracture mechanics symposium*, ASTM, 447-458

Marshek, K. M. Hudson, W., Connell, R., Chen, H., Saraf, C. (1985a). 'Experimental Investigation of Truck Tire Inflation Pressure On Pavement Tire Contact Area and Pressure Distribution', *Report 386-1. Center For Transportation Research*, University of Texas at Austin.

Marshek, K. M., Hudson, W., Connell, R., Chen, H., Saraf, C. (1985b). 'Effect of Truck Tire Inflation Pressure and Axle load On Pavement Performance', *Report 386-2F. Center For Transportation Research*, University of Texas at Austin.

Marshek, K. M., Chen, H., Connell, R., Saraf, C. (1989). 'Effect of Truck Tire Inflation Pressure and Axle load On Flexible and Rigid Pavement Performance', *Transportation Research Record No 1070*, 14-21.

Masters, T. (1993). Practical Neural Network Recipes in C++, Academic Press, Inc., San Diego, CA 493 pp.

Matthews, J. L. and Monismith, C. (1993). 'Investigation of laboratory fatigue testing procedures for asphalt aggregate mixtures', *Journal of Transportation Engineering*, 119(4), 634-654.

Meguid, S. A. (1989). Engineering Fracture Mechanics, Elsevier Applied Science.

Mehta, P. K. (1986). Concrete Structure, Properties, and Materials, Prentice Hall, Inc., Englewood Cliffs, N. J. 07632.

Mellor and Johnson, (1973). Engineering Plasticity, Van Nostrand Reinhold Co.

Mitchell, C. G. B. (1991). 'An Experimental Assessment of Steel, Rubber and Air Suspensions for Heavy Goods Vehicles'. *Proc. I. Mech. E. Seminar Road Wear: The Interaction Between Vehicle Suspensions and The Road*, April 1991, Institution of Mechanical Engineers, London.

Minitab Software and Manual (1992). Minitab Co. Addison-Wesley and Benjamin / Cumminings Publishing Co.

Mizuno, E. and Hatanaka, S. (1992). 'Compressive softening model for concrete', *Journal of Engineering Mechanics*, 118(8), 1546-1563.

- Nadai, A. (1950). Theory of flow and fracture of solids, Vol. 1, Second Edition.
- Nazarian, S. (1989). 'Determination of surface deflection of pavements under moving loads', Proc. TRR Annual Meeting, January.
- Neville, A. M. (1996), Properties of Concrete, Fourth Edition, John Wiley and Sons.
- Nirmalendran, S. and Horii, H. (1992). Analytical modeling of microcracking and bridging in fracture of quasi brittle materials. *J. Mech. Phys. Solids*, 40(2), 8t3-886.
- O'Connor, T.; O'Brian, E. J.; and Jacob B. (1996). 'An Experimental Investigation of Spatial Repeatability,' *EF/Vehicle-Infrastructure I* San Diego, pp. 1-17.
- OECD.(1985). 'Strain Measurement in Bituminous Layers', *OECD Road Trans. Research*, Paris.
- Oliver, J. (1989). 'A Consistent Characteristic Length for Smearred Cracking Models', *International Journal for Numerical Methods in Engineering*, 28 , 461-474.
- Ortiz, M. (1984). 'A Constitutive Theory for The Inelastic Behavior of Concrete', *Ph.D. Dissertation*, Division of Engineering, Brown University, RI 02912.
- Padovan, J. (1986a). 'Finite Element Analysis of steady and transiently moving / rolling nonlinear viscoelastic structure-1. Theory, *Computers and Structures*, 27(2), 249-257.
- Padovan, J. (1986b). 'Finite Element Analysis of steady and transiently moving / rolling nonlinear viscoelastic structure-II. Shell and Three-Dimensional Simulations, *Computers and Structures*, 27(2), 259-273.
- Padovan, J. (1986c). 'Finite Element Analysis of steady and transiently moving / rolling nonlinear viscoelastic structure-III. Impact / Contact Simulations, *Computers and Structures*, 27(2), 275-286.

Pande, G. N. and Sharma, K. G. (1983). Multilaminate model of clays-a numerical evaluation of the influence of rotation of principal axes. *Int. J. Numer. Anal. Methods Geomech.*, 7, 397-418.

Papagiannakis, A. (1996). 'Formulations for viscoelastic response of pavements under moving dynamic loads', *Journal of Transportation Engineering*, Vol. 122, No. 2, March/April.

Peattie, K. R. (1978). Flexible Pavement Design, Ch. 1, Developments in Highway Pavement Engineering', Applied Science Publishers Limited, London.

Porter, O. J. (1950). 'Development of the original method for Highway Design: Symposium on Development of CBR Flexible Pavement Design Method for Airfields,' *Transactions*, ASCE, pp. 461-467.

Potter, T. C.; Cebon, D.; and Cole, D. J. (1995), 'An investigation of road damage due to measured dynamic tire forces', *Proceedings of the Institution of Mechanical Engineers Part D-Journal of Automobile Engineering*, Vol. 209, No. 1, pp. 9-24.

Press, W. (1992). Numerical Recipes in Fortran, Cambridge University Press, Cambridge, England.

RILEM (1985). *Materials and Structures*, 18 (106), p:285-290.

Roelfstra, P. E., Sadouki, H. and Wittmann, F. H. (1985) Le beton numerique. *Mat. et Constr.*, 107, 327-335.

Roque, R. and Butlar, W. (1992). 'The development of a measurement and analysis system to accurately determine asphalt concrete properties using the indirect tensile mode', *Asphalt paving Technology: Proceedings*, 61, 304-332.

Roque, R. and Butlar, W. (1994). 'Development and evaluation of the SHRP measurement and analysis system for indirect tensile testing at low temperatures', *Transportation Research Board*, Jan. 9-13, SHRP Report no. 940773.

Ross, P. J. (1988), Taguchi Techniques for Quality Engineering, McGraw Hill Book Company.

Roy, R. K. (1990), A Primer on the Taguchi Method, Van Nostrand Reinhold, New York.

Schreyer, H. (1990). 'Analytical solutions for Nonlinear strain gradient softening and localization', *Journal of Applied Mechanics*, 57, 522-528.

Sebaaly, P. (1988a). 'Development of dynamic fatigue failure criterion', *ASCE J. of Trans. Engr.*, 114(4), 450-464.

Sebaaly, P. (1988b). 'Pavement response to dynamic loads', *FHWA Load Equivalence Workshop*, Washington D. C., 299 p.

Shah, S. and Jenq, Y. (1991). 'Features of mechanics of quasi brittle crack propagation in concrete', *International Journal of Fracture* , 103-120.

Shah, S. (1991). Fatigue of Concrete Structures, American Concrete Institute, Detroit, Michigan .

SHRP Report (1993). 'Development and validation of performance prediction models and specifications for asphalt binders and paving mixes', SHRP report no. A-357, *National Research Council*, Washington, DC.

Souma, V. E. (1994). 'Fractals, Fractures, and Size Effects in Concrete', *Journal of Engineering Mechanics*, 120(4), 835-854.

Stevens, D. and Liu, D. (1992). 'Strain based constitutive model with mixed evolution rules for concrete', *Journal of Engineering Mechanics*, 118(6), 1184-1200.

Stroud, A. H. (1971). Approximate Calculation of Multiple Integrals. Prentice Hall Publications.

Streit, D. A., Kulakowski, B. T., and Wollyung R. J. (1995). 'Dynamic Vehicle Forces on Pavements,' *Draft Report*, the Pennsylvania Transportation Institute, Pennsylvania. USA, Federal Highway Administration Contact No. DTFH61-90-C-00084.

SUPERWAVE (1993). Software developed at Pennsylvania Transportation Institute, Penn State University.

Taguchi, G. and Konishi, S. (1987), Orthogonal Arrays and Linear graphs-Tools for Quality Engineering, Dearborn: American Supplier Institute, Inc.

Taylor, G. I. (1938), 'Plastic Strain in Metals', *J. Inst. Metals* , 62, 307-324.

Taylor, L. M., Chen, E. P, and Kuszmaul, J. S. (1986). 'Microcrack induced damage accumulation in brittle rock under dynamic loading', *Journal of computer methods in Applied Mechanics and Engineering*, Vol. 55, 1986, 301-320.

Toi, Y., and Che, J. S. (1993). 'Mesoscopic simulation of microcracking behaviors of brittle polycrystalline solids', *Proceedings of the Japanese Society of Mechanical Engineers*, 59 (557), 240-247. (in Japanese)

Toi, Y., and Kiyosue, T. (1995). 'Three-dimensional mesomechanical analysis of brittle solids containing microinclusions', *Proceedings of the Japanese Society of Mechanical Engineers*, 61 (582), 237-243. (in Japanese).

Tvergaard, V. (1985). 'On Bifurcation and stability under elastic plastic deformation.' *Plasticity Today*. A. Sawczuk and G. Bianchi, Elsevier Science Publishers, New York, N.Y.

Uzan, J., Lytton, R., Fernando, E., Roque, R., Hiltunen, D., Stoffels, S. (1994). 'Development and Validation of Realistic Pavement Response Models', *Proc. of the 7th Int. Conf. on Asphalt Pavements*, Vol. 1, 334-350.

Van Dijk, W., and Visser W. (1977). *Proc. The Energy Approach to Fatigue for Pavement Design*, AAPT, 46, 1-40.

Van Dijk, W. (1975). *Proc. Practical Fatigue Characteristics of Bituminous Mixes*, AAPT, 38, 38-72.

van Mier, J. G. M. (1984). 'Strain softening of concrete under multiaxial loading conditions'. *Dissertation*, Eindhoven University of Tech, The Netherlands.

Wang, C. and Salmon, C. (1992). Reinforced Concrete Design, Harper-Collins Publishing Co.

Westergaard, H. M. (1933). 'Analytical tools for judging results of structural tests of concrete pavements', *Public Roads*, Vol. 14, No. 10, pp. 185-188.

Yoder, E. J. and Witczak, M. W. (1975). Principles of Pavement Design, Wiley, New York.

Ziegler, H. (1968). Principles of Structural Stability. Blaisdell Publishing Co., Waltham, Mass.

Zienkiewicz, O. C. (1992). The Finite Element Method, McGraw-Hill, London, 4th Edition.

Zienkiewicz, O. C. (1977). 'Time dependent multi-laminate model of rocks', *The I. J. of Numer. Anal. Methods. Geomech. 1*, 219-247 .

## APPENDIX A

### Derivation of The Incremental Tangent Stiffness Matrix

The incremental tangential stiffness matrix of the Microplane Theory is rederived below.

Using hypothesis III in Chapter 4, and the principle of virtual work, we have the incremental macroscopic stress tensor:

$$d\sigma_{ij} = d\sigma_v \delta_{ij} + \frac{3}{2\pi} \int_{\Omega} d\sigma_d n_i n_j d\Omega + \frac{3}{2\pi} \int_{\Omega} \frac{d\sigma_{tr}}{2} (n_i \delta_{rj} + n_j \delta_{ri} - 2n_i n_j n_r) d\Omega \quad (\text{A.1})$$

From Bazant (1992), the increments of stresses at the microplane level must be replaced by their incremental expressions in terms of the current volumetric, deviatoric and tangent modulus and the increments of strain at that level. These are for the volumetric component,

$$d\sigma_v = E_v^{\tan} d\varepsilon_v \quad (\text{A.2})$$

or,

$$d\sigma_v = E_v^{\tan} \frac{d\varepsilon_{kk}}{3} \quad (\text{A.3})$$

or,

$$d\sigma_v = E_v^{\tan} \frac{d\varepsilon_{kl} \delta_{kl}}{3} \quad (\text{A.4})$$

For the deviatoric component, we have

$$d\sigma_D = E_D^{\tan} d\varepsilon_D \quad (\text{A.5})$$

or,

$$d\sigma_D = E_D^{\tan} (d\varepsilon_{kl} n_k n_l - d\varepsilon_v) \quad (\text{A.6})$$

or,

$$d\sigma_D = E_D^{\tan} (d\varepsilon_{kl} n_k n_l - \frac{d\varepsilon_{kl} \delta_{kl}}{3}) \quad (\text{A.7})$$

or,

$$d\sigma_D = E_D^{\tan} (n_k n_l - \frac{\delta_{kl}}{3}) d\varepsilon_{kl} \quad (\text{A.8})$$

Using the definition for tangential component, we have

$$d\sigma_{T_r} = H_{rs}^{\tan} d\epsilon_s \quad (\text{A.9})$$

or, 
$$d\epsilon_s = (\delta_{sk} - n_s n_k) n_l \epsilon_{kl} \quad (\text{A.10})$$

or, 
$$d\sigma_{T_r} = H_{rs}^{\tan} (\delta_{sk} - n_s n_k) n_l d\epsilon_{kl}. \quad (\text{A.11})$$

Using the constitutive law (Bazant, 1988b), we have

$$d\sigma_{ij} = Z_{ijkl} d\epsilon_{kl}. \quad (\text{A.12})$$

Now to produce a matrix which is symmetry-consistent,  $Z_{ijkl}$  is to be replaced by  $D_{ijkl}$ ,

where

$$D_{ijkl} = \frac{1}{2} (Z_{ijkl} + Z_{ijlk}) \quad (\text{A.13})$$

Substituting the equations A.4, A.8 and A.11 into A.1 and using equation A.13, we then have the expression for the incremental tangential stiffness matrix:

$$\begin{aligned} D_{ijkl}^{\tan} = & \frac{E^{\tan}_v}{3} \delta_{ij} \delta_{kl} + \frac{3}{2\pi} \int_{\Omega} E_D^{\tan} n_i n_j (n_k n_l - \delta_{kl} / 3) d\Omega \\ & + \frac{3}{2\pi} \int_{\Omega} \frac{H_{rs}^{\tan}}{4} (n_i \delta_{rj} + n_j \delta_{ri} - 2n_i n_j n_r) (n_k \delta_{sl} + n_l \delta_{sk} - 2n_k n_l n_s) d\Omega \end{aligned} \quad (\text{A.14})$$

## APPENDIX B

### Taguchi Method

Dr. Genichi Taduchi espoused an excellent philosophy for quality control in the manufacturing industry. His philosophy has far reaching consequences, yet it is founded on three very simple and fundamental concepts (Taguchi et al., 1987). These concepts are:

- Quality should be designed into the product and not inspected into it.
- The deviation from the target has to be minimized to improve the performance of the product.
- The cost should be measured as a function of deviation from the standard and the losses should be measured system wide.

These concepts had tremendous industrial use after the second world war by Electrical Communications Laboratory (ECL) in Japan and then gave birth to the 'quality based manufacturing design' in the USA. Ford Motor Company, for example has decreed that all Ford Motor engineers be trained in the Taguchi Methodology and use the above principles to resolve quality issues to improve the product.

In the nineties, different industries used the Taguchi method for other design applications, that were non-quality or manufacturing related. The second concept from above was utilized to optimize designs and rank the sensitive factors that influence any desired response (Ross, 1988; Roy, 1990). This concept which later became known as 'Taguchi's Design of Experiments' was used in this research and is pertinent to our discussion.

There are two essential steps to guide the Design of Experiments that are explained as follows. First, the Taguchi Method clearly defined a way of selecting

information (through experiments or analyses) by the use of specially constructed tables, known as 'Orthogonal Arrays' (OA). A set of OAs that can be used for many experimental situations is constructed and the dimension of the OA depends on the number of factors and the level of information available for each factor. Taguchi's OAs represent a partial factorial design in contrast to a full factorial design (Fisher, 1951). For example, in a case involving 7 factors, the total number of runs/experiments will be 128 ( $2^8$ ) for a full factorial design. The Taguchi Method selects a small set out of that to reduce the number to only 8 runs.

Taguchi's arrays (OAs) are tables that describe the order of arranging the experimental results involving several factors. Based on the number of factors and levels, the dimension of the arrays vary. For example, the design involving 4 and 7 factors, may all be accomplished by using the same orthogonal array  $L_8$ . The OAs contain both the number as well as the configuration of the experiment. The  $L_8$  OA was applied throughout this research. Once the results have been tabulated in a  $L_8$  array, the average effects of the variables can be computed and are usually represented in a plot known as the 'Main Effect'. This plot gives the influence of the factors when each factor assumes a statistical average number between the ranges considered. Two sets of extreme combinations among the factors are possible as observed in the Main Effects plot. In one combination, the factors combine to give the highest value of response (Case 1) and in the other combination, the factors combine to give the lowest value of the response (Case 2). Taguchi recommends that depending on the objective of the experiment, either of the criteria is to be chosen to proceed to the next step.

The second step is to determine the contribution (in percentage) for each of the factors that were used in the OA. This step involves a statistical treatment of those factors such that the ones which contribute the most will end up with a higher percent contribution. This statistical treatment is known as 'Analysis of Variation' (ANOVA). The steps involved in carrying out ANOVA are discussed in the Appendix C.

## APPENDIX C

### Steps to Calculate ANOVA

The steps to calculate ANOVA are summarized below:

- Step 1: Calculate Total of all results (T)

$$T = \sum_{n=1}^2 Y_n \quad (C.1)$$

where Y is the result and n is the number of experiments.

- Step 2: Correction Factor (C.F.) calculation.

$$CF = T^2 / N \quad (C.2)$$

- Step 3: Calculate Total Sum of Squares.

$$S_t = \sum_{i=1}^8 y_i^2 - C.F. \quad (C.3)$$

- Step 4: Calculate Factor Sum of Squares.

$$S_i = (i_1^2 / N_{i1} + i_2^2 / N_{i2}) - C.F. \quad (C.4)$$

where i denotes factors A, B, etc.

- Step 5: Total and Factor Degrees of Freedom (f) Calculation.

$$f_t = \text{Total Dof} = \text{No. of test runs} - 1 \quad (C.5)$$

$$f_i = \text{No. of levels of factor } i - 1 \quad (C.6)$$

- Step 6: Calculate Mean Square (variance V).

$$V_i = S_i / f_i \quad (C.7)$$

- Step 7: Calculate Percentage Contribution (P).

$$P = (S_i / S_t) \times 100 \quad (C.8)$$

## Appendix D

### Table of Dowel Diameter and Length

The recommended dowel diameter, length of the dowel for a spacing of 0.3 m (1 ft) as recommended by the Portland Cement Association in 1991 and reproduced from Huang (1993) follows.

| Slab Thickness (in.) | Dowel Diameter (in.) | Dowel Length (in.) |
|----------------------|----------------------|--------------------|
| 5                    | 5/8                  | 12                 |
| 6                    | 3/4                  | 14                 |
| 7                    | 7/8                  | 14                 |
| 8                    | 1                    | 14                 |
| 9                    | 9/8                  | 16                 |
| 10                   | 5/4                  | 18                 |
| 11                   | 11/8                 | 18                 |
| 12                   | 3/2                  | 20                 |

Table D.1: Recommended Dowel Dimensions

**APPENDIX E**

**The Developed Program**

```

CCCCCCCCCCCCCCCCCCCCCCCCCCCCCCCCCCCCCCCCCCCCCCCCCCCCCCCCCCCCCCCC
C 19 th MAY 1996
CCCCCCCCCCCCCCCCCCCCCCCCCCCCCCCCCCCCCCCCCCCCCCCCCCCCCCCCCCCCCCCC
C
C
C ***** EXPLICIT CODE *****
C
C THIS IS ARUN'S SAMPLE USER SUBROUTINE.
C THIS IS TO BE USED IN A NONLINEAR FINITE ELEMENT CODE.
C THIS INVOLVES A DAMAGE PHENOMENA.
C THIS CODE IS WRITTEN BY ARUN BHATTACHARYA
C AT UNIVERSITY OF CALIFORNIA AT DAVIS. THIS WAS
C WRITTEN AT THE AHMCT LAB. (STATRED IN SEPTEMBER 1994).
C
CCCCCCCCCCCCCCCCCCCCCCCCCCCCCCCCCCCCCCCCCCCCCCCCCCCCCCCCCCCCCCCC
C JULY 18 th,1995, NEW FROM 1992 paper , from umat.f324
C NOTE THAT OTHER LOADING UNLOADING SCHEMES HAVE
C BEEN USED> IN THIS ONE SCHEME AS PER BAZ92 have been used
CCCCCCCCCCCCCCCCCCCCCCCCCCCCCCCCCCCCCCCCCCCCCCCCCCCCCCCCCCCCCCCC
CCCCCCCCCCCCCCCCCCCCCCCCCCCCCCCCCCCCCCCCCCCCCCCCCCCCCCCCCCCCCCCC
C Constants needed as input (in Abaqus file)
C
C E,NU,A,B,P,Q
C
C Constants defined in this subroutine
C CVZ,CDZ,M=M1,N,E1=E11,ETA,ALPHA,BETA,AK,
C
CCCCCCCCCCCCCCCCCCCCCCCCCCCCCCCCCCCCCCCCCCCCCCCCCCCCCCCCCCCCCCCC
CCCCCCCCCCCCCCCCCCCCCCCCCCCCCCCCCCCCCCCCCCCCCCCCCCCCCCCCCCCCCCCC
C
SUBROUTINE VUMAT(
CCCCCCCCCCCCCCCCCCCCCCCCCCCCCCCCCCCCCCCCCCCCCCCCCCCCCCCCCCCCCCCC
C Read Only -
1 NBLOCK, NDIR, NSHR, NSTATEV, NFIELDV, NPROPS, LANNEAL,
2 STEPTIME, TOTALTIME, DT, CMNAME, COORDMP, CHARLENGTH,
3 PROPS, DENSITY, STRAININC, RELSPININC,
4 TEMPOLD, STRETCHOLD, DEFGRADOLD, FIELDOLD,
5 STRESSOLD, STATEOLD, ENERINTERNOLD, ENERINELASOLD,
6 TEMPNEW, STRETCHNEW, DEFGRADNEW, FIELDNEW,
C Write Only -
7 STRESSNEW, STATENEW, ENERINTERNNEW, ENERINELASNEW)
C
INCLUDE 'VABA_PARAM.INC'
C
C23456789123456789123456789123456789123456789123456789123456789
C
REAL N,NU,M1,M2,M
C
C23456789123456789123456789123456789123456789123456789123456789
C
C All Arrays dimensioned by (*) are not used in this algorithm
C
DIMENSION PROPS(NPROPS), DENSITY(NBLOCK),COORDMP(*),
1 CHARLENGTH(*),STRAININC(NBLOCK,NDIR+NSHR),
2 RELSPININC(*),TEMPOLD(*),
3 STRETCHOLD(*),DEFGRADOLD(NBLOCK,NDIR+NSHR),
4 FIELDOLD(*),STRESSOLD(NBLOCK,NDIR+NSHR),
5 STATEOLD(NBLOCK,NSTATEV),ENERINTERNOLD(NBLOCK),

```

```

6 ENERINELASOLD (NBLOCK) , TEMPNEW (*),
7 STRETCHNEW (*), DEFGRADNEW (*),
8 FIELDNEW (*),
9 STRESSNEW (NBLOCK, NDIR+NSHR) , STATENEW (NBLOCK, NSTATEV) ,
1 ENERINTERNNEW (NBLOCK) , ENERINELASNEW (NBLOCK)
C
C
C23456789123456789123456789123456789123456789123456789123456789
C
    DIMENSION SN (3, 3) , DSN (3, 3) , EN (21) , DEN (21) , ENN (21) ,
1 EDP (NBLOCK, 21) , EDN (NBLOCK, 21) , DED (NBLOCK, 21) , DSD (NBLOCK, 21) ,
2 SDN (NBLOCK, 21) , EDMAX (NBLOCK, 21) , EDMIN (NBLOCK, 21) , SDP (NBLOCK, 21) ,
3 ETP (NBLOCK, 21) , ETN (NBLOCK, 21) , DET (NBLOCK, 21) ,
4 ETMAX (NBLOCK, 21) , ETMIN (NBLOCK, 21) , EVMAX (NBLOCK) , EVMIN (NBLOCK) ,
5 SIGT1 (NBLOCK, 21) , SIGT2 (NBLOCK, 21) , SIGT3 (NBLOCK, 21) ,
6 GAMMAN (NBLOCK, 21) , SIGMVP (NBLOCK) , TAU (NBLOCK, 21) ,
7 SIGMVN (NBLOCK) , DELSV (NBLOCK) , WC (21) , TAUGA (NBLOCK, 21) ,
8 STRAN (NBLOCK, 6) , DSTRAN (NBLOCK, 6)
C
    DIMENSION ETP1 (NBLOCK, 21) , ETP2 (NBLOCK, 21) , ETP3 (NBLOCK, 21) ,
1 ETN1 (NBLOCK, 21) , ETN2 (NBLOCK, 21) , ETN3 (NBLOCK, 21) , DET1 (NBLOCK, 21) ,
2 DET2 (NBLOCK, 21) , DET3 (NBLOCK, 21) , EPVP (NBLOCK) , EPVN (NBLOCK) ,
3 DEPV (NBLOCK) , EPVDV (NBLOCK)
C
    DIMENSION TB11 (NBLOCK, 21) , TC11 (NBLOCK, 21) , TB22 (NBLOCK, 21) ,
1 TC22 (NBLOCK, 21) , TB33 (NBLOCK, 21) , TC33 (NBLOCK, 21) ,
2 TB12 (NBLOCK, 21) , TC12 (NBLOCK, 21) , TB23 (NBLOCK, 21) ,
3 TC23 (NBLOCK, 21) , TB31 (NBLOCK, 21) , TC31 (NBLOCK, 21) ,
4 BT11 (NBLOCK) ,
5 CT11 (NBLOCK) , BT22 (NBLOCK) , CT22 (NBLOCK) , BT33 (NBLOCK) ,
6 CT33 (NBLOCK) , BT12 (NBLOCK) , CT12 (NBLOCK) , BT23 (NBLOCK) ,
7 CT23 (NBLOCK) , BT31 (NBLOCK) , CT31 (NBLOCK)
C
    DIMENSION SVMAX (NBLOCK) , SVMIN (NBLOCK) , EV1 (NBLOCK)
    DIMENSION SDMAX (NBLOCK, 21) , SDMIN (NBLOCK, 21) , ED1 (NBLOCK, 21) ,
1 ET1 (NBLOCK, 21) , STMAX (NBLOCK, 21) , EN1 (21)
C
    DIMENSION N (21, 3)
C
    DIMENSION ZERO3 (NBLOCK) , ZERO (NBLOCK, 21)
    DIMENSION WV (NBLOCK) , WD1 (NBLOCK, 21) , WT1 (NBLOCK, 21) ,
2 WD (NBLOCK) , WT (NBLOCK)
C23456789123456789123456789123456789123456789123456789123456789
C
    CHARACTER*8 CMNAME
C
CCCCCCCCCCCCCCCCCCCCCCCCCCCCCCCCCCCCCCCCCCCCCCCCCCCCCCCCCCCCCCCC
C If romano, etc is used (at ASB)
    OPEN (UNIT=10, FILE='/acs_mnt/users3/a/abhatac/PHD/CHECK.OUT' ,
C If canard etc is used (at Bainer)
    OPEN (UNIT=10, FILE='/u/arun/PHD/CHECK.OUT' ,
1 STATUS='OLD' , ACCESS='APPEND' )
CCCCCCCCCCCCCCCCCCCCCCCCCCCCCCCCCCCCCCCCCCCCCCCCCCCCCCCCCCCCCCCC
C
C
C
    DO 100 KM=1, NBLOCK
C
CCCCCCCCCCCCCCCCCCCCCCCCCCCCCCCCCCCCCCCCCCCCCCCCCCCCCCCCCCCCCCCC
CC Dimenioning N matrix: Direction cosine matrix, for 21
C microplanes and 3 components in space.

```

C  
C Orthogonal symmetries; Bazant p 571  
C23456789  
Ca CHECKED WELL READ  
C  
C microplanes and 3 components in space.  
C The numbers below obtained from microplane calc program  
C based on 87-88 and 95/96 papers  
C  
C

N(1,1)=1.0  
N(1,2)=0.0  
N(1,3)=0.0  
N(2,1)=0.0  
N(2,2)=1.0  
N(2,3)=0.0  
N(3,1)=0.0  
N(3,2)=0.0  
N(3,3)=1.0  
N(4,1)=0.707106781187  
N(4,2)=0.707106781187  
N(4,3)=0.000  
N(5,1)=0.707106781187  
N(5,2)=-0.707106781187  
N(5,3)=0.0  
N(6,1)=0.707106781187  
N(6,2)=0.0  
N(6,3)=0.707106781187  
N(7,1)=0.707106781187  
N(7,2)=0.0  
N(7,3)=-0.707106781187  
N(8,1)=0.0  
N(8,2)=0.707106781187  
N(8,3)=0.707106781187  
N(9,1)=0.0  
N(9,2)=0.707106781187  
N(9,3)=-0.707106781187  
N(10,1)=0.387907304067  
N(10,2)=0.387907304067  
N(10,3)=0.836095596749  
N(11,1)=0.387907304067  
N(11,2)=0.387907304067  
N(11,3)=-0.836095596749  
N(12,1)=0.387907304067  
N(12,2)=-0.387907304067  
N(12,3)=0.836095596749  
N(13,1)=0.387907304067  
N(13,2)=-0.387907304067  
N(13,3)=-0.836095596749  
N(14,1)=0.387907304067  
N(14,2)=0.836095596749  
N(14,3)=0.387907304067  
N(15,1)=0.387907304067  
N(15,2)=0.836095596749  
N(15,3)=-0.387907304067  
N(16,1)=0.387907304067  
N(16,2)=-0.836095596749  
N(16,3)=0.387907304067  
N(17,1)=0.387907304067  
N(17,2)=-0.836095596749

N(17,3)=-0.387907304067  
N(18,1)=0.836095596749  
N(18,2)=0.387907304067  
N(18,3)=0.387907304067  
N(19,1)=0.836095596749  
N(19,2)=0.387907304067  
N(19,3)=-0.387907304067  
N(20,1)=0.836095596749  
N(20,2)=-0.387907304067  
N(20,3)=0.387907304067  
N(21,1)=0.836095596749  
N(21,2)=-0.387907304067  
N(21,3)=-0.387907304067

C  
C

WC(1)=0.0265214244093  
WC(2)=0.0265214244093  
WC(3)=0.0265214244093  
WC(4)=0.0199301476312  
WC(5)=0.0199301476312  
WC(6)=0.0199301476312  
WC(7)=0.0199301476312  
WC(8)=0.0199301476312  
WC(9)=0.0199301476312  
WC(10)=0.0250712367487  
WC(11)=0.0250712367587  
WC(12)=0.0250712367587  
WC(13)=0.0250712367587  
WC(14)=0.0250712367587  
WC(15)=0.0250712367587  
WC(16)=0.0250712367587  
WC(17)=0.0250712367587  
WC(18)=0.0250712367587  
WC(19)=0.0250712367587  
WC(20)=0.0250712367587  
WC(21)=0.0250712367587

CCCCCCCCCCCCCCCCCCCCCCCCCCCCCCCCCCCCCCCCCCCCCCCCCCCCCCCCCCCC

C  
C   CONSTANTS CALCULATED  
C

E= PROPS(1)  
NU=PROPS(2)  
P= PROPS(3)  
A= PROPS(4)  
Q= PROPS(5)  
B= PROPS(6)

CCCCCCCCCCCCCCCCCCCCCCCCCCCCCCCCCCCCCCCCCCCCCCCCCCCCCCCCCCCC

C VUMAT11.f addition, EF is strain coresp to fracture strength  
C Source Chen & Han: 'plasticity for structural engineers' p-350  
C from Springer-Verlag  
C case 2

EF= -0.13

C Case 3

EF= -0.001  
EF= -0.1  
EF= -0.01

CCCCCCCCCCCCCCCCCCCCCCCCCCCCCCCCCCCCCCCCCCCCCCCCCCCCCCCCCCCC

CCCCCCCCCCCCCCCCCCCCCCCCCCCCCCCCCCCCCCCCCCCCCCCCCCCCCCCCCCCC

C  
C Virgin Volumetric Tangent Stiffness Modulus



```

CCCCCCCCCCCCCCCCCCCCCCCCCCCCCCCCCCCCCCCCCCCCCCCCCCCCCCCCCCCC
C.Volumetric strain at the beginning and its Increment
C
      EPVP(KM) = (STRAN(KM,1)+STRAN(KM,2)+STRAN(KM,3))/3.0
      DEPV(KM) = (DSTRAN(KM,1)+DSTRAN(KM,2)+DSTRAN(KM,3))/3.0
C
C          PRINT *, 'NBLOCK=' ,NBLOCK
C          PRINT *, 'NSTATEV=' ,NSTATEV
C          PRINT *, 'STRAININC=' ,STRAININC(1,3)
C          PRINT *, 'DSTRAN(1)=' ,DSTRAN(KM,1)
C          PRINT *, 'DSTRAN(2)=' ,DSTRAN(KM,2)
C          PRINT *, 'DSTRAN(3)=' ,DSTRAN(KM,3)
C          PRINT *, 'DSTRAN(4)=' ,DSTRAN(KM,4)
C          PRINT *, 'DSTRAN(5)=' ,DSTRAN(KM,5)
C          PRINT *, 'DSTRAN(6)=' ,DSTRAN(KM,6)
C          PRINT *, 'STRAN(1)=' ,STRAN(KM,1)
C          PRINT *, 'STRAN(2)=' ,STRAN(KM,2)
C          PRINT *, 'STRAN(3)=' ,STRAN(KM,3)
C          PRINT *, 'DEPV=' ,DEPV(KM)
C          PRINT *, 'EPVP=' ,EPVP(KM)
CC
CCCCCCCCCCCCCCCCCCCCCCCCCCCCCCCCCCCCCCCCCCCCCCCCCCCCCCCCCCCC
CCCCCCCCCCCCCCCCCCCCCCCCCCCCCCCCCCCCCCCCCCCCCCCCCCCCCCCCCCCC
C
C NEW Volumetric Strain
C
      EPVN(KM) = EPVP(KM)+DEPV(KM)
C          PRINT *, 'EPVN=' ,EPVN(KM)
      EPSINC=1.0/(10.0**18.0)
C
      EPVDV(KM) = EPVP(KM)*DEPV(KM)
C
CCCCCCCCCCCCCCCCCCCCCCCCCCCCCCCCCCCCCCCCCCCCCCCCCCCCCCCCCCCC
CCCCCCCCCCCCCCCCCCCCCCCCCCCCCCCCCCCCCCCCCCCCCCCCCCCCCCCCCCCC
C
      M1=0.5
CCCCCCCCCCCCCCCCCCCCCCCCCCCCCCCCCCCCCCCCCCCCCCCCCCCCCCCCCCCC
      E11=0.0004
      E11=0.00005
C
CCCCCCCCCCCCCCCCCCCCCCCCCCCCCCCCCCCCCCCCCCCCCCCCCCCCCCCCCCCC
C Volumetric constitutive relationship
CCCCCCCCCCCCCCCCCCCCCCCCCCCCCCCCCCCCCCCCCCCCCCCCCCCCCCCCCCCC
C Working with 2 state variables : Volumetric Behavior
C
      IF (EPVN(KM).GE.STATEOLD(KM,1)) THEN
          STATENEW(KM,1)=EPVN(KM)
      ELSE
          STATENEW(KM,1)=STATEOLD(KM,1)
      ENDIF
C
C
      IF (EPVN(KM).LT.STATEOLD(KM,2)) THEN
          STATENEW(KM,2)=EPVN(KM)
      ELSE
          STATENEW(KM,2)=STATEOLD(KM,2)
      ENDIF
C
CC
C Defining the maximum and minimum strain then

```

```

C
      EVMAX (KM) =STATENEW (KM, 1)
      EVMIN (KM) =STATENEW (KM, 2)
      SVMAX (KM) =CVZ*EVMAX (KM) * ((1.0+(ABS (EVMAX (KM) ))/A) ** (-P) +
3      ((ABS (EVMAX (KM) ))/B) ** (Q) )
      SVMIN (KM) =EVMIN (KM) *CVZ* (EXP (- ((ABS (EVMIN (KM) ))/E11) **M1) )
C
CCCCCCCCCCCCCCCCCCCCCCCCCCCCCCCCCCCCCCCCCCCCCCCCCCCCCCCCCCCCCCCCCCCCCCCCCCCC
C Check the value of EPVP for loading and unloading.
C
      IF (EPVN (KM) *DEPV (KM) .GE.0.0 .AND. (EPVN (KM) -EVMAX (KM) ) *
1      (EPVN (KM) -EVMIN (KM) ) .GE.0.0) THEN
C      Loading occurs
      IF (EPVN (KM) .GT.0.0) CV=CVZ* ((1.0+(ABS (EPVN (KM) ))/A) ** (-P) +
2      ((ABS (EPVN (KM) ))/B) ** (Q) )
C      Loadin Stiffness in Tension
      IF (EPVN (KM) .LE.0.0) CV=CVZ* (EXP (- ((ABS (EPVN (KM) ))/E11) **M1) )
      SIGMVN (KM) =CV*EPVN (KM)
ELSE
C      Unloading and Reloading occurs
C      PRINT *, 'UNLOADING volumetric WATCH1'
      IF (EPVN (KM) .GT.0.0) THEN
          SIGMVN (KM) =STATEOLD (KM, 72) +CVZ*DEPV (KM)
          EV1 (KM) =EVMAX (KM) -SVMAX (KM) /CVZ
          IF (EV1 (KM) .LT.EPSINC) EV1 (KM) =0.0
C
          IF (SIGMVN (KM) .GE.0.0) GO TO 11
          IF (SIGMVN (KM) .LT.0.0) SIGMVN (KM) =CVZ* (EPVN (KM)
4          -EV1 (KM) ) * (EXP (- ((ABS (EPVN (KM) -EV1 (KM) ))/E11) **M1) )
      ELSE
          IF (EPVN (KM) .EQ.0.0) SIGMVN (KM) =0.0
          IF (EPVN (KM) .LT.0.0) SIGMVN (KM) =EPVN (KM) *
5          (SVMIN (KM) /EVMIN (KM) )
      ENDIF
C
      ENDIF
C
      ENDIF
CCCCCCCCCCCCCCCCCCCCCCCCCCCCCCCCCCCCCCCCCCCCCCCCCCCCCCCCCCCCCCCCCCCCCCCCCCCC
11      STATENEW (KM, 72) =SIGMVN (KM)
C
CCCCCCCCCCCCCCCCCCCCCCCCCCCCCCCCCCCCCCCCCCCCCCCCCCCCCCCCCCCCCCCCCCCCCCCCCCCC
C DAMAGE RULE (VOLUMETRIC)
      IF (EPVN (KM) .LE.0.0) THEN
          WV (KM) =EXP (- ((ABS (EPVN (KM) ))/E11) **M1)
      ELSE
          WV (KM) =0.0
      ENDIF
CCCCCCCCCCCCCCCCCCCCCCCCCCCCCCCCCCCCCCCCCCCCCCCCCCCCCCCCCCCCCCCCCCCCCCCCCCCC
C Redefining STRAN(NTENS) INTO A 2-D ARRAY SN(I,J)
CCCCCCCCCCCCCCCCCCCCCCCCCCCCCCCCCCCCCCCCCCCCCCCCCCCCCCCCCCCCCCCCCCCCCCCCCCCC
C
      SN (1, 1) =STRAN (KM, 1)
      SN (2, 2) =STRAN (KM, 2)
      SN (3, 3) =STRAN (KM, 3)
      SN (1, 2) =STRAN (KM, 4)
      SN (2, 3) =STRAN (KM, 5)
      SN (1, 3) =STRAN (KM, 6)
C
      SN (2, 1) =STRAN (KM, 4)
      SN (3, 2) =STRAN (KM, 5)
      SN (3, 1) =STRAN (KM, 6)

```

```

C
C Incremental Strain (GLOBAL); matrix form.
C
      DSN(1,1)=DSTRAN(KM,1)
      DSN(2,2)=DSTRAN(KM,2)
      DSN(3,3)=DSTRAN(KM,3)
      DSN(1,2)=DSTRAN(KM,4)
      DSN(2,3)=DSTRAN(KM,5)
      DSN(1,3)=DSTRAN(KM,6)
C
      DSN(2,1)=DSTRAN(KM,4)
      DSN(3,2)=DSTRAN(KM,5)
      DSN(3,1)=DSTRAN(KM,6)
C
CCCCCCCCCCCCCCCCCCCCCCCCCCCCCCCCCCCCCCCCCCCCCCCCCCCCCCCCCCCCCCCCCCCCCCCC
C Normal Strain EN & its increment DEN for # M-Planes.
C NEW Normal Strain ENN at the end.
C
      DO 10 K=1,21
          EN(K) = 0.0
          DEN(K)=0.0
C
C
      DO 20 I=1,3
          DO 20 J=1,3
              EN(K)=SN(I,J)*N(K,I)*N(K,J)+EN(K)
              DEN(K)=DSN(I,J)*N(K,I)*N(K,J)+DEN(K)
          20 CONTINUE
C
CCCCCCCCCCCCCCCCCCCCCCCCCCCCCCCCCCCCCCCCCCCCCCCCCCCCCCCCCCCCCCCCCCCCCCCC
C23456789123456789123456789123456789123456789123456789123456789123456789
CCCCCCCCCCCCCCCCCCCCCCCCCCCCCCCCCCCCCCCCCCCCCCCCCCCCCCCCCCCCCCCCCCCCCCCC
      EN1(K)=SN(1,1)*N(K,1)*N(K,1)+SN(1,2)*N(K,1)*N(K,2)+SN(1,3)*N(K,1)
      1 *N(K,3)+SN(2,1)*N(K,2)*N(K,1)+SN(2,2)*N(K,2)*N(K,2)+SN(2,3)*
      2 N(K,2)*N(K,3)+SN(3,1)*N(K,3)*N(K,1)+SN(3,2)*N(K,3)*N(K,2)+
      3 SN(3,3)*N(K,3)*N(K,3)
C      PRINT*,'EN1(K)=' ,EN1(K)
C      PRINT*,'EN(K)=' ,EN(K)
          ENN(K)=EN(K)+DEN(K)
C
CCCCCCCCCCCCCCCCCCCCCCCCCCCCCCCCCCCCCCCCCCCCCCCCCCCCCCCCCCCCCCCCCCCCCCCC
C (Normal) Deviatoric Strain; Begin=EDP, New=EDN, Incr=DED
CCCCCCCCCCCCCCCCCCCCCCCCCCCCCCCCCCCCCCCCCCCCCCCCCCCCCCCCCCCCCCCCCCCCCCCC
C DEVIATORIC BEHAVIOR
C
      EDP(KM,K)=EN(K)-EPVP(KM)
      EDN(KM,K)=ENN(K)-EPVN(KM)
      DED(KM,K)=EDN(KM,K)-EDP(KM,K)
CCCCCCCCCCCCCCCCCCCCCCCCCCCCCCCCCCCCCCCCCCCCCCCCCCCCCCCCCCCCCCCCCCCCCCCC
C      IF (EDP(KM,K).GT.0.0.AND.EDN(KM,K).LT.0.0) PRINT*,'WATCH4
Cj  1      DED=' ,DED(KM,K)
C      IF (EDP(KM,K).LT.0.0.AND.EDN(KM,K).GT.0.0) PRINT*,'WATCH5
C      2      DED=' ,DED(KM,K)
CCCCCCCCCCCCCCCCCCCCCCCCCCCCCCCCCCCCCCCCCCCCCCCCCCCCCCCCCCCCCCCCCCCCCCCC
C      PRINT*,'K=' ,K,' EDN=' ,EDN(KM,K),' EDP=' ,EDP(KM,K)
C
C Using state variables no. 3 to 23.
C
      IF (EDN(KM,K).GE.STATEOLD(KM,2+K)) THEN
          STATENEW(KM,2+K)=EDN(KM,K)

```



```

      IF (EDN(KM,K).GT.0.0) THEN
C          PRINT*, 'EDN .GT. 0.0'
            ED1(KM,K)=EDMAX(KM,K)-SDMAX(KM,K)/CDZ
            IF (ED1(KM,K).LT.EPSINC) ED1(KM,K)=0.0
            SDN(KM,K)=STATEOLD(KM,I)+CDZ*DED(KM,K)
C          PRINT*, 'SDN=inter=',SDN(KM,K)
C          PRINT*, 'CDZ=',CDZ
            IF (SDN(KM,K).GE.0.0) GO TO 12
C          IF (SDN(KM,K).LT.0.0) PRINT*, 'WATCH7'
            IF (SDN(KM,K).LT.0.0) SDN(KM,K)=CDZ*(EDN(KM,K)-
2              -ED1(KM,K))*EXP(-(ABS(EDN(KM,K)-ED1(KM,K))/E2)**M2)
C          ELSE
            PRINT*, 'EDN .LE. 0.0'
            IF (EDN(KM,K).EQ.0.0) SDN(KM,K)=0.0
            IF (EDN(KM,K).LT.0.0) SDN(KM,K)=EDN(KM,K)*
3              (SDMIN(KM,K)/EDMIN(KM,K))
C          ENDIF
C      ENDIF
C
C          PRINT*, 'SDN=',SDN(KM,K)
CCCCCCCCCCCCCCCCCCCCCCCCCCCCCCCCCCCCCCCCCCCCCCCCCCCCCCCCCCCCCCCCCCCC
C          Updating state variables
12         STATENEW(KM,I)=SDN(KM,K)
Cn        PRINT*, 'STOLD=',STATEOLD(KM,I)
C         PRINT*, 'I=',I, 'STNEW=',STATENEW(KM,I)
CCCCCCCCCCCCCCCCCCCCCCCCCCCCCCCCCCCCCCCCCCCCCCCCCCCCCCCCCCCCCCCCCCCC
C          DAMAGE RULE (DEVIATORIC)
C
C          WD1(KM,K)=EXP(-(ABS(EDN(KM,K))/E1)**M)
CCCCCCCCCCCCCCCCCCCCCCCCCCCCCCCCCCCCCCCCCCCCCCCCCCCCCCCCCCCCCCCCCCCC
10        CONTINUE
CCCCCCCCCCCCCCCCCCCCCCCCCCCCCCCCCCCCCCCCCCCCCCCCCCCCCCCCCCCCCCCCCCCC
C
C          TANGENTIAL/INPLANE COMPONENTS
C
CCCCCCCCCCCCCCCCCCCCCCCCCCCCCCCCCCCCCCCCCCCCCCCCCCCCCCCCCCCCCCCCCCCC
C
C          DO 30 K=1,21
C
C          Components of ETN:New ten strain vector as ET1, ET2,ET3
C
C          Change January 23, 95
C
CCCCCCCCCCCCCCCCCCCCCCCCCCCCCCCCCCCCCCCCCCCCCCCCCCCCCCCCCCCCCCCCCCCC
C23456789123456789123456789123456789123456789123456789123456789123456789
CCCCCCCCCCCCCCCCCCCCCCCCCCCCCCCCCCCCCCCCCCCCCCCCCCCCCCCCCCCCCCCCCCCC
C
      ETP1(KM,K)=SN(1,1)*N(K,1)+SN(1,2)*N(K,2)+SN(1,3)*N(K,3)
1      -EN(K)*N(K,1)
      ETP2(KM,K)=SN(2,1)*N(K,1)+SN(2,2)*N(K,2)+SN(2,3)*N(K,3)
1      -EN(K)*N(K,2)
      ETP3(KM,K)=SN(3,1)*N(K,1)+SN(3,2)*N(K,2)+SN(3,3)*N(K,3)
1      -EN(K)*N(K,3)
C234567
C
      ETP(KM,K)=SQRT(ETP1(KM,K)**2.+ETP2(KM,K)**2.+ETP3(KM,K)**2.)
C
      DET1(KM,K)=DSN(1,1)*N(K,1)+DSN(1,2)*N(K,2)+DSN(1,3)*N(K,3)-
1      DEN(K)*N(K,1)

```

```

      DET2 (KM, K) =DSN (2, 1) *N (K, 1) +DSN (2, 2) *N (K, 2) +DSN (2, 3) *N (K, 3) -
1   DEN (K) *N (K, 2)
      DET3 (KM, K) =DSN (3, 1) *N (K, 1) +DSN (3, 2) *N (K, 2) +DSN (3, 3) *N (K, 3) -
1   DEN (K) *N (K, 3)
C
C
C
      ETN1 (KM, K) =ETP1 (KM, K) +DET1 (KM, K)
      ETN2 (KM, K) =ETP2 (KM, K) +DET2 (KM, K)
      ETN3 (KM, K) =ETP3 (KM, K) +DET3 (KM, K)
C
      ETN (KM, K) =SQRT (ETN1 (KM, K) **2 . +ETN2 (KM, K) **2 . +ETN3 (KM, K) **2 .)
      GAMMAN (KM, K) =ETN (KM, K)
C
C
      ZERO (KM, K) =ETN1 (KM, K) *N (K, 1) +ETN2 (KM, K) *N (K, 2) +ETN3 (KM, K) *N (K, 3)
      ZERO (KM, K) =ETP1 (KM, K) *N (K, 1) +ETP2 (KM, K) *N (K, 2) +ETP3 (KM, K) *N (K, 3)
C
C
C
      DET (KM, K) =ETN (KM, K) -ETP (KM, K)
C
C
      PRINT *, 'DET (1) =', DET (1)
C
CCCCCCCCCCCCCCCCCCCCCCCCCCCCCCCCCCCCCCCCCCCCCCCCCCCCCCCCCCCCCCCCCCCCCCCCCCCC
C
C CONSTANTS A3 P3 AND CTZ , E33 AND K1 DEFINED
C AK defined
C
      AK=0.0
      A3Z=.0015
      A3=A3Z+AK*EPVN (KM)
CCCCCCCCCCCCCCCCCCCCCCCCCCCCCCCCCCCCCCCCCCCCCCCCCCCCCCCCCCCCCCCCCCCCCCCCCCCC
C
      A3=.0018
      P3=1.5
C
      CTZ=(1.0/3.0) * ((5.0-10.0*NU) / (1.0+NU) -2.0*ETA) *CVZ
C
CCCCCCCCCCCCCCCCCCCCCCCCCCCCCCCCCCCCCCCCCCCCCCCCCCCCCCCCCCCCCCCCCCCCCCCCCCCC
C Using state variables no.45 to 65.
C
      IF (ETN (KM, K) .GE. STATEOLD (KM, 44+K)) THEN
          STATENEW (KM, 44+K) =ETN (KM, K)
      ELSE
          STATENEW (KM, 44+K) =STATEOLD (KM, 44+K)
      ENDIF
C
CCCCCCCCCCCCCCCCCCCCCCCCCCCCCCCCCCCCCCCCCCCCCCCCCCCCCCCCCCCCCCCCCCCCCCCCCCCC
C Maximum and Minimum Values of tangential Strain so far
C ETMIN is always zero
C
      PRINT*, 'K=', K
C
      ETMAX (KM, K) =STATENEW (KM, 44+K)
      ETMIN (KM, K) =0.0
      STMAX (KM, K) =CTZ*ETMAX (KM, K) *EXP (- (ETMAX (KM, K) /A3) **P3)
C
CCCCCCCCCCCCCCCCCCCCCCCCCCCCCCCCCCCCCCCCCCCCCCCCCCCCCCCCCCCCCCCCCCCCCCCCCCCC
C Inplane (tangential) Constitutive rule
CCCCCCCCCCCCCCCCCCCCCCCCCCCCCCCCCCCCCCCCCCCCCCCCCCCCCCCCCCCCCCCCCCCCCCCCCCCC
CCCCCCCCCCCCCCCCCCCCCCCCCCCCCCCCCCCCCCCCCCCCCCCCCCCCCCCCCCCCCCCCCCCCCCCCCCCC
C STESSES AND INCREMENTAL STRESS

```

```

C
C      PRINT*, 'ETN=' , ETN(KM, K) , ' DET=' , DET(KM, K)
C      PRINT*, 'ETMAX=' , ETMAX(KM, K) , ' STOLD=' , STATEOLD(KM, K+93)
C2345678
C      IF (ETN(KM, K) * DET(KM, K) .GE. 0.0 .AND. (ETN(KM, K) - ETMAX(KM, K)) *
1          (ETN(KM, K) - ETMIN(KM, K)) .GE. 0.0) THEN
C
C          TAU(KM, K) = CTZ * ETN(KM, K) * EXP(- (ETN(KM, K) / A3) ** P3)
C      ELSE
C          PRINT*, 'Unloading -tangential WATCH3', ' K=' , K
C          TAU(KM, K) = STATEOLD(KM, K+93) + DET(KM, K) * CTZ
C          IF (TAU(KM, K) .LT. 0.0) TAU(KM, K) = 0.0
C
C      ENDIF
C      PRINT*, 'TAU=' , TAU(KM, K)
C
C      CCCCCCCCCCCCCCCCCCCCCCCCCCCCCCCCCCCCCCCCCCCCCCCCCCCCCCCCCCCCCCCCC
C      DAMAGE RULE (TANGENTIAL)
C          WT1(KM, K) = EXP(- (ETN(KM, K) / A3) ** P3)
C      CCCCCCCCCCCCCCCCCCCCCCCCCCCCCCCCCCCCCCCCCCCCCCCCCCCCCCCCCCCCCCCCC
C      Defining State variables from 94 to 114
C          STATENEW(KM, K+93) = TAU(KM, K)
C          PRINT*, ' STNEW=' , STATENEW(KM, K+93)
C      CCCCCCCCCCCCCCCCCCCCCCCCCCCCCCCCCCCCCCCCCCCCCCCCCCCCCCCCCCCCCCCCC
C
C          IF (GAMMAN(KM, K) .LE. 0.0) THEN
C              TAUGA = 0.0
C          ELSE
C              TAUGA(KM, K) = TAU(KM, K) / GAMMAN(KM, K)
C          ENDIF
C
C      Tangential Stresses 1, 2 and 3
C          SIGT1(KM, K) = TAUGA(KM, K) * ETN1(KM, K)
C          SIGT2(KM, K) = TAUGA(KM, K) * ETN2(KM, K)
C          SIGT3(KM, K) = TAUGA(KM, K) * ETN3(KM, K)
C
C      30      CONTINUE
C      CCCCCCCCCCCCCCCCCCCCCCCCCCCCCCCCCCCCCCCCCCCCCCCCCCCCCCCCCCCCCCCCC
C
C      C
C      C
C      C      NEW GLOBAL STRESS= TERMA + TERMB + TERMC
C      C
C      C
C
C          TA12 = 0.0
C          TA13 = 0.0
C          TA31 = 0.0
C          TA23 = 0.0
C
C      CCCCCCCCCCCCCCCCCCCCCCCCCCCCCCCCCCCCCCCCCCCCCCCCCCCCCCCCCCCCCCCCC
C
C      DO 201 K=1, 21
C          TB11(KM, K) = SDN(KM, K) * N(K, 1) * N(K, 1)
C23456
C          TC11(KM, K) = SIGT1(KM, K) * (N(K, 1) - N(K, 1) ** 3.)
1              - SIGT2(KM, K) * (N(K, 2) * N(K, 1) ** 2.)
2              - SIGT3(KM, K) * (N(K, 3) * N(K, 1) ** 2.)
C
C
C

```

```

201      CONTINUE
C
      BT11 (KM) =0.0
      CT11 (KM) =0.0
C
      DO 202 K=1,21
          BT11 (KM) =TB11 (KM, K) *WC (K) +BT11 (KM)
          CT11 (KM) =TC11 (KM, K) *WC (K) +CT11 (KM)
202      CONTINUE
C
C
      STRESSNEW (KM, 1) =SIGMVN (KM) +6.0* (BT11 (KM) +CT11 (KM) )
CCCCCCCCCCCCCCCCCCCCCCCCCCCCCCCCCCCCCCCCCCCCCCCCCCCCCCCCCCCCCCCC
C
      DO 203 K=1,21
          TB22 (KM, K) =SDN (KM, K) *N (K, 2) *N (K, 2)
C234567
          TC22 (KM, K) =-SIGT1 (KM, K) *N (K, 1) * (N (K, 2) **2.) +
          1          SIGT2 (KM, K) * (N (K, 2) -N (K, 2) **3.)
          2          -SIGT3 (KM, K) * (N (K, 2) **2.) *N (K, 3)
C
203      CONTINUE
C
      BT22 (KM) =0.0
      CT22 (KM) =0.0
C
      DO 204 K=1,21
          BT22 (KM) =TB22 (KM, K) *WC (K) +BT22 (KM)
          CT22 (KM) =TC22 (KM, K) *WC (K) +CT22 (KM)
C
204      CONTINUE
C
      STRESSNEW (KM, 2) =SIGMVN (KM) +6.0* (BT22 (KM) +CT22 (KM) )
CCCCCCCCCCCCCCCCCCCCCCCCCCCCCCCCCCCCCCCCCCCCCCCCCCCCCCCCCCCCCCCC
      DO 205 K=1,21
          TB33 (KM, K) =SDN (KM, K) *N (K, 3) *N (K, 3)
C23456
          TC33 (KM, K) =-SIGT1 (KM, K) *N (K, 1) * (N (K, 3) **2.)
          1          -SIGT2 (KM, K) *N (K, 2) * (N (K, 3) **2.)
          2          +SIGT3 (KM, K) * (N (K, 3) -N (K, 3) **3.)
C
205      CONTINUE
C
      BT33 (KM) =0.0
      CT33 (KM) =0.0
C
      DO 206 K=1,21
          BT33 (KM) =TB33 (KM, K) *WC (K) +BT33 (KM)
          CT33 (KM) =TC33 (KM, K) *WC (K) +CT33 (KM)
206      CONTINUE
C
C
      STRESSNEW (KM, 3) =SIGMVN (KM) +6.0* (BT33 (KM) +CT33 (KM) )
CCCCCCCCCCCCCCCCCCCCCCCCCCCCCCCCCCCCCCCCCCCCCCCCCCCCCCCCCCCCCCCC
CCCCCCCCCCCCCCCCCCCCCCCCCCCCCCCCCCCCCCCCCCCCCCCCCCCCCCCCCCCCCCCC
      DO 207 K=1,21
          TB12 (KM, K) =SDN (KM, K) *N (K, 1) *N (K, 2)
C
          TC12 (KM, K) =0.5*SIGT1 (KM, K) * (N (K, 2) -2.0*N (K, 2) *N (K, 1) **2.0)
          1          +0.5*SIGT2 (KM, K) * (N (K, 1) -2.0*N (K, 1) *N (K, 2) **2.0)

```





## APPENDIX F

### Stress-Strain Equations

The explicit equation for the stress strain curve in the Microplane Theory (Bazant, 1992a) can be written as follows:

For volumetric behavior:

$$\begin{cases} \sigma_v = E_v^0 \varepsilon_v \left[ e^{-(|\varepsilon_v|/a1)^{p1}} \right] & \text{for } \varepsilon_v \geq 0 \\ \sigma_v = E_v^0 \varepsilon_v \left[ \left( 1 + \frac{|\varepsilon_v|}{a} \right)^{-p} + \left( \frac{|\varepsilon_v|}{b} \right)^{-q} \right] & \text{for } \varepsilon_v < 0. \end{cases} \quad (\text{G.1})$$

For deviatoric behavior:

$$\begin{cases} \sigma_d = E_d^0 \varepsilon_d \left[ e^{-(|\varepsilon_d|/a1)^{p1}} \right] & \text{for } \varepsilon_d \geq 0 \\ \sigma_d = E_d^0 \varepsilon_d \left[ e^{-(|\varepsilon_d|/a2)^{p2}} \right] & \text{for } \varepsilon_d < 0. \end{cases} \quad (\text{G.2})$$

For tangential behavior:

$$\tau = E_t^0 \gamma e^{-(\gamma/a3)^{p3}} \quad (\text{G.3})$$

where

$$\tau = \sqrt{\sigma_t \cdot \sigma_t} \quad (\text{G.4})$$

and

$$\gamma = \sqrt{\varepsilon_t \cdot \varepsilon_t}. \quad (\text{G.5})$$

There are 14 parameters for the explicit version of the Microplane Theory (1992a). These parameters can be divided into 4 categories as follows:

- Elastic parameters:  $E$ ,  $\nu$ ,  $\eta_o$ . The elastic parameter  $E$  represents the Young's Modulus,  $\nu$  is the Poisson's ratio, and  $\eta_o$  is the additional elastic parameter that is linked with the deviatoric behavior.
- Volumetric law parameters:  $a$ ,  $b$ ,  $p$ ,  $q$ ,  $a1$  and  $p1$ . The parameters  $a$ ,  $b$ ,  $p$  and  $q$  represent the constants used in describing the material behavior in volumetric compression. The parameters  $a1$  and  $p1$  represent the same in volumetric tension.
- Deviatoric law parameters:  $a2$  and  $p2$ . These parameters represent the material behavior in deviatoric compression.
- Tangential law parameters:  $a3$ ,  $Ka$  and  $p3$ . The parameters represent the in-plane stress-strain response for each microplane. The equations shown from G.3 to G.5 relate the resultant in-plane response  $\tau$  in a microplane to a given absolute magnitude of the shear strain  $\gamma$ .

## APPENDIX G

### Nomenclature

|            |                                      |
|------------|--------------------------------------|
| $A_s$      | Cross sectional area of steel        |
| $C$        | Green Deformation Tensor             |
| $C_v$      | Volumetric Secant Modulus            |
| $C_d$      | Deviatoric Secant Modulus            |
| $C_t$      | Tangential Secant Modulus            |
| $D_{ijkl}$ | Incremental Tangent Stiffness Tensor |
| $E$        | Elastic Modulus                      |
| $F$        | Deformation Gradient                 |
| $K_a$      | Parameter used in tangential law     |
| $L$        | Length of the pavement slab          |
| $M$        | Mass                                 |
| $P$        | Load applied on the pavement         |
| $S$        | Dowel Spacing                        |
| $SF1$      | Section forces in the dowel          |
| $T$        | Time                                 |
| $W$        | Width of the joint                   |
| $a$        | Volumetric parameter (compression)   |
| $a1$       | Volumetric parameter (tension)       |
| $a2$       | Deviatoric parameter (compression)   |
| $a3$       | Tangential parameter 1               |
| $a^03$     | Tangential parameter 2               |
| $b$        | Volumetric parameter (compression)   |

|                       |                                         |
|-----------------------|-----------------------------------------|
| $d$                   | Dowel diameter                          |
| $h$                   | Depth of the dowel                      |
| $h_1$                 | Thickness of the concrete layer         |
| $h_2$                 | Thickness of the base or subbase        |
| $n$                   | Number of microplanes                   |
| $n_{i \text{ or } j}$ | Unit normal vector defining microplanes |
| $p$                   | Volumetric parameter (compression)      |
| $p_1$                 | Volumetric parameter (tension)          |
| $p_2$                 | Deviatoric parameter (compression)      |
| $p_3$                 | Tangential parameter 3                  |
| $q$                   | Volumetric parameter (compression)      |
| $u$                   | Nodal displacement                      |
| $w_v$                 | Volumetric damage                       |
| $w_d$                 | Deviatoric damage                       |
| $w_t$                 | Tangential damage                       |
| $\Delta t$            | Time increment                          |
| $\delta_{ij}$         | Kronecker Delta                         |
| $\epsilon_{ij}$       | Strain Tensor                           |
| $\epsilon_n$          | Normal Strain                           |
| $\epsilon_v$          | Volumetric Strain Tensor                |
| $\epsilon_d$          | Deviatoric Strain Tensor                |
| $\epsilon_t$          | Tangential Strain Tensor                |
| $\phi$                | Surface traction                        |
| $\gamma$              | Shear Strain                            |
| $\eta_0$              | Additional elastic constant             |
| $\nu$                 | Poisson's ratio                         |
| $\rho$                | Mass density                            |

|               |                          |
|---------------|--------------------------|
| $\sigma_c$    | Max. Stress in concrete  |
| $\sigma_{11}$ | Longitudinal Stress      |
| $\sigma_{ij}$ | Stress Tensor            |
| $\sigma_v$    | Volumetric Stress Tensor |
| $\sigma_d$    | Deviatoric Stress Tensor |
| $\sigma_t$    | Tangential Stress Tensor |
| $\tau$        | Shear Stress             |